Analytical and Numerical Methods for Assessing the Aquifer Support and its Application to the Sabah Field

A MASTER THESIS
SUBMITTED TO THE
DEPARTMENT OF PETROLEUM ENGINEERING
UNIVERSITY OF LEOBEN, AUSTRIA,

written by
Dipl.-Ing. Christoph Steiner
October 2015

Advisor: O.Univ.Prof. Dipl.-Ing. Dr.mont. Dr.h.c. Zoltán E. HEINEMANN

Affidavit

I declare in lieu of oath that I did this work by myself using only literature cited at the end of this volume.

_____

Dipl.-Ing. Christoph Steiner
Leoben, October 2015

Acknowledgments

First of all I would like to thank O.Univ.Prof. Dipl.-Ing. Dr.mont. Dr.h.c. Zoltán E. Heinemann for his advice and support during the development of this master thesis. I am grateful for the opportunity to write my master thesis with him and for the knowledge I was able to gain from him.

Special thanks also to Dr. Georg Mittermeir of Heinemann Consulting GmbH Leoben who supported me in the development of this work and taught me valuable reservoir engineering skills.

I want to thank Dr. Mohamed Gharsalla for his support and help in understanding the Sabah Field.

I also want to express my gratitude to Dr. Pavle Matijevic Technologie und Forschungsimpulszentrum GmbH, Professors Heinemann's Doctorate Group (PHDG) and PM Lucas Enterprises for providing office room and the necessary software packages. PHDG's proprietary software package H5/PRS was essential to the success of this master thesis.

I would also like to thank Zueitina Oil Company (ZOC) for providing the necessary data of the Sabah Field.

The quality of the English, spelling and grammar, was corrected in a friendly turn by my sister Mag. Maria Steiner and I also want to thank her for help.

Last but not least I want to thank my parents for their comprehensive support throughout my studies at the Montanuniversität Leoben.

Abstract

This master thesis presents the application of the Target Pressure Method (TPM) and the material balance method to the Sabah field. The applicability of the TPM is proved and the advantages of this method compared to other techniques are demonstrated. Improvements to the TPM have been suggested and also applied in this thesis.

The Sabah field, a naturally fractured reservoir, is located in the south-western part of the Sirte Basin in Libya. The reservoir is situated on a local high within the Zella graben and has been discovered in 1964 by the Alwerath Oil Company. Since then seventy wells have been drilled into this reservoir.

Both, the material balance method and the TPM, use field data to match the pressure history by determining the water influx requirements. In the TPM water influx occurs through defined boundaries of the productive area. Both methods give the possibility to determine aquifer pressure support and the parameters of analytical aquifer models at a very early stage of the dynamic modeling process. The TPM facilitates the recognition of deficiencies in the geological reservoir model and can be used to provide feedback to the geological modeler. It also allows for the determination of outer (surrounding the productive area) aquifer parameters, an area of the hydrodynamic system that is usually without any direct measurements.

Using both methods analytical aquifer parameters have been determined. The correctness of the analytical aquifer parameters calculated with the TPM was proved by successfully recalculating the history in prediction mode. The main water influx was found to be occurring from the south of the Sabah field. The five target regions could be excellently matched with the TPM. Discrepancies between measured and calculated pressures for the central region - a control region- indicate potential improvements of the geological model.

Kurzfassung

Diese Masterarbeit präsentiert die Anwendung der Target Pressure Method (TPM) und der Materialbilanzmethode auf die Sabah Lagerstätte. Die Anwendbarkeit der TPM wird nachgewiesen und die Vorteile dieser Methode im Vergleich zu anderen Methoden werden aufgezeigt. Verbesserungen der TPM wurden vorgeschlagen und in dieser Abschlussarbeit auch angewandt.

Die Sabah Lagerstätte, eine natürlich geklüftete Lagerstätte, liegt im südwestlichen Teil des Sirte Beckens in Libyen. Die Lagerstätte ist dort in einem lokalen hoch im Zella Graben situiert und wurde 1964 von der Alwerath Oil Company entdeckt. Seitdem wurden siebzig Bohrungen in diese Lagerstätte abgeteuft.

Sowohl die Materialbilanzmethode also auch die TPM gleichen unter Verwendung von Felddaten historische und berechnete Druckverläufe durch Bestimmung des Wasserzuflussbedarfs an. In der TPM findet Wasserzufluss durch definierte Lagerstättengrenzen statt. Beide Methoden ermöglichen die Bestimmung der Aquifer Druckunterstützung und von Parametern analytischer Aquifermodelle in einem sehr frühen Stadion der dynamischen Modellierung. Die TPM ermöglicht das Erkennen von Schwächen des geologischen Lagerstättenmodells, was als Feedback für geologischen Modellierer benutzt werden kann. Zusätzlich kann die Methode herangezogen werden um Parameter des umgebenden Aquifers zu bestimmen, von dem üblicherweise keine direkten Messungen vorhanden sind.

Unter Anwendung beider Methoden wurden Parameter von analytischen Aquifermodellen bestimmt. Die Korrektheit der Parameter der analytischen Aquifermodelle, die mit der TPM bestimmt wurden, wurde durch erfolgreiche Reproduktion der Druckhistorie im Vorhersagemodus nachgewiesen. Hauptsächlich findet der Wasserzufluss vom Süden der Sabah Lagerstätte statt. In den fünf Zielregionen konnten mit der TPM die Druckhistorie sehr gut reproduziert werden. Unterschiede zwischen gemessenen und berechneten Drücken in der Zentralregion – einer Kontrollregion – weisen auf potentielle Verbesserungen des geologischen Modells hin.

Table of Contents

List of Figures

List of Tables

Chapter 1

Introduction

1.1 Problem Description and Objectives

In many reservoirs an aquifer is connected to the hydrocarbon saturated part of the reservoir, providing pressure support to the reservoir in case of depletion. Together, the petroleum reservoir and the aquifer form a hydrodynamic system, which makes it necessary to determine aquifer properties. Knowing the water influx requirements of a hydrocarbon reservoir is of highest importance to predict future reservoir performance. Usually no direct measurement of the aquifer characteristics are possible, which means that indirect methods are required. Typically pressure declines non-uniformly within a reservoir. Geological features like faults, baffles and interbeddings impact fluid flow and thus pressure propagation.

To assess the aquifer support for a petroleum reservoir, different methods can be applied. Both an analytical approach, the material balance method, and a numerical approach, reservoir simulation, can be used to determine the water influx requirements. The material balance method can be viewed as an historically important technique to determine aquifer model parameters, however the contemporary way to evaluate the model parameters is by history matching the historical field data using reservoir simulation. It should be emphasized that despite material balance calculation exists for over 80 years now, it is still a basic, mandatory and reliable tool for the practicing reservoir engineer.

Also the aquifer itself can be defined as an analytical or numerical model. Examples of analytical models would be the Fetkovich aquifer model or the Van Everdingen and Hurst model. Numerically, aquifers can also be represented as gridded aquifers.

To be able to apply material balance calculations to a petroleum reservoir an average pressure for the field is needed. In case of numerical simulation using an automated history matching approach, in this thesis the Target Pressure Method (TPM), the definition of multiple pressure regions and their average pressures is necessary. Both the material balance method and the reservoir simulation using the TPM are able to determine aquifer parameters for analytical aquifers.

Static pressure gradient surveys are a tactic to obtain the required average pressure data. However, this data is not always reliable and can be unrepresentative of the desired average pressure. Multiple reasons can be responsible that the static pressure data has to be rejected, most importantly a too short shut-in time. A method to decide which data is acceptable and which data has to be rejected is necessary to ensure the quality of the average pressure data.

Defining the required pressure regions for the TPM can be done by analyzing the history of the reservoir. The use of validated static pressure data combined with the geological knowledge of the field make it possible to define pressure regions.

The objectives for this thesis are:

- Evaluation of the static pressure data and identification and definition of pressure regions.
- Determination of average pressures for the pressure regions and for the field level.
- Analytical assessment of aquifer model parameters for the Sabah field, which belongs to the National Oil Corporation (NOC) and is operated by the Zueitina Oil Company (ZOC) of Tripoli, Libya.
- Numerical determination of water influx requirements and parameters for analytical aquifer models by matching of field and region pressure history for the Sabah field using the automated history matching method “Target Pressure Method”.

This master thesis is based on previous achievements of numerous scientists and software developers. Many of them have worked at the Petroleum Engineering Department of the Mining University of Leoben under the guidance and leadership of Professor Zoltán E. Heinemann.

The practical work presented in this master thesis was carried out using the research simulator H5. It is designed, developed and coded by Prof. Heinemann. His research simulator is a multipurpose reservoir simulator capable to solve black-oil and compositional problems for fractured and non-fractured reservoirs. Furthermore it offers a large collection of tools for basic reservoir engineering work such as displacement efficiency calculations, material balance calculations, decline curve analysis, etc. The H5 tool is only available to students and researchers of the PHDG, the Professor Heinemann Doctorate group. H5 is the fifth generation of research simulators developed under the supervision of Prof. Heinemann. The first generation was written in FORTRAN-IV in 1968. The development of the fifth generation began in 2006, using FORTRAN-1995 and C++ programing languages. The various “H”-versions served as the foundations for commercial software packages including SIMULA, SURE, PRS-2012 and PRS-2015

For model building the commercial geological software package Petrel from Schlumberger was used. The results of the H5 simulator have been (whenever possible) validated and verified against the results calculated with Schlumbergers ECLIPSE E100 black oil reservoir simulator.

1.2 Content and Organization of this Work

In **Chapter 2** a literature review on aquifer modeling approaches and the historical development of the water influx models is given. Also the procedures of determining the parameters for analytical aquifer models are described. The focus is set on analytical procedures, using the material balance equations, and numerical methods.

Chapter 3 gives definitions that are important for this work. This includes definition of average pressures, static pressure, initial reservoir pressure, analytical aquifer models and the possibilities of defining aquifers in numerical models.

Chapter 4 deals with the Sabah field. The geology of the Sabah field is described on the basis of the dissertation by Gharsalla (2015). Also available RCAL and SCAL data is discussed and the reservoir fluid properties of the Sabah field are listed. Also the available static pressure data and well test data are listed and discussed. Additionally the pressure gradient data is analyzed, which is necessary to prove vertical communication between layers.

Chapter 5 describes the evaluation of the static pressure measurements, the procedure for defining pressure regions and average pressure for regions and the field level. Also included is the application of all these procedures to the Sabah field.

Chapter 6 consists of a description of the reservoir simulation model and the application of two approaches for the determination of the aquifer support assessment. One of the applied methods is the material balance method and the other used method is the simulation of the reservoir with automated history matching using the Target Pressure Method. For the application of the Target Pressure Method the software H5 is used. Also a test of the calculated analytical aquifer parameters using Schlumberger ECLIPSE confirming the correct calculation of these parameters within H5 is included.

Chapter 7 contains the conclusions of this thesis.

Chapter 2

Literature Review

2.1 Aquifer Modeling

In the 1930`s it has been identified that in the subsurface a hydrodynamic system consisting of reservoir and aquifer is formed. This knowledge made it indispensable to treat these two parts of the system together and model the water influx into the reservoir. Material balance formulations for the aquifer behavior have been developed and continued to be prevalent until numerical simulation became more practical during the 1960`s. The development of practical numerical simulators enabled the incorporation of water influx calculations to this area, where novel approaches have been developed.

In the realm of analytical water influx calculations different models for aquifers can be used. What these models have in common is that they describe aquifer behavior in terms of water influx rate as a function of the reservoir conditions. Customarily aquifer models with known analytical solutions are assumed.

There are two distinct ways to establish such an aquifer behavior model. The first approach starts with an idealized mathematical reservoir model. In this mathematical model simplifying assumptions regarding the petrophysical properties like porosity or permeability and the geometry of both the reservoir and the aquifer are made. This means that for example the porosity is assumed to be uniform and the geometry is represented by radial or linear aquifer models.

The second approach does not make use of simplifying assumptions regarding the petrophysical properties or the flow geometry. The aquifer behavior model is directly derived from measured field data.

Schilthuis (1936) published a steady-state aquifer model by assuming an idealized reservoir. Therefore the development of this model corresponds to the first approach described. The steady-state assumption means that this water influx model can only be used when the aquifer pressure can be considered to be constant even though water influx into the reservoir happens. Because this is only true for an infinitely large aquifer, this approach is not suitable for all cases.

A more detailed description of the Schilthuis model can be found in Section 3.4.1.

When the aquifer dimension is limited and the pressure of the aquifer changes as a function of time, a different approach has to be chosen. Through the solution of the differential diffusivity equation two models have been developed. Van Everdingen and Hurst (1941) solved the equation for radial symmetrical aquifers and Carslaw and Jaeger (1959) for linear aquifers. The Van Everdingen and Hurst model is described in Section 3.4.3.

The shortcomings of both models is that the solutions are only valid for a certain aquifer shape and solutions for arbitrary shapes are not offered. Furthermore the principle of superposition is applied for the calculation of the time dependent aquifer pressure, which causes the calculation to become effortful and time-consuming.

Carter and Tracy (1960) proposed a model based on the Van Everdingen and Hurst water influx model. The aim of this modification was to reduce the calculation effort originating from the principle of superposition. Therefore the assumption of a constant water influx rate for any given time step was made, which presents an inaccuracy compared to the Van Everdingen and Hurst model. A description of this model can be found in Section 3.4.3.1.

Vogt and Wang (1987) published another and enhanced model based on the Van Everdingen and Hurst model. Instead of using piecewise constant boundary pressure approximations they introduced piecewise linear approximations. Particularly at early times, where the gradient of the pressure change over time is high, this presents a more accurate solution. Another advantage of the Vogt and Wang solution is the improved integrability in numerical simulators. In Section 3.4.3.2 a more detailed description of the Vogt and Wang solution can be found.

Numbere (1989) developed a water influx calculation method for complex flow geometries. This was done to eliminate the restriction of the other methods, which are only applicable to simple reservoir-aquifer geometries. In his publication a generalized method for calculation the dimensionless water influx function is presented.

Fetkovich (1969) developed a method for calculating the water influx without prior knowledge of the reservoir-aquifer geometry. The Fetkovich aquifer model describes a pseudo steady-state flow behavior and can therefore be used when the transient flow period is negligible. No fixed set of rules of when this aquifer model is applicable is available because this model is largely of empirical nature. In Section 3.4.2 a description of the Fetkovich aquifer model is provided.

When the aquifer behavior model is developed according to the second approach, which means directly from field data, the hereby generated model is valid solely for one particular reservoir-aquifer geometry. This implies that the with this approach gained influence function F(t), which describes the water influx depending on pressure and time, is only applicable to one unique case. However, this influence function includes the heterogeneities and the complex geometry for the specific hydrodynamic system. Hutchinson and Sikora (1959) and Katz et al. (1962) developed methods to define aquifer influence functions. However, problems originating from inaccurate field data have been encountered and smoothness requirements for the field data are present.

Coats et al. (1964) published an aquifer modeling method based on a general aquifer. This

means that the aquifer was considered to be heterogeneous and arbitrarily shaped. It was also assumed that permeability, porosity and total system compressibility are not a function of pressure. They made use of the linear programming technique and proved that the three basic flow behaviors of water influx models (transient, pseudo steady-state and steady state) are simply distinct cases of their general formulation. Ding (1990) presented an alternative to the linear programming technique to improve computer storage and calculation time as well as the robustness to inaccuracies of field data. Menissi et al. (1998) then published a method for assessing water influx using influence functions for undersaturated oil reservoirs using a semi-analytical approach. However, all of these models still have the shortcoming that an estimation of the water influx is necessary for matching the influence function.

2.2 Determination of Analytical Aquifer Model Parameters

The model parameters for the analytical aquifer models can be determined with analytical, numerical and experimental methods. Analytical determination of aquifer model parameters can be done with the use of material balance calculations. Numerical methods are dealing with reservoir simulation and the history matching of the pressure in the reservoir. Experimental methods aim to a direct measurement of properties defining the model parameters.

2.2.1 Analytical Determination of Aquifer Parameters

Van Everdingen et al. (1953) published a statistical method for deriving aquifer parameters for the Van Everdingen and Hurst aquifer model based on a material balance approach. The cumulative water influx is represented as an proportionality factor times the water pressure drop per period and the dimensionless inflow function. For each available data point the proportionality factor can be calculated. When the correct aquifer parameters have been chosen the proportionality factor should remain constant for each material balance calculation step. An improvement for this method was published by Mueller (1962), who expanded the applicability of the method to aquifers with linearly varying aquifer properties.

McEwen (1962) developed a technique for assessing water influx parameters where initially only the oil in place is calculated and the water influx constant is taken as proportional to the oil in place. This leads to better results than the method by Van Everdingen et al. when the reservoir pressure data is erratic. The ratio between the proportionality factor and the oil in place is calculated as a function of initial formation volume factor, effective aquifer fluid compressibility and the water saturation of the reservoir before water influx.

Havlena and Odeh (1963) proposed straight-line material balance relationships. By plotting the ratio of net production in reservoir barrels, F, and the expansion of oil, E_O, against the ratio of aquifer influx function, S, and expansion of oil (i.e. F/E_O vs. S/E_O) the correctness of the

assumed aquifer parameters can be tested. In case of a correct water influx this plot shows a straight line. The intercept of the straight line with the ordinate gives a value for the original oil in place and the slope of the line gives the aquifer influx constant. Tehrani (1985) published an improved method for calculating the water influx constant from a different but algebraically equivalent form to the one proposed by Havlena and Odeh.

Sills (1996) then combined the Havlena Odeh straight line approach with the Tehrani approach. Also this method was developed for the Van Everdingen and Hurst unsteady-state radial aquifer model. A combined aquifer/reservoir expansion term is introduced. When the water influx parameters in the aquifer model are correct, a plot of the net production in reservoir barrels against this combined aquifer/reservoir expansion term should give a straight line. The best fit values for the original oil in place are determined with the technique developed by Tehrani.

2.2.2 Numerical Determination of Aquifer Parameters

Numerical determination of analytical aquifer properties can be done via the history matching procedure. History matching is a process where reservoir model properties are varied until measured field data reasonably matches the output of the dynamic reservoir model calculated with a reservoir simulator. Adjustable parameters include permeabilities, porosities, fault transmissibilities and throws, compressibilities, initial fluid contact depths and also aquifer properties. History matching mainly deals with aquifer properties, since this part of the hydrodynamic system is of great importance for the pressure match and typically only sparse information about this domain is available.

Generally two approaches can be taken. One method is to manually adjust the reservoir model parameters and the second one is to automatically determine the parameters within a given range.

Williams et al. (1998) described a manual, traditional history matching approach, where the aquifer model parameters are one of the first adjusted parameters within the process of the pressure matching. It should be noted that this history matching approach is not specifically designed for the determination of parameters for analytical aquifer models, but a general approach that can be applied also for gridded or other aquifer models.

Anterion et al. (1989) developed a method that assists history matching, which can be viewed as a first step towards automated history matching, but this method itself cannot be understood as an automated history matching technique. In this approach gradients of the components of the objective function as a function of the history matching parameters are calculated. However, it is still the decision of the reservoir engineer which parameters have to be changed and by what amount.

In recent years many different approaches to automated history matching have been developed. Gradient methods, based on the approach presented by Anterion et al. (1989), are one of the main methods. Bissel et al. (1994) applied this approach for automated history matching on a full field case, by finding a local minimum of the objective function using non-linear regression

algorithms.

Another type of automated history matching is the use of stochastic samplers or optimizers. Within this category fall ant colony optimization (e.g. Hajizadeh et al. 2009), genetic algorithms (e.g. Castellini et al. 2005), evolutionary algorithms (e.g. Schulze-Riegert et al. 2002) and other similar strategies. The advantage of these approaches is that they are more able to find a global minimum, but difficulties with the quantification of uncertainties are a shortcoming of this method (Christie et al. 2013).

The third category of automated history matching methods is the use of filtering techniques. An example is the Ensemble Kalman Filter. A comprehensive literature review on this filter can be found in Aanonsen et al. (2009). When faced with realistic field cases, problems originating from ensemble collapse have been observed (Myrseth and Omre 2010). Also no specific case of aquifer parameter determination using this technique could be found in the literature.

Another approach specifically designed for the determination of aquifer parameters has been presented by Mittermeir et al. (2004) and Pichelbauer (2003). They published the Target Pressure Method (TPM), which is a numerical method for the determination of aquifer parameters, well suited for reservoir simulation and can be easily introduced in any simulation package. This method presents a tool for the automated matching of the pressure history. It is an explicit method that determines the required water influx at every step of the history run to match measured pressure data. At the end of the history simulation the best fitting aquifer parameters for the Fetkovich, Carter-Tracy and Vogt-Wang aquifer models are calculated, which can be viewed as the minimization of an objective function.

2.2.3 Experimental Determination of Aquifer Parameters

Experimental methods for determining aquifer parameters are very uncommon in the oil industry. Direct measurement of the model parameters for a Van Everdingen and Hurst radial aquifer would require the determination of the following aquifer properties: reservoir drainage radius, effective reservoir radius, aquifer permeability, reservoir thickness, aquifer porosity, total aquifer compressibility and the aquifer water viscosity.

Because of the this approach presents an unusual way of defining aquifer properties in the context of reservoir engineering, no detailed description of the measurement techniques will be presented in this thesis.

Chapter 3

Definitions

3.1 Initial Reservoir Pressure

The initial reservoir pressure is the average pressure of the reservoir before production starts. It is possible to determine the initial reservoir pressure at different steps of the life cycle of the reservoir. The following methods can be used to determine the initial reservoir pressure:

1. Performing tests on an appraisal well in the very early stages before production of the reservoir starts.
2. Calculation of the initial pressure by evaluation of pressure buildup test data at a later point, after some production from the reservoir occurred.

3.1.1 Initial Pressure from Appraisal Wells

Before any production, when a reservoir is discovered the initial pressure equals the static reservoir pressure. Determining the initial reservoir pressure in an appraisal well is possible with a so-called RFT (repeat formation tester) tool, which not only gives an initial reservoir pressure for a specific depth, but is able to provide pressure gradient data across the reservoir section (Dake 2001). However, the so-called effect of supercharging, an effect that can be caused by mud filtrate invasion. This effect has been discussed already by Pelissier-Combescure et al. (1979), when they analyzed this phenomenon using a field example from the Middle East. Low permeability section of the reservoir are more prone to be supercharged, because the pressure perturbation caused by the drilling mud takes longer to dissipate than in high permeability regions. Methods to deal with this effect of supercharging have been proposed by different authors. For example Stewart and Wittmann (1979) proposed the superposition of a point sink, representing the RFT, and a point source, representing the filtrate influx, assuming that the pressure buildup due to the spurt loss has already dissipated. Also other authors dealt with this problem of supercharging, e.g. Phelps et al. (1984), who expanded the problem to a two-phase problem.

3.1.2 Initial Pressure Calculated from Transient Well Testing

In the case of transient well testing it is necessary to distinguish two different drainage area types. In the beginning, during the time of transient flow, the drainage area is expanding, thus the drainage area is called infinite. During this period the pressure perturbation does not reach a boundary. Once a boundary is reached the drainage area gets limited and is called finite drainage area (Smith et al. 1992).

In the period of infinite drainage area it is possible to use a so-called Horner plot. This widely used method, proposed by Horner (1951), consists of plotting the bottom hole pressure vs. the logarithm of the Horner-time. Horner's (1951) solution for an infinite acting, homogeneous reservoir containing a single well and a low compressibility fluid can be seen in Equation 3.1.

$$p_{ws} = p_i - \frac{q\mu}{4\pi kh} \ln \frac{t_0 + \vartheta}{\vartheta} \tag{3.1}$$

In Equation 3.1 p_{ws} [atm] is the well pressure after shut-in, p_i [atm] is the initial pressure of the reservoir. Horner-time is defined as follows: $(t_0 + \vartheta)/\vartheta$, where ϑ [s] is the shut-in time and t_0 [s] is the time of constant production before the well is shut-in. The slope of the buildup curve, $m = \frac{q\mu}{4\pi kh}$, allows to estimate permeability, k, and skin factor, s. In the case of an infinite acting reservoir it is also possible to determine the initial reservoir pressure, p_i, by extrapolating the slope to $\log\left(\frac{t_0 + \vartheta}{\vartheta}\right) = 0$, which means that the shut-in time, ϑ, is infinite. Figure 3.1 shows a pressure buildup curve. At the beginning skin and wellbore storage effects can be seen. Following the these effects the points can be expected to follow a straight line in the plot (Horner 1951). The line is then extrapolated to 1, which is equivalent to $\log\left(\frac{t_0 + \vartheta}{\vartheta}\right) = 0$. At this point p* can be read, which is equivalent to the initial pressure, as long as the reservoir can still be considered to be an infinite reservoir (Horner 1951). As mentioned before this means that no boundary effects have been experienced. The extrapolation of the pressure points for real field data, however, can be very subjective, as mentioned also by Dake (2001). Sometimes it is not completely clear when the straight line starts and the early time effects have vanished.

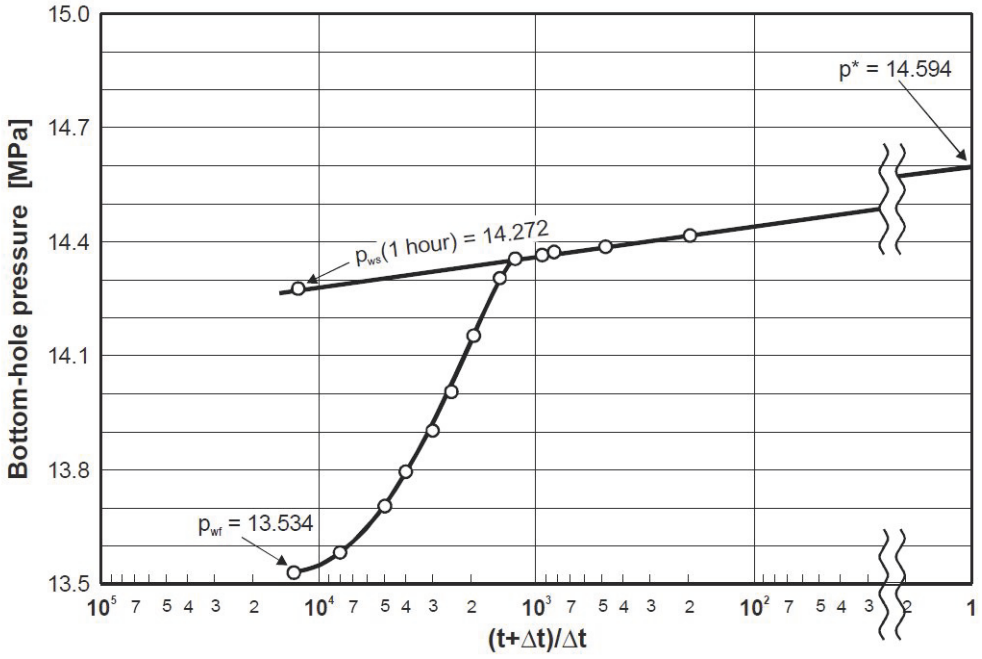

Figure 3.1: Pressure buildup curve with skin effect and wellbore storage (Heinemann and Mittermeir 2013)

3.2 Static Reservoir Pressure

The static reservoir pressure is a pressure that is present in the reservoir when all fluid motion stopped, therefore the name "static". Depending on the time when this pressure is measured or calculated, it can either be called the initial reservoir pressure, p_i (Horner 1951), or the average reservoir pressure, $\bar{p}$ (Satter et al. 2008). After production started, because of the depletion of the reservoir, the initial reservoir pressure will no longer be the same as the average reservoir pressure.

3.3 Average Pressures

The average pressure is the pressure that would be obtained after an infinite long shut in time. It can be seen in Figure 3.2 that the extrapolated pressure from the slope gives a higher value than the average reservoir pressure, which could be found at the end of the pressure buildup curve. This is because the well is no longer producing from an infinite acting drainage area, but from a finite drainage area. This means that boundary effects are already experienced. As a side note, the here found value p* is also no longer the same as the initial reservoir pressure, but will be lower. This difference between initial pressure and p* is a reflection of some depletion that

already happened in the reservoir (Matthews and Russel 1967).

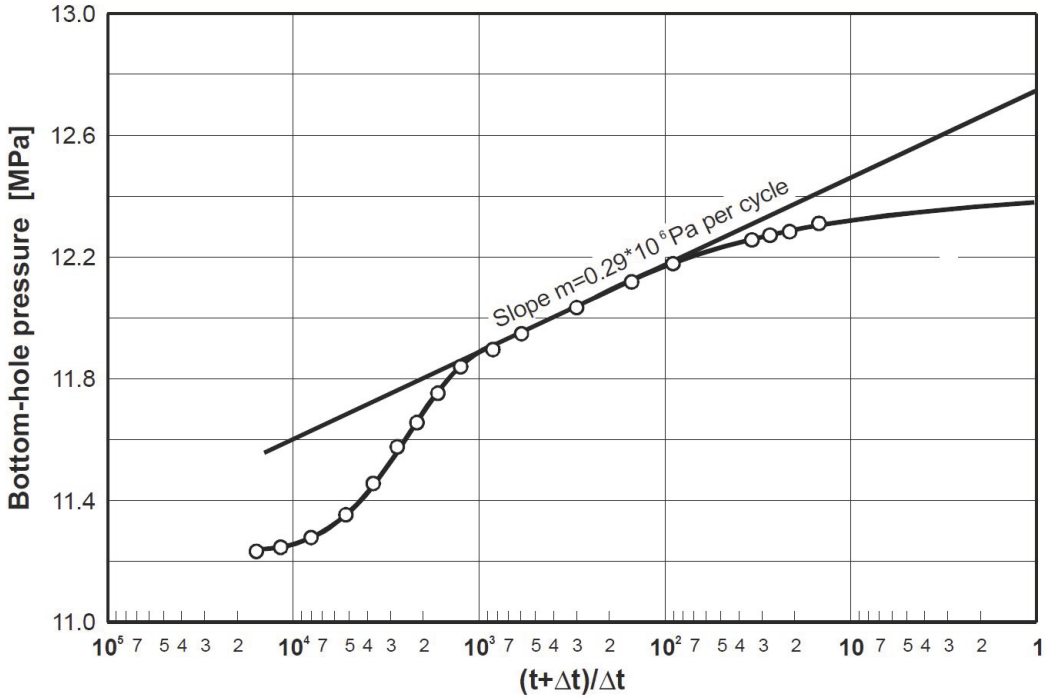

Figure 3.2: Pressure buildup curve with a limited drainage area (Heinemann and Mittermeir 2013)

Different methods for the determination of the static reservoir pressure in a finite drainage area are known. Traditional methods for determining the average reservoir pressure are:

- Matthews, Brons and Hazebroek (MBH) method (Matthews, Brons and Hazebroeck 1954)
- Dietz (Dietz 1965)
- Miller, Dyes and Hutchinson (MDH) method (Miller, Dyes and Hutchinson 1950)
- Muskat (Muskat 1937)

3.3.1 Average Reservoir Pressure

The average reservoir pressure is a single value of pressure for a certain time that is defined for the entire reservoir. It is the pressure that would be present in the reservoir when all fluid motions stops (Satter et al. 2008), which is equivalent to the static pressure.

3.3.2 Average Region Pressure

Because it is often not possible to find a single value of pressure that is valid for the entire reservoir, regions of different pressures can be defined. It can be defined as the pore-volume weighted average pressure, that is valid for a certain part of the reservoir, called a region (Shiralkar and Stephenson 1994). Korteland et al. (2010) stated that the majority of the available literature on fluid flow in porous media defines the average macroscale pressure as the phase-volume average pressure, as can be seen in Equation 3.2.

$$\overline{p_\alpha} = \frac{1}{V_\alpha} \int_{V_\alpha} p_\alpha dV \tag{3.2}$$

Where $\bar{p}_\alpha$ [Pa] is the phase-volume average pressure of phase α, V_α [m^3] is the volume of integration of phase α and p_α [Pa] is the pressure in phase α.

3.3.3 Drainage Area

When a well is producing it tends to produce from a certain area, which is called drainage area (Dake 2001). This area is significant in the estimation of the average reservoir pressure in methods like the MBH method. It is, however, very difficult to exactly define drainage areas for all wells in a complex reservoir.

3.3.4 Productive Area

Mittermeir, Pichelbauer and Heinemann (2004) defined the productive area, as this is an expression used in the context of reservoir simulation with H5/PRS. The entire grid model can be split in aquifer grid and productive area grid. It is important that the productive area not only covers the hydrocarbon part but also parts that are saturated with water. The definition of the productive area is important, because at the boundaries of the productive area analytical aquifers can then be linked in the later used Target Pressure Method.

3.4 Aquifer

Aquifers are water saturated permeable rocks surrounding a hydrocarbon reservoir, often of much greater volume than the hydrocarbon part of the reservoir (Ahmed 2006). For a significant amount of hydrocarbon reservoirs this aquifer provides a drive mechanism. Smith et al. (1992) list different mechanism, which result in the driving force:

- Water expansion
- Contraction of the pore volume due to the pressure decline from production and the compressible nature of the rock
- Expansion of another hydrocarbon accumulation that shares the same aquifer with the reservoir in production
- Artesian flow, where surface water recharges the aquifer

Although early on it is difficult to determine if a natural water influx is taking place into the reservoir, there can be some hints. A low and decreasing reservoir pressure decline rate during increasing cumulative withdrawal of the reservoir can be a hint to an aquifer, although the reason for this phenomenon could also be influx of another fluid from a yet undeveloped region of the reservoir (Ahmed and McKinney 2005). Ahmed and McKinney (2005) warned that early water production, although a possible hint towards an active aquifer, can be easily misinterpreted. This is especially true in the case of a fractured reservoir or a reservoir with high-permeability streaks.

If enough dynamic data is available material balance can be used to detect an aquifer. Already Havlena and Odeh (1963) presented a method on how to fit to dynamic data. Campbell and Campbell (1978) also presented a plot based on material balance that can be used to identify natural water influx into the reservoir. In Figure 3.3 the so-called Campbell plot can be seen, which makes it possible to identify the presence of an aquifer and its relative strength.

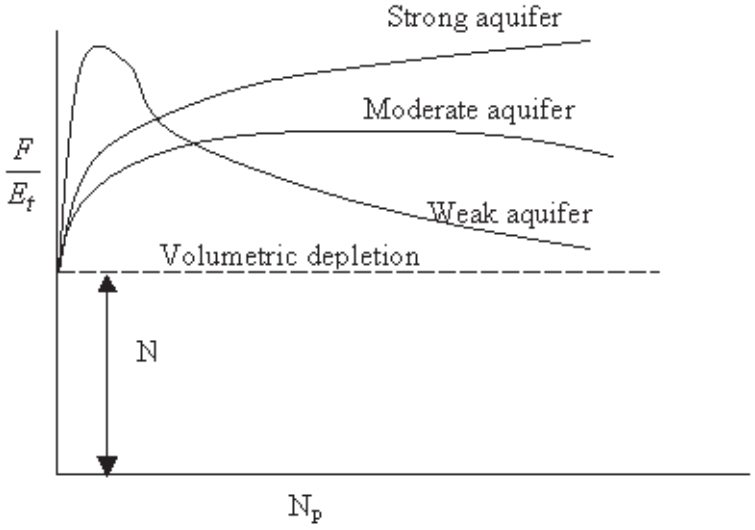

Figure 3.3: Campbell plot for the identification of an aquifer.

Different analytical aquifer models are available to model the natural water influx into the reservoir. Because there is usually little data known about the aquifer parameters, models have to be calibrated based on the production history of the reservoir (Smith et al. 1992). The following analytical aquifer models exist:

- Schilthuis (Schilthuis 1936)
- van Everdingen and Hurst (van Everdingen and Hurst 1949)
- Fetkovich (Fetkovich 1971)
- Carter-Tracy (Carter and Tracy 1960)

- Vogt-Wang (Vogt and Wang 1987)
- Pot aquifer (Coats 1970)

3.4.1 Schilthuis Model

This aquifer model, presented by Schilthuis (1936), can be used to describe a steady-state aquifer. The water influx rate, $q_w(t)$ [m³/day], can be calculated as follows:

$$q_w(t) = C[p_{\mathrm{Aq}} - p(t)] \tag{3.3}$$

where C [m³/bar.day], is the constant of proportionality, p_{Aq} [bar] is the constant aquifer pressure and $p(t)$ [bar] is the reservoir boundary pressure as a function of time. Equation 3.3 shows that the water influx rate is a linear function of the reservoir boundary pressure. The cumulative water influx, $W_e(t)$ [m³], can then simply be calculated by integrating the water influx rate over the time interval [0,t]:

$$W_e(t) = C\int_0^t [p_{\mathrm{Aq}} - p(t)]dt \tag{3.4}$$

The value for the constant, C, can be calculated as follows for a radial symmetric aquifer:

$$C = \frac{2\pi hk}{\mu \ln \frac{r_e}{r_w}} \tag{3.5}$$

where h is the thickness of aquifer [m], k is the permeability of aquifer [m²], μ is the water viscosity of the aquifer [Pa.s], r_e is the outer aquifer radius [m] and r_w is the inner radius of aquifer [m]

3.4.2 Fetkovich Model

The Fetkovich model (Fetkovich 1971) can be used to describe pseudo steady-state aquifers. This means this model can be used when the transient period is negligible. This model requires two input parameters, J_w [m³/bar.day], the productivity index of the aquifer, and W_{ei} [m³], the maximum encroachable water. The water influx rate, $q_w(t)$ [m³/day], can be calculated as follows:

$$q_w = J_w(\bar{p} - p_w) \tag{3.6}$$

where $\bar{p}$ is the average aquifer pressure [bar] and p_w is the boundary pressure of the reservoir

[bar]. Using the from material balance derived value for W_{ei}:

$$W_{ei} = c_t \cdot W \cdot p_i \tag{3.7}$$

where c_t is the total compressibility [1/bar], W is the water volume of the aquifer [m³] and p_i is the initial aquifer pressure [bar], the average aquifer pressure can be calculated as follows:

$$\bar{p} = -\frac{p_i}{W_{ei}} W_e + p_i \tag{3.8}$$

where W_e is the cumulative outflow of the aquifer [m³].

3.4.3 Van Everdingen-Hurst Model

The van Everdingen-Hurst model (van Everdingen and Hurst 1949) also is an unsteady state model. Van-Everdingen and Hurst presented an solution foe the diffusivity equation which can be used for edge-water drive systems, bottom-water drive systems and linear-water drive systems (Ahmed and McKinney 2008). The dimensionless influx function, $Q_D(t_D)$, can be calculated as follows:

$$Q_D(t_D) = \int_0^{t_D} \left(\frac{\partial P_D}{\partial r_D} \right)_{r_D = 1} dt_D \tag{3.9}$$

where t_D is the dimensionless time (Equation 3.10), P_D is the dimensionless pressure (Equation 3.11) and r_D is the dimensionless radius (Equation 3.12).

$$t_D = \frac{k}{\phi \mu c_t r_w^2} t = At \tag{3.10}$$

$$P_D = \frac{p_i - p}{p_i - p_w} = \frac{p_i - p}{\Delta p_w} \tag{3.11}$$

$$r_D = r / r_w \tag{3.12}$$

where ϕ is the porosity of the aquifer [-], r_w is the inner radius [m], k is the permeability [m²], μ is the viscosity of the water [Pa.s], c_t is the total compressibility of the aquifer [1/Pa], A is the real time multiplier and p_i is the aquifer boundary pressure of calculation interval i [bar]

With the assumptions of a radial aquifer, constant pressure drop across the aquifer and uniform aquifer properties the cumulative water influx, $Q(t)$ [m³], can be determined as:

$$Q(t) = 2\pi h \phi r_w^2 c_t \Delta p_w Q_D(t_D) \tag{3.13}$$

where h is the thickness of the aquifer [m], ϕ is the porosity of the aquifer [-], r_w is the inner radius [m], c_t is the total compressibility of the aquifer [1/Pa] and Δp_w is the constant pressure drop at the reservoir boundary.

By using a stepwise calculation with different pressure differences, as illustrated in Figure 3.4 the cumulative water influx, W_e [m³], can be calculated as can be seen in Equation 3.14. This basically is applying the principle of superposition, by adding solutions of different pressure differences.

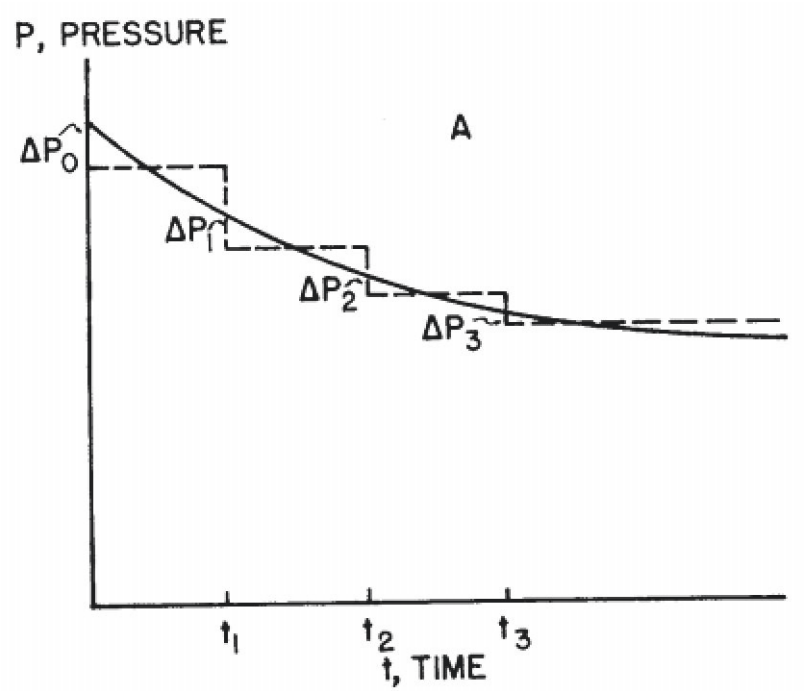

Figure 3.4: Stepwise calculation procedure for the cumulative water influx (van Everdingen and Hurst 1949)

$$W_e(t_{D_n}) = -C\left[\frac{p_1 - p_0}{2} \cdot Q_D(t_{D_n}) + \frac{p_2 - p_0}{2} \cdot Q_D(t_{D_n} - t_{D_1}) + \ldots + \frac{p_n - p_{n-2}}{2} \cdot Q_D(t_{D_n} - t_{D_{n-1}})\right] \tag{3.14}$$

where C is an aquifer related constant [m^3/bar] and n is the number of calculation intervals. The aquifer related constant is defined as:

$$C = \alpha \phi h c_t r_w^2 \tag{3.15}$$

where α is the angle subtended by the boundary between the reservoir and the aquifer.

Tables for values of the water influx are available as a function of dimensionless time and dimensionless radius for both infinite and limited aquifers. To fully define a van Everdingen-Hurst aquifer the following as to be defined:

- A, the constant real time multiplier
- C, the aquifer related constant
- Q_D, the dimensionless inflow function

3.4.3.1 Carter-Tracy Solution

This method, published by Carter and Tracy (1960) is based on the van-Everdingen and Hurst model, as described above. In uses the constant terminal rate solution of the diffusivity equation. This solutions aims to eliminate the superposition calculations by combining it with the material balance equation of the Schilthuis method. Ahmed and McKinney (2008) described that the main difference between the Carter-Tracy solution and the original van Everdingen and Hurst methodology is that Carter-Tracy assume a constant water influx rate for a certain time interval. The water influx rate for the *i*th time interval, q_{wi} [m³/day], is determined as follows:

$$q_{w_{i-1}} = \frac{C \cdot \Delta p(t_{D_i}) - W_e(t_{D_{i-1}})P'(t_{D_i})}{P(t_{D_i}) - t_{D_{i-1}}P'(t_{D_i})} \tag{3.16}$$

where C again is the constant of proportionality, P' is the derivative of P with respect to dimensionless time [-] and P is the van Everdingen-Hurst dimensionless function [-].

The cumulative water influx can be calculated with:

$$W_e(t_{D_i}) = W_e(t_{D_{i-1}}) + q_{w_{i-1}} \cdot (t_{D_i} - t_{D_{i-1}}) \tag{3.17}$$

Because of the availability of computational power this simplification of the van-Everdingen and Hurst model is no longer of use.

3.4.3.2 Vogt-Wang Solution

Vogt and Wang (1987) presented an improved method for evaluating the water influx integral. Instead of a stepwise pressure function a piecewise linear pressure function is used. This improves the accuracy especially at early times, which makes it possible to compute aquifer parameters early in the reservoir's life.

The cumulative water influx can then be calculated as follows:

$$W_e(t_{D_n}) = -C\left[\frac{p_1 - p_0}{t_{D_1}} \cdot \tilde{Q}_D(t_{D_n}) + \left(\frac{p_2 - p_1}{t_{D_2} - t_{D_1}} - \frac{p_1 - p_0}{t_{D_1}}\right) \cdot \tilde{Q}_D(t_{D_n} - t_{D_1}) \right. \tag{3.18}$$
$$\left. + \ldots + \left(\frac{p_n - p_{n-1}}{t_{D_n} - t_{D_{n-1}}} - \frac{p_{n-1} - p_{n-2}}{t_{D_{n-1}} - t_{D_{n-2}}}\right) \cdot \tilde{Q}_D(t_{D_1} - t_{D_{n-1}}) \right]$$

where

$$\tilde{Q}_D(t_D) = \int_0^{t_D} Q(u)du \tag{3.19}$$

is the dimensionless inflow.

To define a Vogt-Wang aquifer the following as to be defined:

- A, the constant real time multiplier
- C, the aquifer related constant
- Q_D, the dimensionless inflow function

3.4.4 Aquifers in Numerical Simulation

For reservoir simulation there is the option to model the aquifer with a gridded aquifer model or with an analytical aquifer model.

Figure 3.5 shows a simulation grid with a blue boundary, that represents the where the analytical aquifer can be attached to the simulation grid. The parameters for the analytical aquifer model can be calculated with e.g. the Target Pressure Method.

Figure 3.6 shows a grid model with a gridded aquifer. The reservoir, or area of interest, is in the center of the grid. The principle is to extend the finite difference grid that it covers both the reservoir and the aquifer and it is therefore necessary to assign rock and fluid properties also for the aquifer regions, which results in higher computer storage requirements (Fanchi 2005).

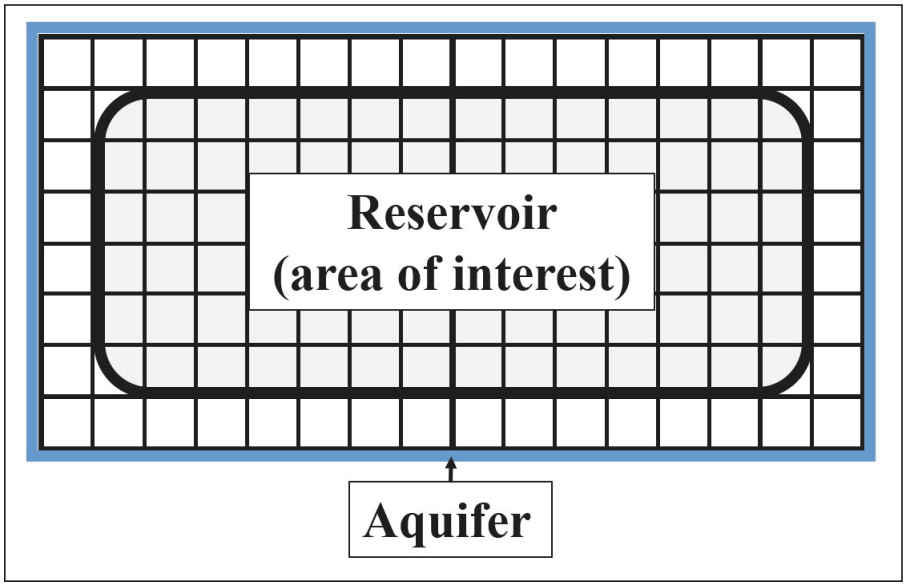

Figure 3.5: Simulation grid with an analytical aquifer

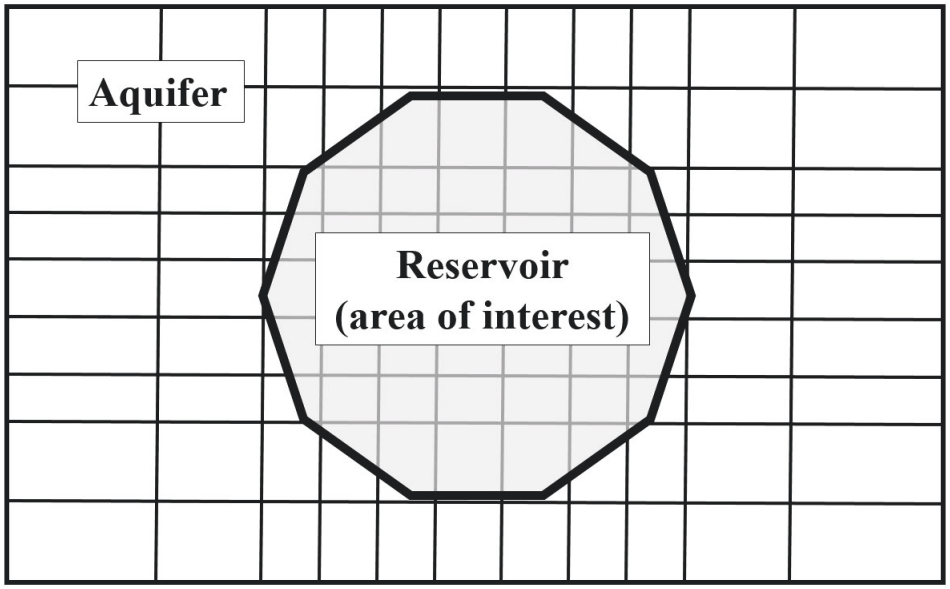

Figure 3.6: Simulation grid with a gridded aquifer

Chapter 4

Introduction to the Sabah Field

4.1 Geology of the Sabah Field

The geology of the Sabah field was already described in detail by Gharsalla (2015) and HOT Engineering GmbH (2004). Therefore the sections geology of the Sabah field, the geology of Sirte Basin, the stratigraphy of the Sabah field and the structural model of the Sabah field are based on these works.

The Sabah field, located in the south-western part of the Sirte Basin in Libya, extends in the two concession regions NC74F and NC131. The reservoir is situated on a local high within the Zella graben (Figure 4.1). With the well G01 the field has been discovered in 1964 by the Alwerath Oil Company. Since then seventy wells have been drilled into this naturally fractured carbonate reservoir.

4.1.1 Regional Geology of Sirte Basin

In the Early Cretaceous rifting in the basement complex of North Africa occurred. The main direction of the generated rifts is in the NNW (Van der Meer and Cloething 1993). After the tectonic activity of the Early Cretaceous a tectonically quiet time period followed in the Mid Cretaceous. In the Late Cretaceous the collision of two continental plates, the African-Arabian and the Eurasian plate, ensued. This resulted in folding and even inversion of basins along the African-Arabian Tethyan margin. Recommencement of rifting transpired when the compressional forces relaxed and a tensional stress regime was formed. This rifting period lasted until the end of the Cretaceous and created multiple troughs in NW-SE orientation in Northern Libya, including the Sirt-Kalash trough. The boundary between the Cretaceous and Cenozoic shows unconformities induced by tectonic events.

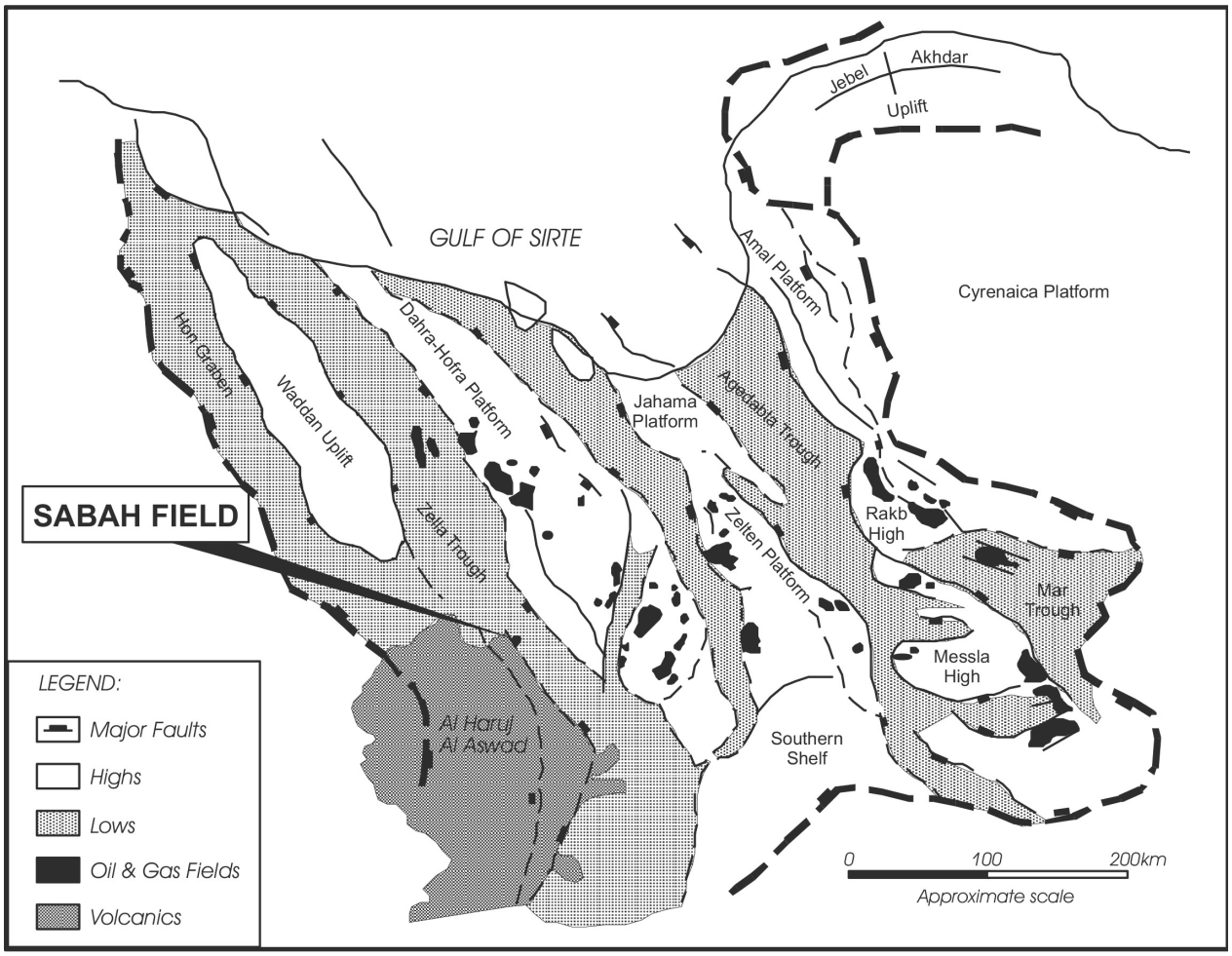

Figure 4.1: Schematic structural map of the Sirte Basin with Location of Sabah Field (with courtesy of Mansur (1987))

4.1.2 Sabah Field Stratigraphy

The stratigraphic sequence in the western Sirte Basin (Figure 4.2) can be grouped into five stratigraphic intervals:

- Pre-Cretaceous (I): This interval consists of a metamorphic and igneous basement, poorly sorted clastics and orhthoquarzite clastics.
- Lowermost Upper Cretaceous to the top of the Upper Cretaceous (II): In this part the evolution from a pure intracratonic basin to continental margin type failed-rift basin can be observed.
- Uppermost Upper Cretaceous to the middle of the Lower Eocene (III): The deposition of carbonate and shale during a time of regionally and accelerating subsidence can be observed. The deposition of the marine carbonates and shales was interrupted twice by emergence or near-emergence. During the time of emergence evaporites were

deposited in a Sabkha environment.
- Mid-Lower Eocene to the upper Middle Eocene (IV) : This stratigraphic group consists of interbeds of evaporites, carbonates, limestone, shales, silts and sandstones.
- Upper Middle Eocene to the Present (V): Rocks of these stratigraphic group have been eroded in the NC74F area or have not been deposited.

The Bahi sandstones, sandstones of unknown thickness and structure, overlie the basement in the Sabah field. The Bahi sandstones are then followed by the Lindam formation, which consists of fine-grained limestones and calcarenite. The rest of the Upper Cretaceous sediments consist of roughly 2000 [ft] marine shale and minor carbonates of the Rakb Groud and Kalash Formation. The Hagfa shales, deposited in the Paleocene, succeeds the Kalash formation and build the base of the Beda formation. This Beda C reservoir is contained in this formation and is overlaid by anhydrites forming the seal for the reservoir. On top of the Beda formation follows the Dahra formation. The uppermost 200 [ft] of Dahra are limestone with good porosity. With increasing depth the Dahra formation becomes shalier. The top of the Paleocene is formed by the Zelten (fine-grained limestone) and Kheir (shaly carbonate) formations, which overlay the Dahra. The base of the Eocene is formed by dolomites and limestones of the Facha Member, which is the base of the Gir formation. The Hon Member of the Gir formation then consists of anhydrites with interbedded dolomite and limestone. The Gattar formation, consisting of carbonates, the Bu'Mras formation, comprised of sandstones and carbonates, and overlying basalt are the final formation of the mid-lower Eocene to upper middle Eocene (IV).

The main reservoir of the Sabah field is located in the Beda C interval. The Beda C was formed in the early Paleocene during a third order regressional cycle. Depositional patterns and the resulting selective changes to the rock by dolomitization significantly influenced the reservoir rock properties. The reservoir itself can be divided into three main zones:

- Zone 1: This dolomite zone has porosities of up to 35% and high permeability values. The reason for these properties are the significant diagenetic alterations, most importantly dolomitization.
- Zone 2: This zone consists of limestone and shows dolomitization only in a few spots. A downward deterioration of porosity and permeability can be observed.
- TIGHT Zone: This is a porosity layer separating Zone 1 and Zone 2 with porosities between zero and 8%.

Zones 1 and 2 can be further subdivided based on geological features and reservoir quality observed from logs. The subdivision can be seen in Figure 4.3, where Zone 1 is split into 4 subzones and Zone 2 is split into 5 subzones.

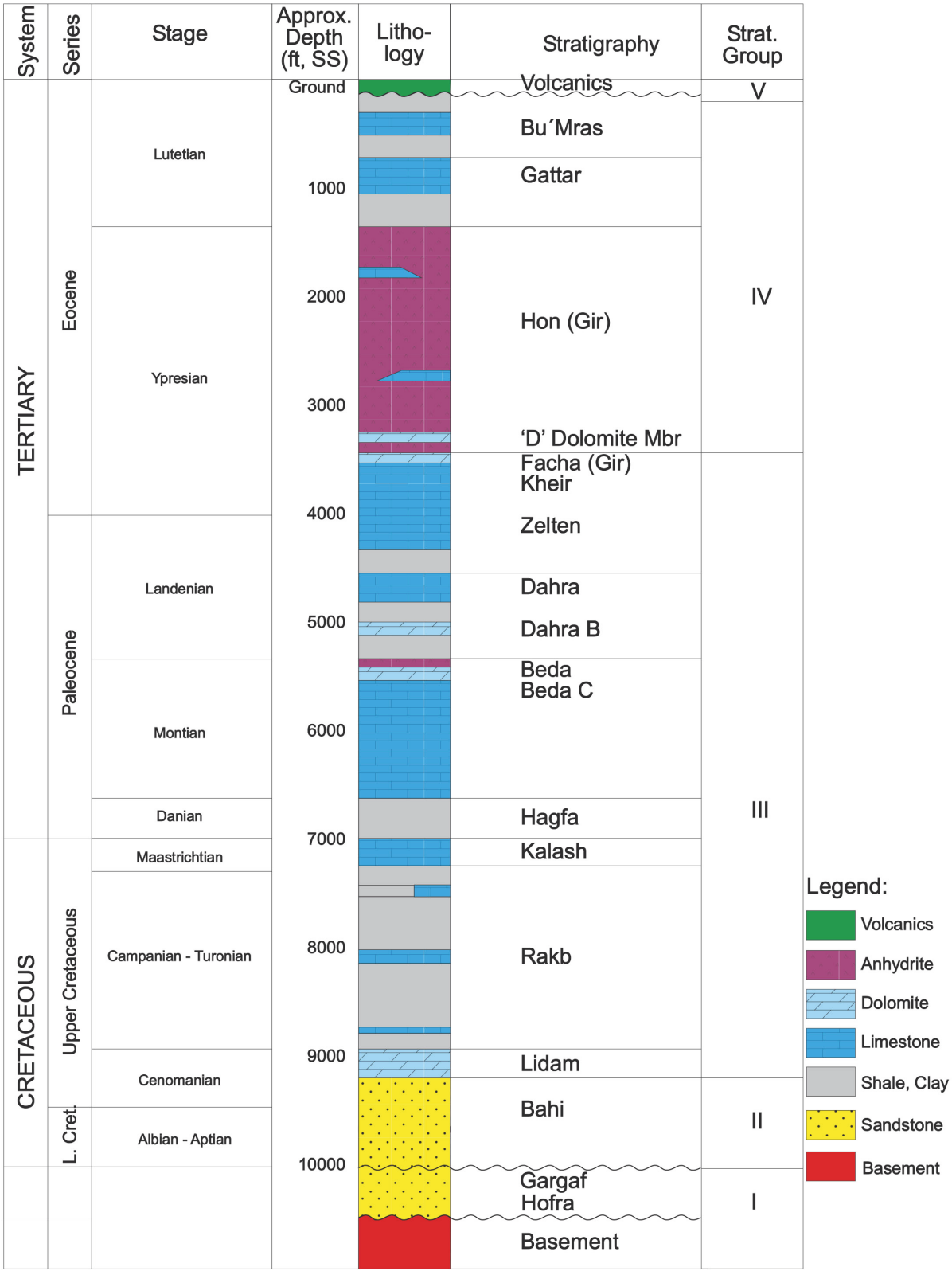

Figure 4.2: Stratigraphic type column of western Sirte Basin (modified after Gokturk and Tarhouni (1999) and Knytl et al. (1996).)

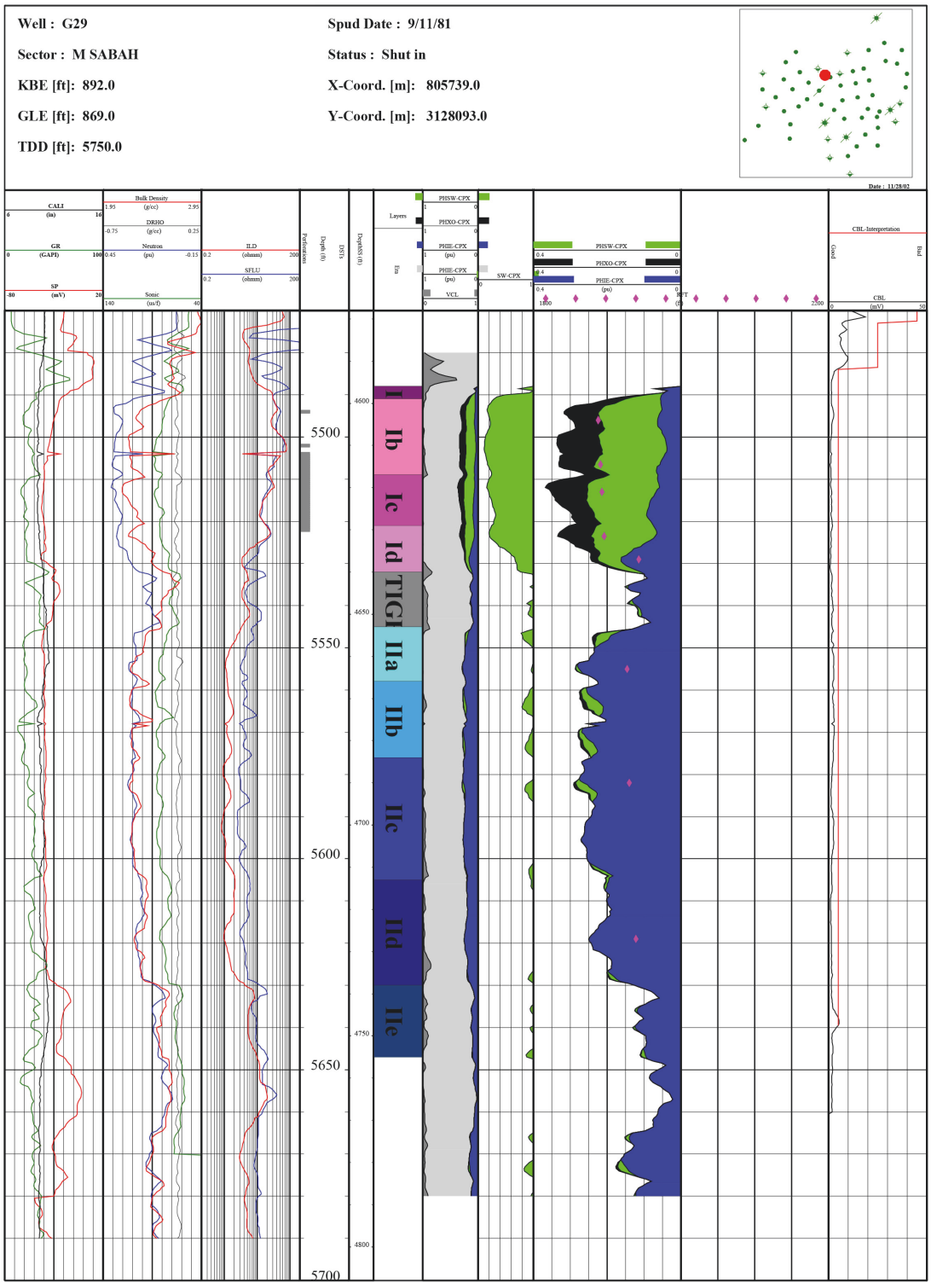

Figure 4.3: Stratigraphic positions of Sabah reservoir sub-zones based on reservoir quality (Gharsalla 2015).

4.1.3 Sabah Field Structural Model

The structure of the Sabah field is divided by NW-SE oriented normal faults. The anticline containing the reservoir is roughly 8000 [m] long in East-West direction and extends 5000 [m] in North-South direction. Between the Lower Cretaceous and into the Oligocene indications of seven periods of tectonic activity have been observed in well logs. Knytl et al. (1996) stated that the Sabah field is part of a sequence of right-lateral strike-slip anticlinal structures that have been formed in a post-Oligocene compressional regime. Faulting happened in a compressional and wrench-dominated environment.

The faults are not sealing, as indicated by the non-observable compartmentalization of the reservoir. Many indications of natural fractures have been observed, including the loss of drilling mud, patterns on dipmeter logs, indications on Formation MicroImager logs, permeability tests and the production performance as well as direct visibility of fractures in analyzed cores. Figure 4.4 shows the structural map for the top of the Beda C reservoir, including wells and faults.

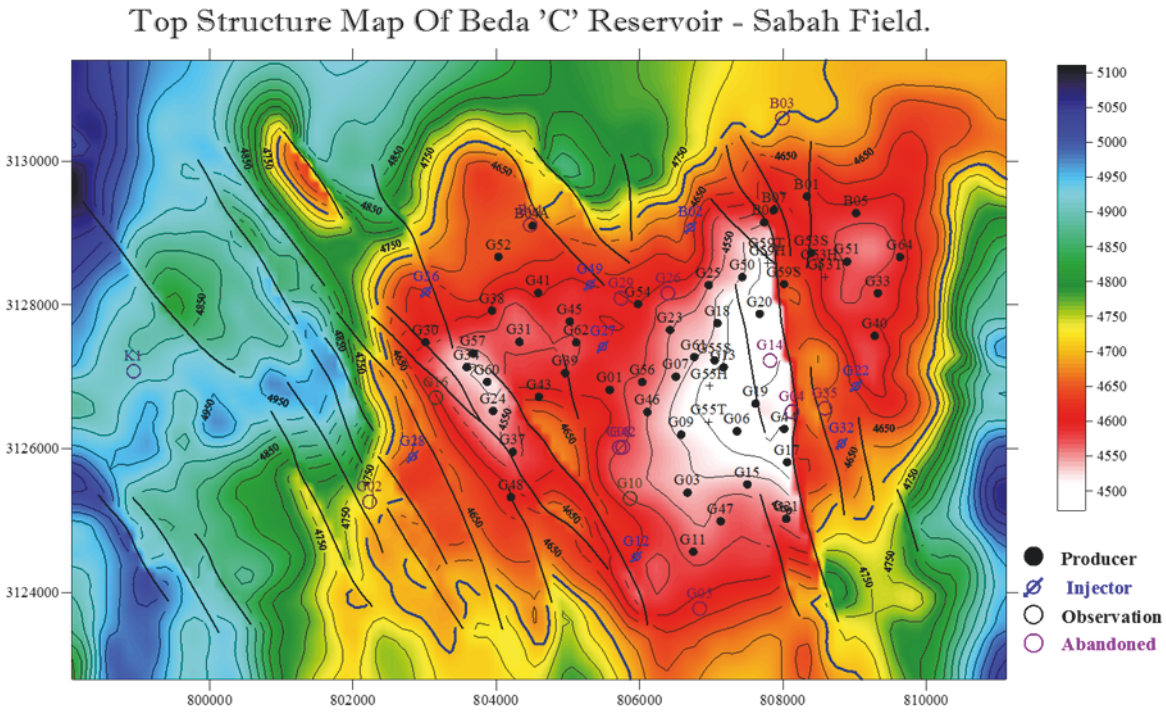

Figure 4.4: Top Structure Map of Beda C Reservoir –Sabah Field (Gharsalla 2015)

4.2 Routine Core Analysis (RCAL)

RCAL data is available for the wells B01, B03, B04, G01, G04, G06, G41, G42, G43, G48, G50 and G53. RCAL data consists of porosity, permeability and grain density measurements. Permeabilities from transient pressure tests are much higher than the measured permeabilities by the RCAL, which indicates the presence of natural fractures in the reservoir. Another indication for natural fractures is the measured vertical to horizontal permeability ratio of greater than one. Grain density measurements showed the presence of limestone in Zone II and of dolomite in Zone 1. Also anyhdrite and celestite grain densities have been observed in many plugs.

4.3 Special Core Analysis (SCAL)

SCAL measurements focus on the rock/fluid interactions. The goal is to get information about the multi-phase-flow behavior. SCAL data is available for the wells G06, G43, G48, G50 and G53. For these wells samples have been analyzed in terms of cementation and saturation exponents, water oil relative permeabilities and capillary pressure. However, for samples of G53 no capillary pressure measurements exist.

The Sabah reservoir is considered to be mixed wet, which means that parts of the rock are water wet and other parts of the rock are oil wet.

Hot Engineering GmbH (2004) used the available SCAL data for the creation of the 11 rock regions and the assignment of capillary pressure curves and relative permeability curves to each region. For the fracture rock region no capillary pressure measurement is possible, thus it is assumed to be zero. The relative permeability curve for the fracture region is therefore linear.

4.4 Fluid properties

PVT measurements are available for two measurements from the wells G03 and G18 (CORE LABORATIES 1977 and 1991). The sample from G03 was a subsurface sample and the sample from G18 was a separator oil sample with a synthetically prepared gas. HOT Engineering GmbH listed the most important data from the PVT analysis, which can be seen in Table 4.1. The water properties, which are also taken from the HOT Engineering GmbH report (2004) can be seen in Table 4.2.

Table 4.1: Oil properties

		G03	G18
Pb	[psia]	438	445
Rs	[ft^3/stb]	211	199
FVF at Pb	[bbl/stb]	1.204	1.18
Density at Pb	[g/cm^3]	0.731	0.743
Viscosity at Pb	[cp]	0.706	0.529
Stock tank density	[API]	42.6	40
Compressibility	[1/psi]	1.04E-05	9.95E-06
Viscosibility	[1/psi]	7.50E-05	1.13E-04

Table 4.2: Water properties

Salinity	[ppm]	45000
Viscosity	[cP]	0.4
Compressibility	[1/psi]	2.87E-06
Formation volume factor	[-]	1.028
Density	[g/cm3]	1.003
Density (@14.7 psia, 60°F)	[g/cm3]	1.031

4.5 Pressure and well test data

All the available static pressure data, a total of 561 values, can be seen in Figure 4.5. It can be seen that the pressure varies in a range of roughly 500 [psi] during the depletion of the reservoir. The measured data originates from static pressure measurements that have been conducted when a workover of the well has been necessary. The procedure was to pull the artificial lift system, ESP pumps, out of the wellbore and then the pressure gauge was run. Due to this process it is not guaranteed that for all available pressure points the static pressure has been reached, because a too short shut-in time is possible.

Regarding well test data a total of 27 pressure build up tests are available. Most of these tests have been performed in the very early times of the reservoir life between the years 1978 and

1983. No recent pressure build up test has been performed. The last recorded test was conducted in 1996, which is the only build up test conducted after 1983. Changing reservoir conditions, (i.e. differences in phase, pressure and skin) drastically reduce the value of this information for the presence. It cannot be assumed that the measured well test data from the early times of the reservoir are still representative of the current state.

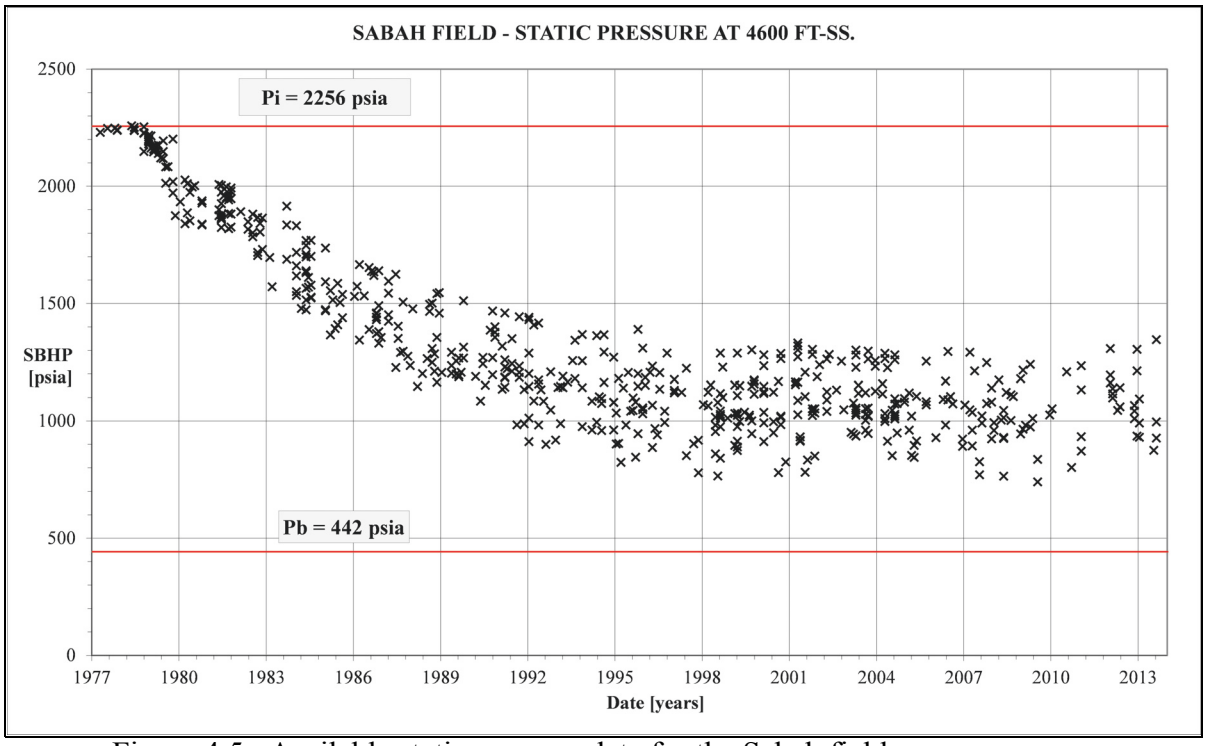

Figure 4.5: Available static pressure data for the Sabah field.

4.6 Pressure gradient data

Pressure gradient measurements have been performed and the thereby gained data is important to the interpretation of static pressure data. The reservoir stratigraphy, as described in Section 4.1.2, shows that two main parts of the reservoir, Zone I and Zone II, are divided by the TIGHT layer. In case vertical pressure communication through this layer can be proven, Zone 1 and Zone 2 can be expected to equilibrate. Because pressure gradient data is available, a look on the behavior of the gradient can show whether the two zones are in equilibrium or not. Formation tester pressures (RFT) are available for 16 wells. Because no unusual pressure differences can be observed across the TIGHT zone, this zone must be permeable. Otherwise the unequal production from the two surrounding zones would cause pressure differences.

As an example Figure 4.6 shows RFT measurement data for the well G43 from July 1989. It is obvious that no clear pressure discrepancy is present over the tight layer, which is located between Zone 1 and Zone 2. To illustrate this two linear trend lines are also displayed in this figure.

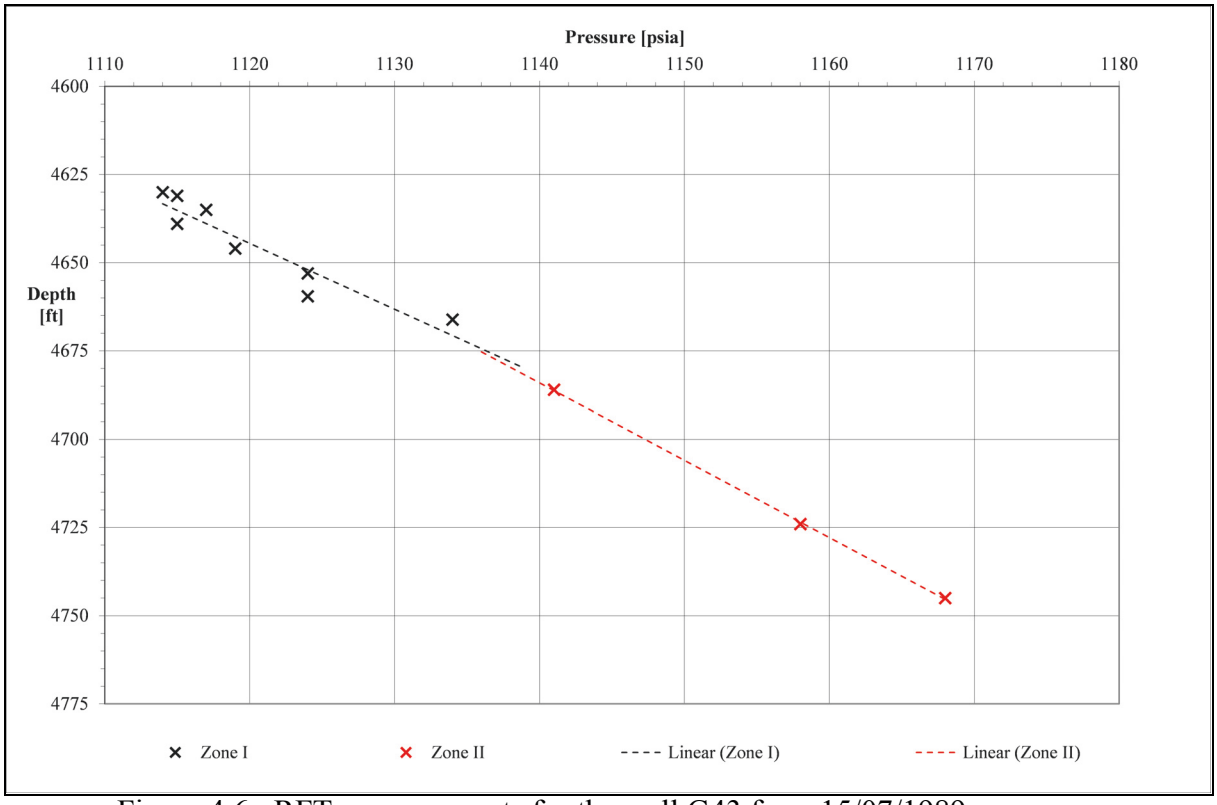

Figure 4.6: RFT measurements for the well G43 from 15/07/1989

The behavior of the measured pressure gradient in G43 can also be seen in other wells. HOT Engineering GmbH (2004) mentioned in their report the same finding and concluded that me most likely reason for this behavior is the presence of natural fractures. Because also the later shown production history indicates the presence of natural fractures, this explanation is considered to be true.

4.7 Production and injection data

Figure 4.7 shows the historical oil production, water injection and water cut for the Sabah field. Production from the Sabah field started in October 1978. Oil production peaked at roughly 41000 [bbl/d] in November 1982. In 1999 water injection into the reservoir started.

The water cut rises rapidly already at the beginning of the production period of the reservoir. This is an indicator that this reservoir is naturally fractured and therefore the water production starts very early. Birks (1963) described the effect of water coning in naturally fractured reservoirs and developed a method for calculating the critical production rate in order to avoid premature water production.

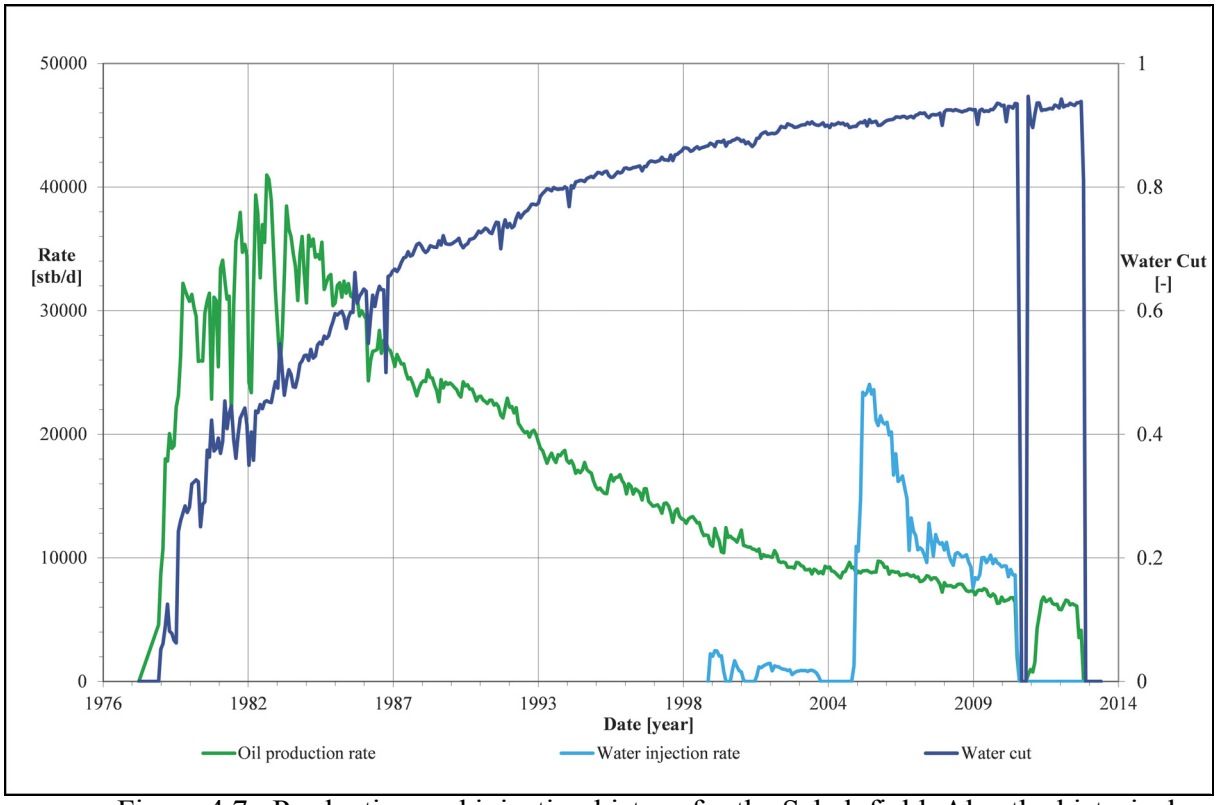

Figure 4.7: Production and injection history for the Sabah field. Also the historical water cut of the production can be seen.

Chapter 5

Pressure Region Definition, Evaluation of Static Pressures and Average Pressure Determination

Average reservoir and regional pressure data are necessary if material balance or numerical simulation tools are used to evaluate the production history and to predict reservoir performance. In some cases, as for high permeability gas reservoirs, the assessment of the historical pressure decline is straight forward, but in most cases it is a complex and time consuming task with sometimes uncertain results. The definitions and of the average reservoir and average region pressure are given in Chapter 3. Also the classical methods, with which the necessary pressure data can be determined are described in Chapter 3. The available input data can be found in Chapter 4.

5.1 Used Input Data

Static gradient survey data are available, from which shut-in bottom hole pressures have been extracted. Here it is important to consider, that the pressure measurements have taken place at different depths. To correct for this, all pressure points have been converted to pressure at the datum, which in this case is 4600 [ft] SS. 6819 pressure measurements for 62 well locations are available. In addition, pressure buildup tests for 27 wells are available. However, as mentioned earlier, the most recent buildup test data is from the year 1996 and all of the other buildup data was recorded in the years between 1978 and 1983. Because the reservoir conditions, including pressure and saturation, changed significantly since these measurements, it can not be assumed that this data is still representative. Also, from the records it was not possible to determine exact shut-in times for the measured static pressures, therefore it was not possible to apply a minimum shut-in time filtering for the available static pressure data.

5.2 Pressure Region Definition Procedure

It is difficult, if not impossible, to determine the drainage are of individual wells. On top of that, the extension of the drainage area changes over time. Instead, fixed pressure regions should be defined, by considering all relevant geological and engineering background information.

The fundamental workflow can be seen in Figure 5.1. Within this procedure it is necessary to consider all available data. This includes geological information, like the position of faults, as well as dynamic data, e.g. production data.

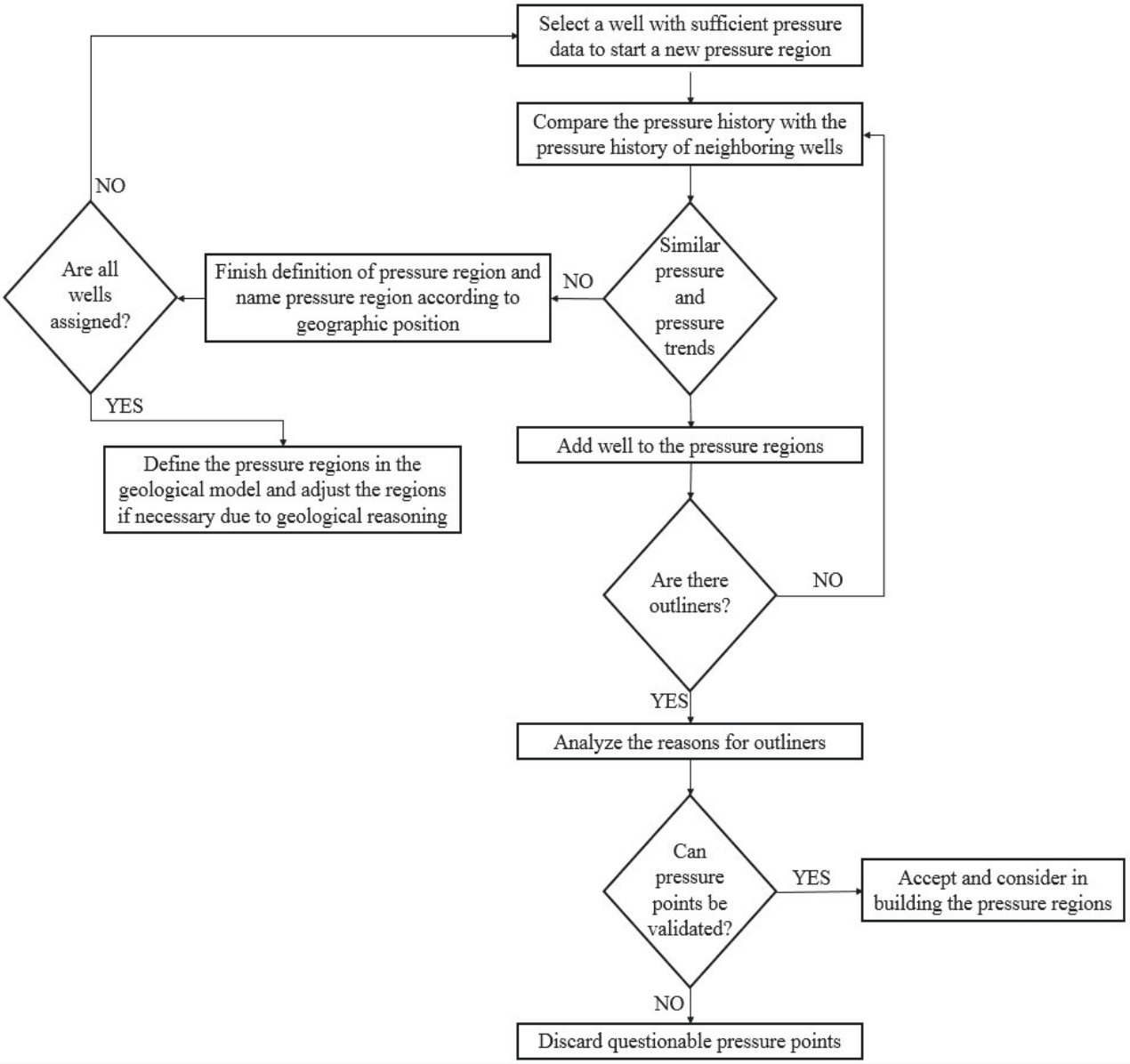

Figure 5.1: Fundamental workflow for the definition of pressure regions

The first step to start a pressure region is to find a suitable well. If only one ore few pressure

points are available, it is not possible to determine a trend. The next step is to compare the pressure history with the pressure history of neighboring wells. If both the absolute value of pressure and also the pressure trends are similar the wells can be added to the pressure region. If the neighboring wells no longer show similar trends or absolute pressure values, the pressure region cannot be expanded any further.

Often it is the case that outliners are present, although most of the static pressure measurement values fit the pressure region. Every outliner has to be analyzed. Explanations for outliners could be casing leaks, too short shut-in time or nearby injection wells. If a reasonable explanation for the out of line behavior of a measurement can be found and the measurement can be considered to be valid, the pressure point can be accepted and the pressure point must be considered when building the pressure regions. If no explanation for the out of line pressure measurement can be found, or if the pressure measurement is invalidated by e.g. a too-short shut-in time, the measurement should be discarded. This assures that no invalid pressure points are used when the average pressure of the region is determined and is a method to evaluate the quality of the static pressure data in absence of recent transient well tests. Also a plot of the regional average pressures and the reservoir production rate versus time can be created. The plots must follow opposite trends, i.e. when production rate increases, the pressure should drop. However, it must me considered that a certain lag time between the production and pressure behavior exists.

Once all pressure wells have been assigned based on the dynamic data, both pressure data and production data, also all available geological information should be included in the process of the definition of pressure regions. This can be accomplished by introducing the pressure regions into the geological model. By comparing the created boundaries of the pressure regions with natural boundaries like faults, an improvement of the exact region boundary definitions can be achieved. In the case when only one or few pressure measurements for a well are available, the geological reasoning for the assignment of wells to pressure regions gains importance compared to cases where abundant dynamic data is available.

5.3 Pressure Regions for the Sabah Field

By applying the procedure discussed in Section 5.2 the initial pressure regions have been created in the geological model using Schlumberger Petrel. The resulting 2D window view of the pressure regions can be seen in Figure 5.2. The text fields in the figure show the name of the regions. A total of 8 pressure regions are defined and the pressure regions NE and NW are split into Zueitina Oil Company (ZOC) and Arabian Gulf Oil Company (AGOCO) regions, because a license boundary exists. The names of the pressure regions give hints about the geographic position of the region based on a coarse division of the reservoir into 6 parts that has been conducted before any region has been assigned. The pressure regions are:

- SE_NE: South-East and North-East
- NE: North-East
- NW: North-West
- MN_MS: Main-North and Main-South
- MN_MS_NW: Main-North, Main-South and North-West
- SW: South-West
- MS: Main-South
- MSS: Main-South-South

Figure 5.2 shows the initial pressure regions after the dynamic data has been investigated according to the described procedure. To increase the quality of the pressure region definitions also geological information has to be taken into account. The position of major faults is of significance to pressure region definitions, because faults potentially present flow barriers.

In Figure 5.3 the improved version of the pressure regions can be seen. The differences to the non-corrected version is indicated with arrows and circles. After consideration of the fault position between the SE_NE and the MN_MS region the East side of the fault was considered to be improvable by assigning all blocks on this side to the SE_NE region. Careful investigation of the available dynamic data (static pressure measurements, production data) justified the reassignment of these blocks.

Also a reassignment of blocks between the two faults in the vicinity of the intersections of the regions NE, NW and MN_MS has been done. The in the two faults lying wells G69 and B06 only have a combined 4 data points, which initially led to the wrong assignment of these blocks.

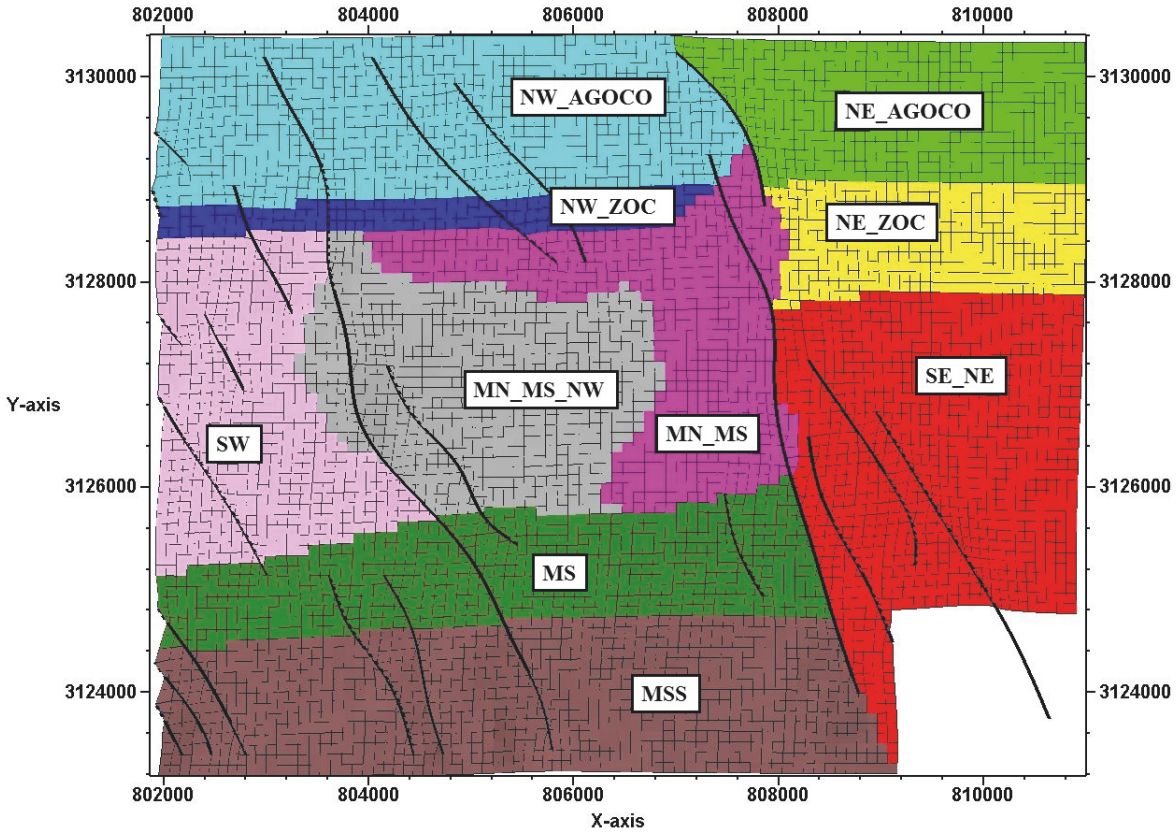

Figure 5.2: Initial pressure regions. X and Y axis are Easting and Northing (m)

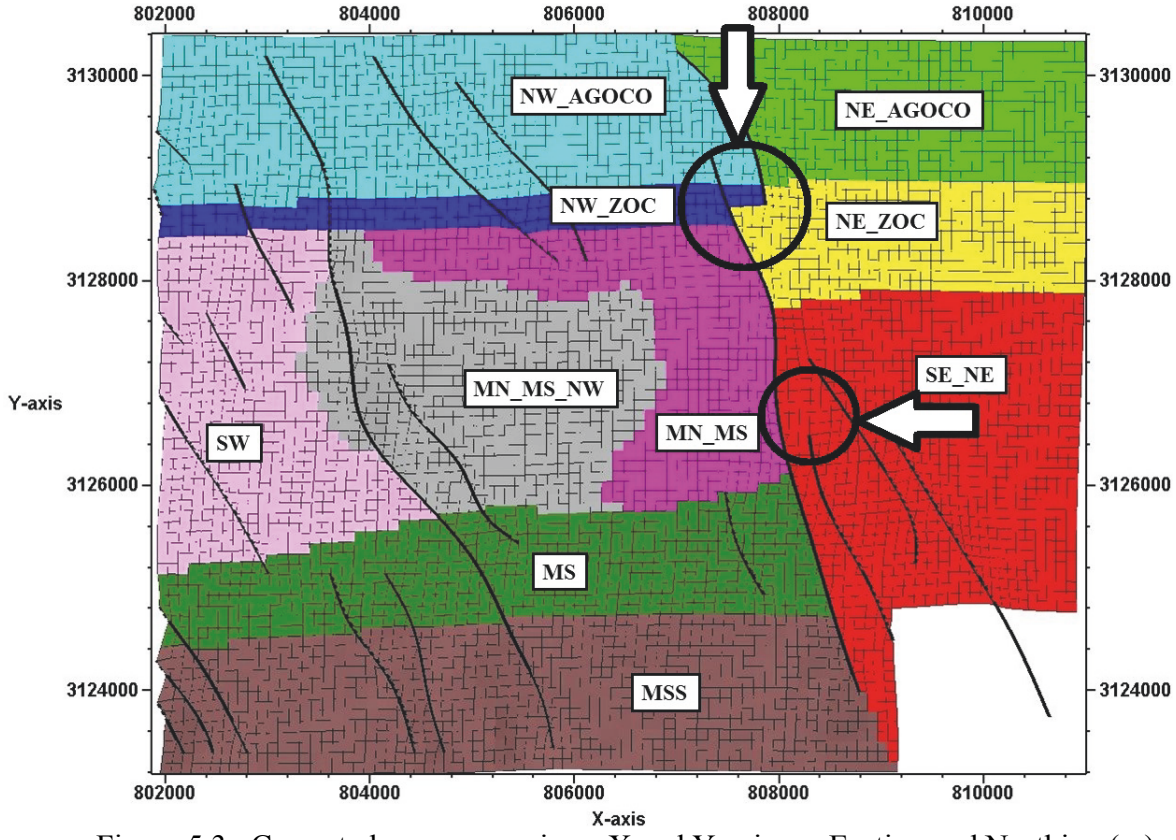

Figure 5.3: Corrected pressure regions. X and Y axis are Easting and Northing (m)

5.4 Average Pressures

It is necessary to find average regions pressures for all regions and also for the field level. The average region pressures are important for the TP M method and the field level average pressure is a needed parameter for a material balance calculation.

As a first step specific dates for which the average pressure should be estimated should be defined. Using all valid pressure measurements the pressure values for the specified dates can be estimated. After a successful pressure region definition and quality control of the pressure data, the static pressure values for a specific area should be very similar and with only marginal deviation from each other for a certain time period.

5.4.1 Average Pressures for the Pressure Regions

The resulting pressure regions for the Sabah field can be plotted in a static bottom hole pressure versus time diagram.

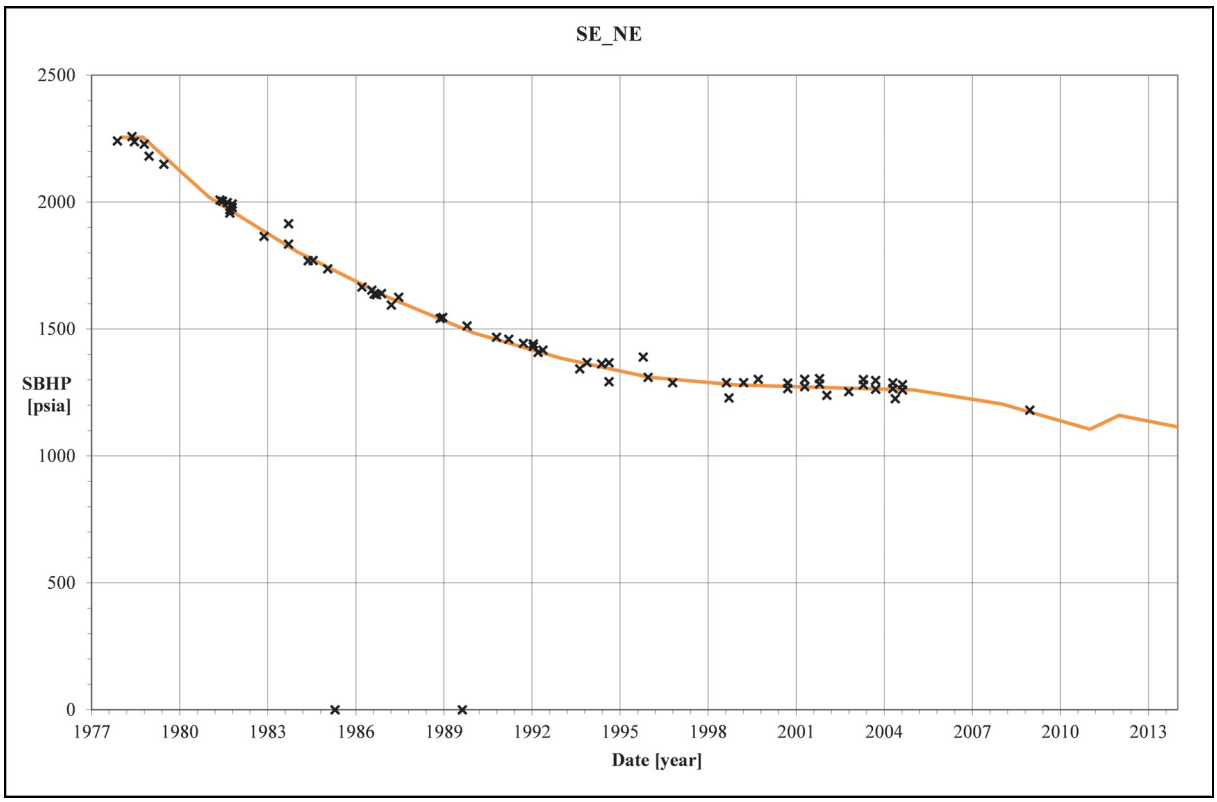

Figure 5.4: Pressure region SE_NE with all measured static pressures. The estimated average region pressure is the orange line.

Figure 5.4 shows the pressure data and the estimated average pressure for the SE_NE region, which is located in the south-east part of the Sabah field. South and east boundary of this region

represent also boundaries of the reservoir. In the north this region shares a boundary with the NE region. Towards the west the region is confined by a major fault. On the other side of the fault are the regions MN_MS, MS and MSS.

After August 2004 data is only sparse. One data point is available for the year 2008 and for the rest the average pressure had to be estimated based on the available data of the other regions, considering the interactions between the pressure regions. The slight increase in average region pressure in 2012 is in accordance to the regions MS and MN_MS. It is necessary to estimate the average region pressure also for this time, because it is a requirement for the simulation to have pressure data available until the end of the history matching period (January 2014) for all regions.

Overall sufficient static pressure data is available for this region and only 2 outliners, originating from the well G04, had to be eliminated. The measurements from April 1985 and August 1989 showed similar values as would have been expected in the MN_MS region, but after shut-in of the well in August 1989 the values fit perfectly to the SE_NE region. After shut-in the values are better representing the average values of the region. A probably too short shut-in time for the two pressure measurements before caused the too low pressure readings. Also the geologic location east of the main north-south fault hints towards the inclusion of the well to the SE_NE region.

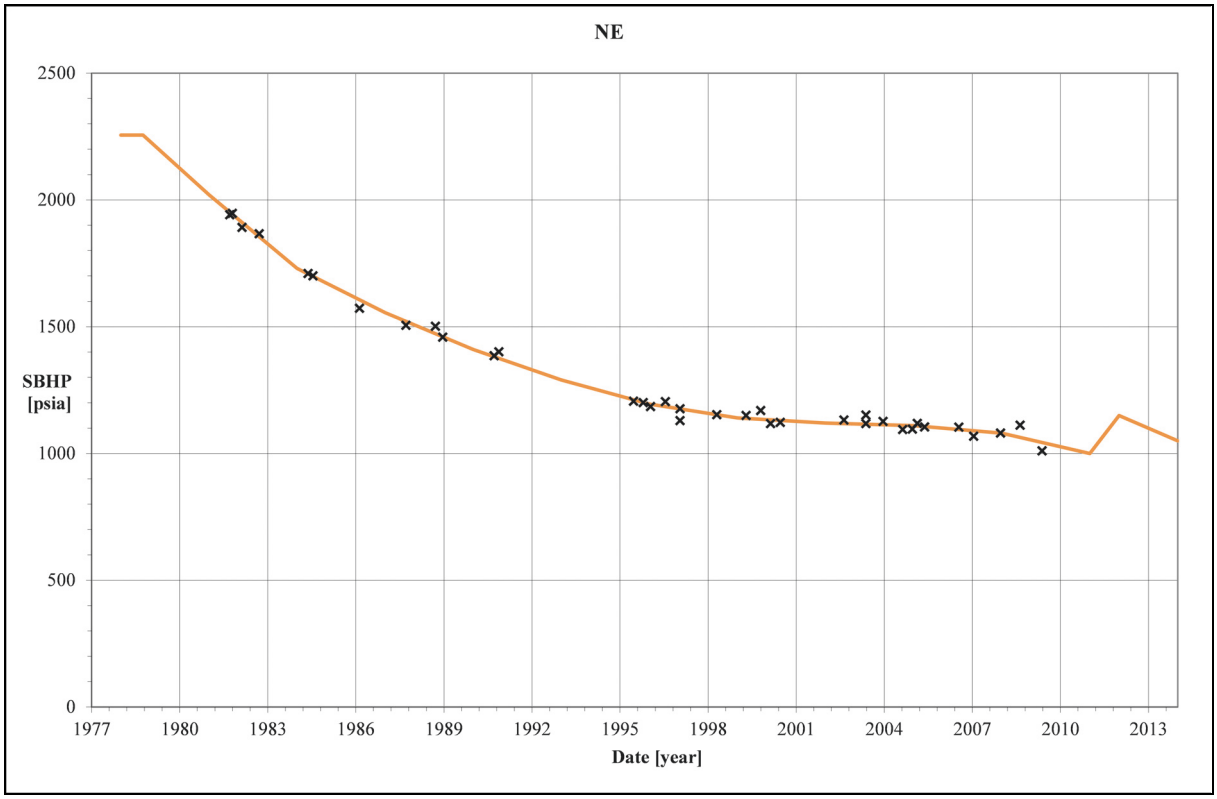

Figure 5.5: Pressure region NE with all measured static pressures. The estimated average region pressure is the orange line.

Figure 5.5 shows the pressure data and the estimated average pressure for the NE region, which

is located in the north-east part of the Sabah field. The NE region is subdivided into two regions, called NE_ZOC and NE_AGOCO, parts of the region that belong to the license of Zueitina Oil Company (ZOC) and Arabian Gulf Oil Company (AGOCO), respectively. To be able to later on estimate volume fluxes between the two regions the NE region had to be divided, but this had no influence on the definition of the pressure region. The north and east boundary of this region is also the boundary of the reservoir. In the south the NE region shares a boundary with the SE_NE region.On the west the region is confined by faults, where it has a common boundary with the NW region and the MN_MS region.

After May 2009 no newer pressure measurement data is available for any of the wells in the NE region. Similar to the SE_NE region, it was therefore necessary to estimate the behavior of the average pressure after this time until January 2014. In this case this has been performed by taking over the trends of the NW and MN_MS region. In this case also the initial pressure had to be estimated, but with the assumption that the initial reservoir pressure is nearly identical for all regions, this is less of an uncertainty than the extrapolation of the later data.

For the NE region also sufficient data is available. The pressure points line up very well in a reasonable way, which makes the determination of the average region pressure straight forward.

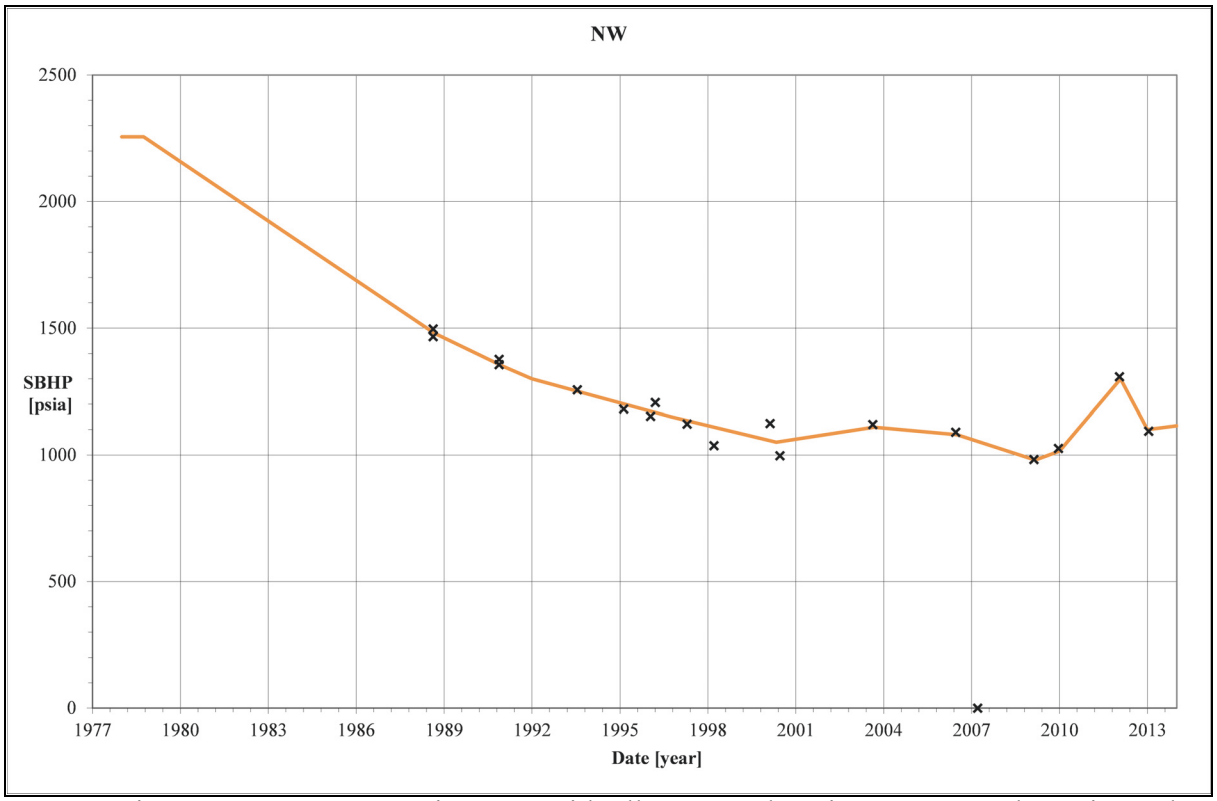

Figure 5.6: Pressure region NW with all measured static pressures. The estimated average region pressure is the orange line.

Figure 5.6 shows the pressure data and the estimated average pressure for the NW region, which is located in the north-west part of the Sabah field. Also the NW region is subdivided into two regions, called NW_ZOC and NW_AGOCO, parts of the region that belong to the license of

Zueitina Oil Company (ZOC) and Arabian Gulf Oil Company (AGOCO), respectively.

Towards the north and the west this region represents a boundary for the productive area. Towards the south it shares region boundaries with SW, MN_MS and MN_MS_NW. The west of the NW region is bounded by one of the main faults of the reservoir.

One measurement at well B06 in March 2007 showed an 200 [psi] higher pressure than other pressure measurements at this time. Also for this measurement not good explanation for the aberration could be identified and this resulted in the discarding of this measurement.

For this region only a small amount of data is available, but in this region data until 2013 is available. In this region the pressure measurements can be easily interpolated to form the average region pressure. In this case also the initial pressure had to be estimated, assuming that the initial reservoir pressure is identical in all pressure regions.

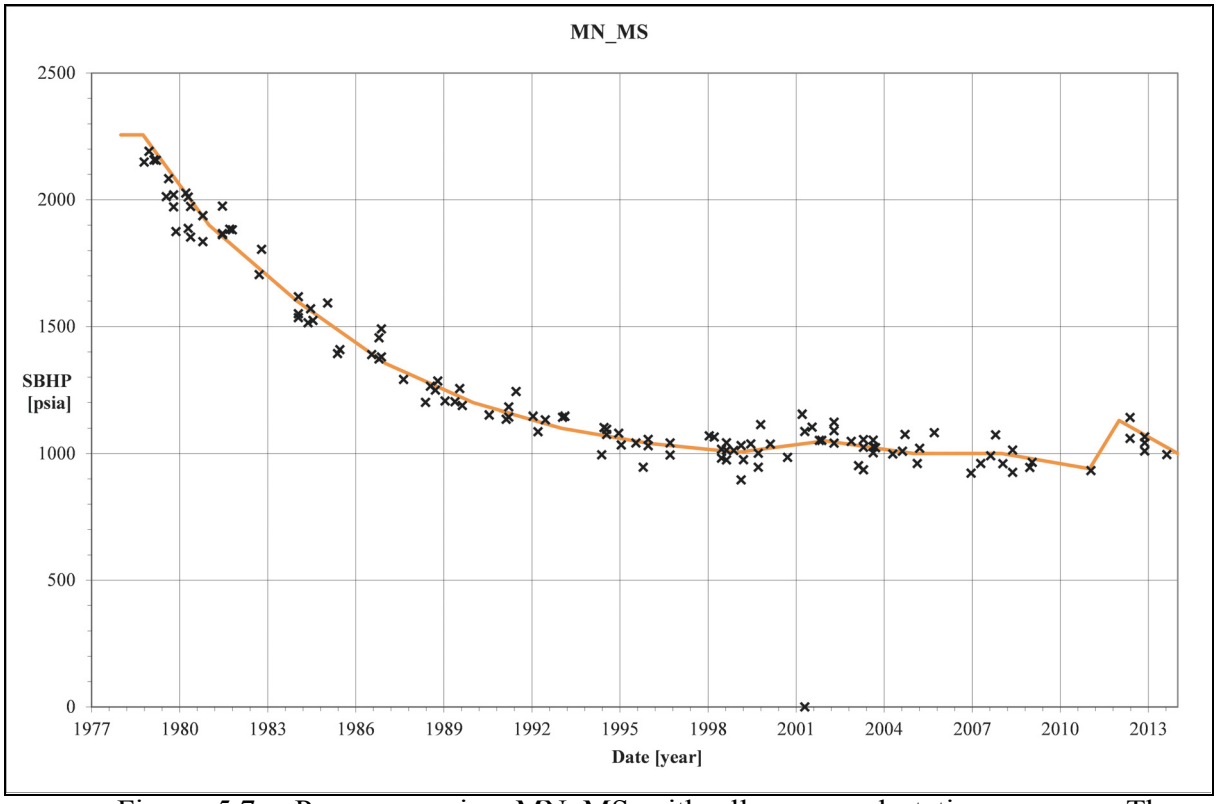

Figure 5.7: Pressure region MN_MS with all measured static pressures. The estimated average region pressure is the orange line.

Figure 5.7 shows the pressure data and the estimated average region pressure for the MN_MS region. This region is located in the center of the productive area and contains 15 wells. Towards the east it is bounded by one of the main faults of the reservoir. In the south and west it shares boundaries with MN_MS_NW and MS. In the west of the region is the region SW.

Because of the high amount of wells in this region, sufficient data is available throughout the productive time of the reservoir. Also here the determination of the average region pressure was

straight forward because of the reasonably good match of pressure measurements at similar times. In this case the initial pressure had to be estimated, assuming that the initial reservoir pressure is identical in all pressure regions.

One measurement at well G49 in April 2001 showed a 150 [psi] too high pressure compared to other measurements in the area. It is unclear why this pressure measurement does not fit the trend or the absolute values of the region or even the well G49 itself. Pressure measurements 6 months later at this well showed again accordance with the other region pressures and also the nearest pressure measurement before in September 1999 shows a good match with other pressure measurements of the region. Therefore the pressure measurement of April 2001 for G49 was discarded.

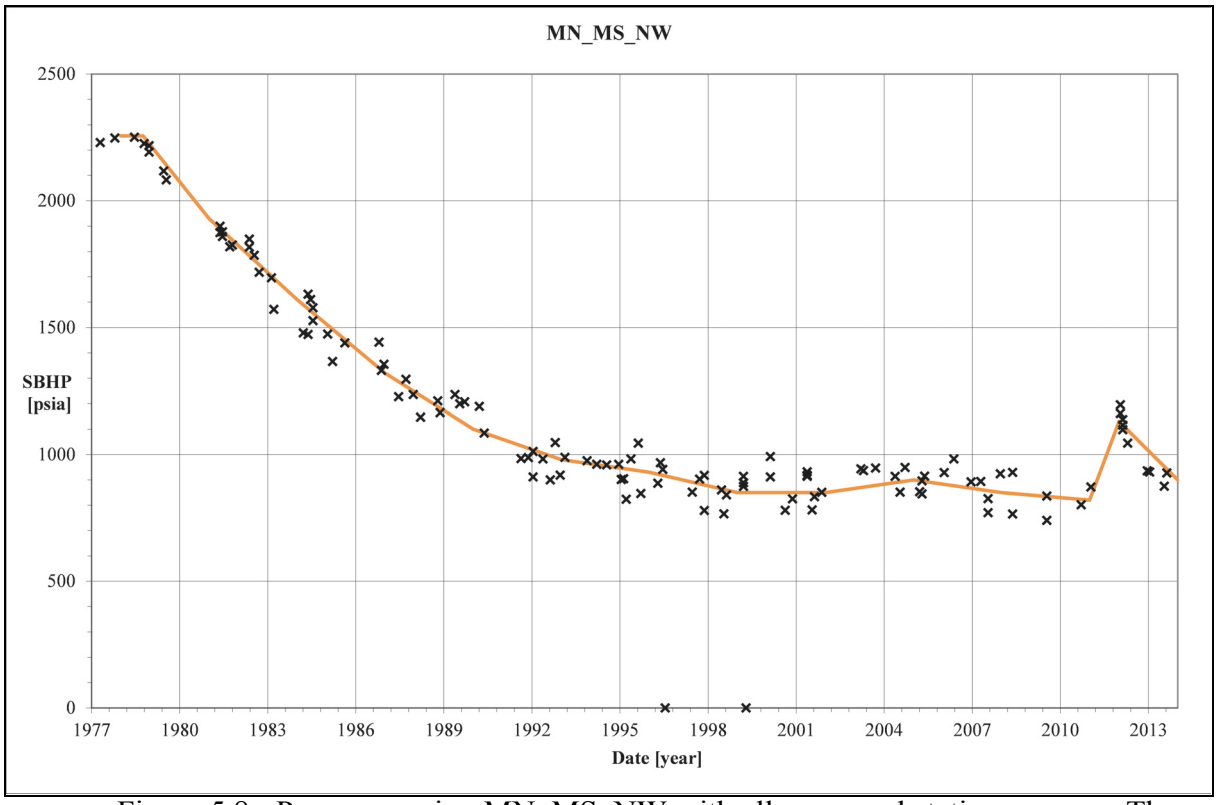

Figure 5.8: Pressure region MN_MS_NW with all measured static pressures. The estimated average region pressure is the orange line.

Figure 5.8 shows the pressure data and the estimated average region pressure for the MN_MS_NW region. This region is located in the center, the main part of the productive area. It includes 16 wells and has pressure data throughout the productive time. This pressure region is completely bounded by other pressure regions and does not represent a reservoir boundary at any location. It shares boundaries with the regions MN_MS, NW, SW and MS.

Similar to MN_MS also here abundant pressure data is available because of the high amount of wells drilled in this area. Also here the determination of the average region pressure done by interpolating pressure points.

Two static pressure measurements had to be discarded for this region, both for the well G01. The two measurements have been conducted in July 1996 and April 1999. Both of these measurements showed a 250 [psi] higher pressure than other wells at this time. Also the measurements at G01 in November 2011, August 2000 and June 1997 showed much lower pressures that fit the trend and values of the other wells in the region.

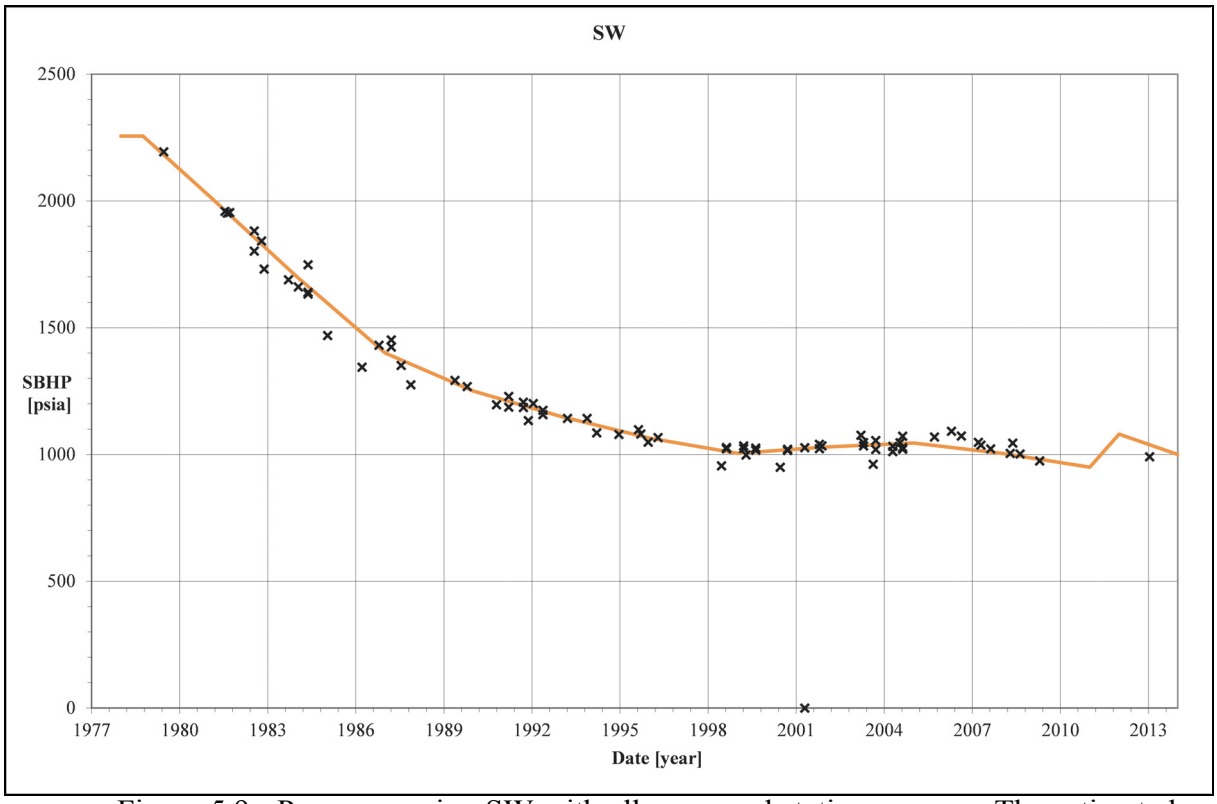

Figure 5.9: Pressure region SW with all measured static pressures. The estimated average region pressure is the orange line.

Figure 5.9 shows the pressure data and the estimated average region pressure for the SW region. The boundary on the west of this region is also a productive area boundary. Towards the north this region is bounded by the region NW, towards the east is shares a boundary with MN_MS_NW and the south of the SW region is bounded by the MS region.

After April 2009 only one pressure measurement data is available for any of the wells in the SW region. It was therefore necessary to estimate the behavior of the average pressure after this time until January 2014. In this case this has been performed by using the trends of the MN_MS_NW and the MS region. In this case also the initial pressure had to be estimated, but with the assumption that the initial reservoir pressure is nearly identical for all regions, this is less of an uncertainty than the extrapolation of the later data, which is similar to region NW.

Also in this pressure region one static pressure measurement had to be discarded. The measurement in G16 from April 2001 showed a 300 [psi] too high pressure compared to other wells at this time and also compared to the history of the well G16. In September 2000 and October 2001 G16 measurements were in line with other pressure measurements and

approximately 300 [psi] lower than the measurement in April 2001.

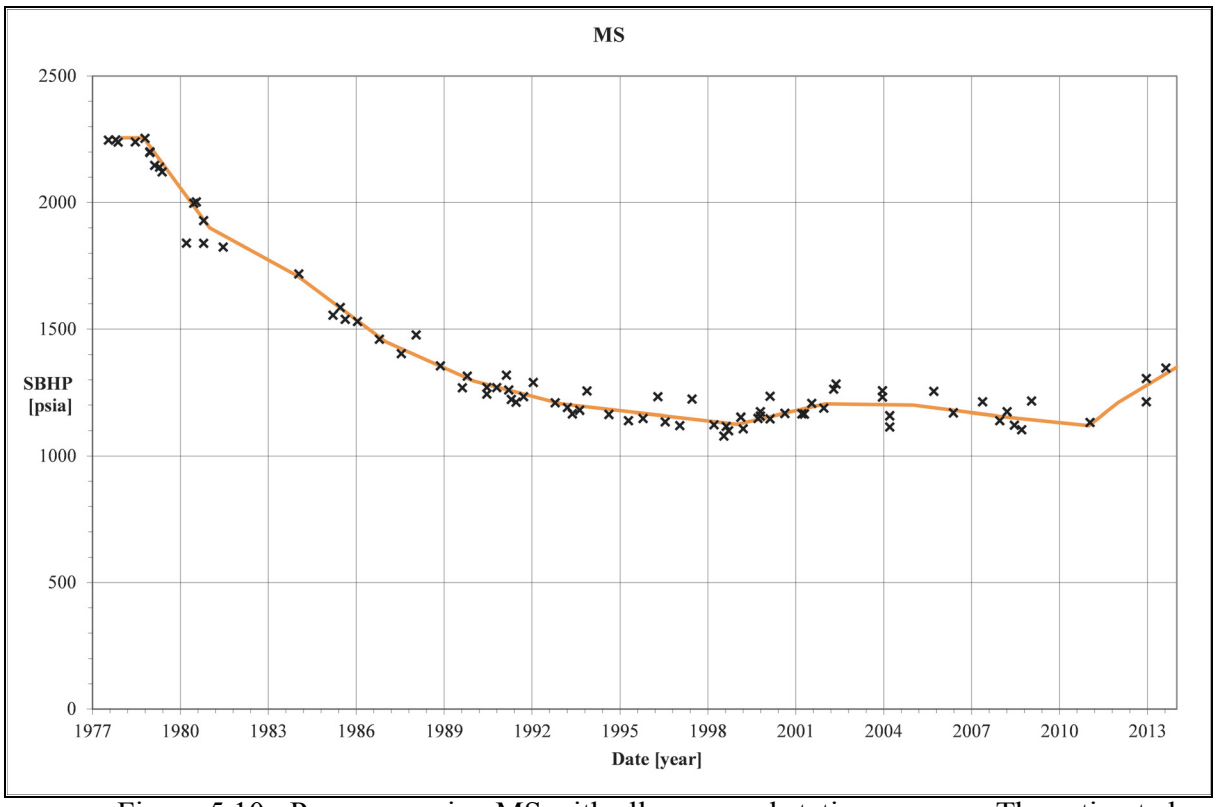

Figure 5.10: Pressure region MS with all measured static pressures. The estimated average region pressure is the orange line.

Figure 5.10 shows the pressure data and the estimated average region pressure for the MS region. This region extends from the eastern boundary of the reservoir to the main fault in the west. In the south the region MSS can be found and in the north the regions SW, MN_MS_NW and MN_MS are neighboring. This region includes 7 wells.

All static pressure measurements for this region were accepted and again the determination of the average region pressure was easy, because many data points are available that share a common trend.

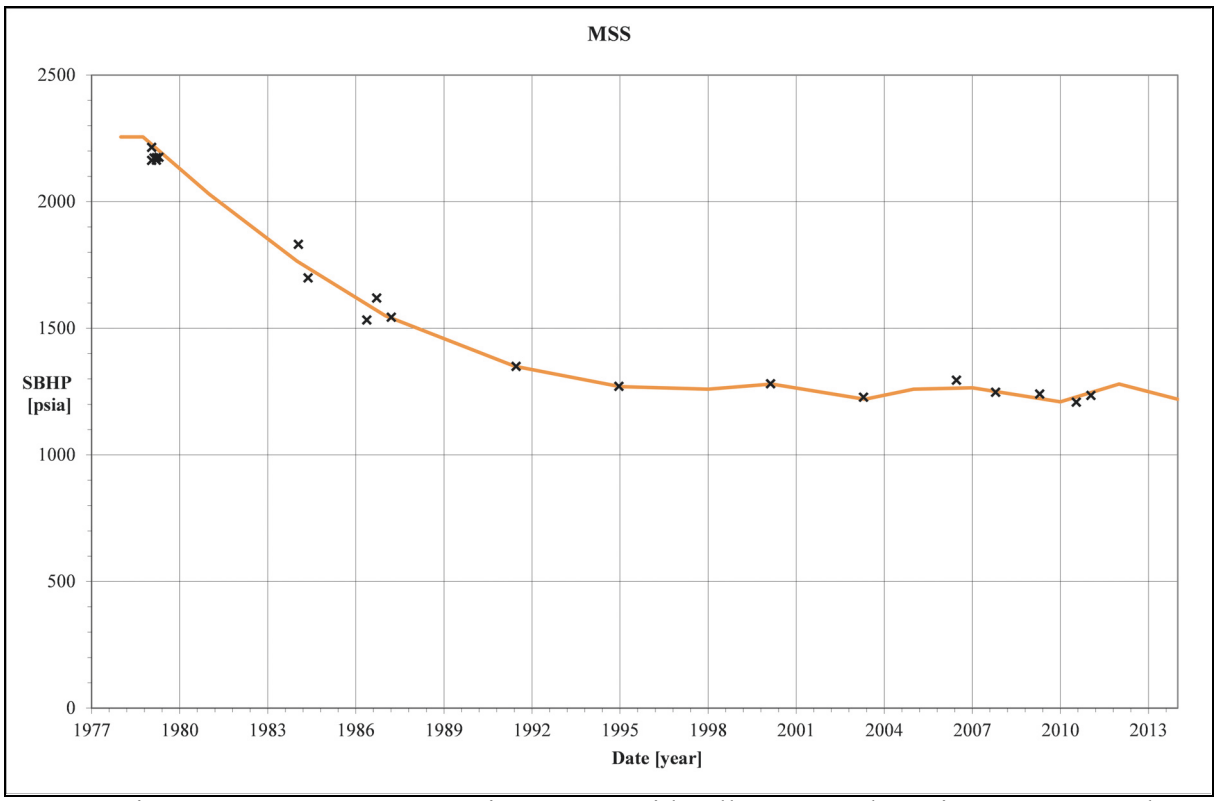

Figure 5.11: Pressure region MSS with all measured static pressures. The estimated average region pressure is the orange line.

Figure 5.11 shows the pressure data and the estimated average region pressure for the MSS region. This region is neighboring to the MS region in the north and the SE_NE region in the east. The western and southern boundaries also represent productive area boundaries.

Only three wells are included in this region, and only two wells have pressure data available (G11 and G12). It was, however, necessary to introduce this region because the absolute values of the static pressures did not fit the values of the MS region. Because only limited data is available the data for the end of the pressure history again had to be estimated based on the trends that are present in the rest of the reservoir.

5.4.2 Average Pressure for the Field Level

The field average pressure can be calculated as the hydrocarbon pore volume weighted average of the individual pressure regions. It is necessary to calculate the average pressure for the field for a later comparison with the pressure values gained by simulation. It is not possible to easily determine an average pressure for the field using all the pressure data (Figure 4.5). No information about the individual drainage areas of all the wells is available.

Therefore the average pressure calculation for the field level was conducted on the basis of the average pressure for the region level. From the geological model the initial hydrocarbon pore

volumes (HCPV) for all regions and for both continua, matrix and fracture, have been extracted and weighting factors have been calculated. The input data and the calculated weighting factors for all regions can be seen in Table 5.1. The last row of the table is the sum of all entries of each column and therefore represents the data for the field level.

Table 5.1: Hydrocarbon pore volumes of the regions and the calculated weighting factors for the average pressure determination

Region	**HCPV Matrix [1000 bbl]**	**HCPV Fracture [1000 bbl]**	**HCPV M&F [1000 bbl]**	**Weighting Factor [-]**
SE_NE	44138	3139	47277	0.060
NE_ZOC	60337	3258	63595	0.081
NE_AGOCO	53240	3264	56504	0.072
NW_AGOCO	21843	1560	23403	0.030
NW_ZOC	26394	1602	27996	0.036
MN_MS	141022	7213	148235	0.188
MN_MS_NW	122638	7203	129841	0.165
SW	56271	3474	59745	0.076
MS	109206	6318	115524	0.147
MSS	108166	6399	114565	0.146
Field	743255	43430	786685	1.000

The here used weighting factor (WF) [-] for a pressure region *i* is defined as:

$$WF_i = \frac{HCPV_i}{\sum_i HCPV_i} \tag{5.1}$$

Using the weighting factors from Equation 5.1 it is then possible to calculate the field HCPV weighted average pressure, $\bar{P}_{field}$ [psia], for a certain time *t* with and regions *i*:

$$\bar{P}_{field}(t) = \sum_i WF_i \cdot P_i(t) \tag{5.2}$$

.

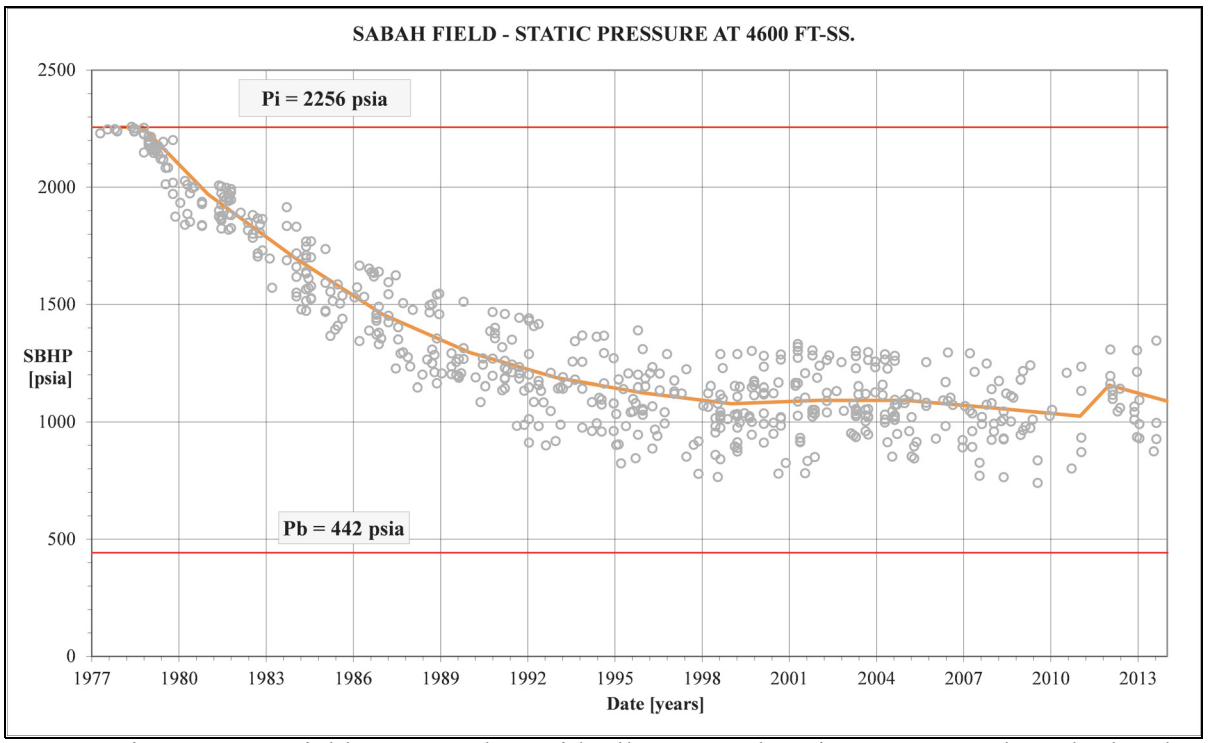

Figure 5.12: Field pressure data with all measured static pressures. The calculated average pressure is the orange line.

The resulting average field pressures can be seen in Figure 5.12. In Figure 5.13 all static pressure data and average region pressure as well as the average field pressure can be seen. Pressure differences of more than 400 [psia] exist between regions MSS and SE_NE. It is also obvious that none of the regions is close to the bubble point pressure at any time during the life of the reservoir.

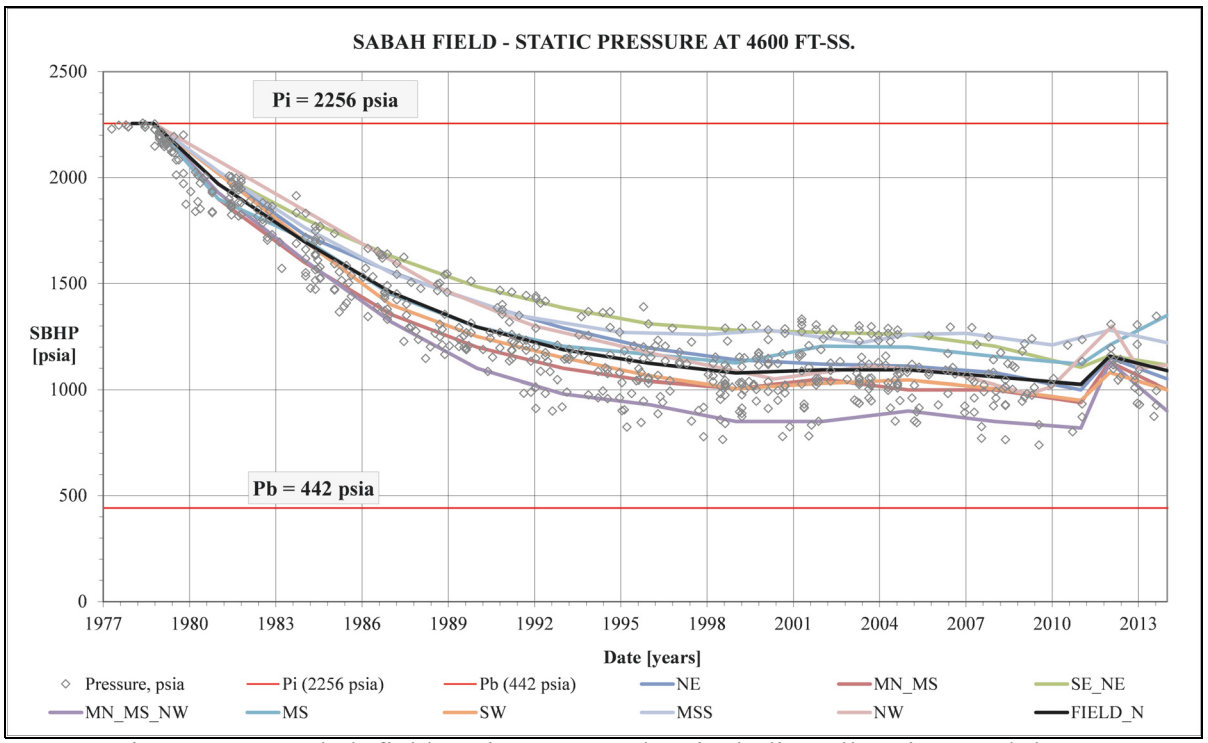

Figure 5.13: Sabah field static pressure data including all regions and the average field pressure.

Chapter 6

Aquifer Support Assessment

The aquifer support assessment can be conducted in analytical or numerical manner. H5 offers multiple solutions for determining water influx requirements. The analytical determination of aquifer parameters is historically significant, but the contemporary method is the use of numerical simulation. Therefore the focus will be set on the numerical determination of aquifer parameters.

For the numerical approach a full field numerical simulation has been performed using the Target Pressure Method (TPM) and by specifying the produced reservoir volume.

6.1 Simulation Model

The simulation grid (see Figure 6.1) has corner-point geometry. General data about the simulation model:

- Dual porosity, single permeability model
- 187440 grid blocks: 93720 for the fracture domain and 93720 for the matrix domain
- Initial OWC is 4700 [ft] SS
- Initial oil in place is 672.2 [MMSTB]
- Initial reservoir pressure is 2259 [psia] (HC-weighted)
- No gas cap is present since the oil is undersaturated
- 10 rock regions for the matrix and one rock region for the fracture: The capillary pressure curves used have been created by Hot Engineering GmbH (2004), which were computed from log derived water saturation versus depth. In the fracture region the capillary pressure is set to zero.
- One PVT region for the entire model, since no compartmentalization is present

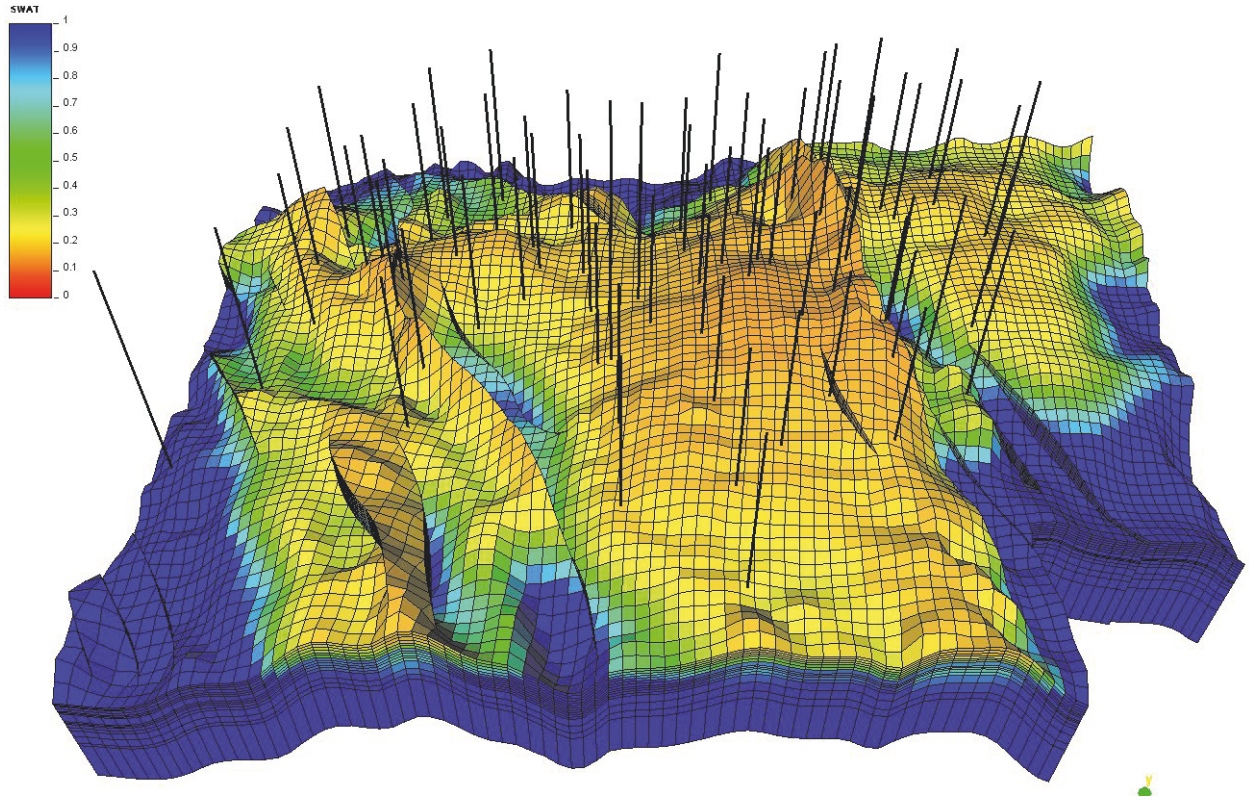

Figure 6.1: Simulation grid showing with initial water saturation of the matrix and wells

6.1.1 Boundaries

Five boundaries have been defined for the simulation model. All boundaries connect to water saturated blocks of the bottom layer. Only the fracture gridblocks are connected to the aquifer, since the model is a single permeability model and the matrix only has connections to neighboring fractures. Figure 6.2 shows the defined boundaries. Different colors represent different boundaries. Gray grid blocks are non-boundary active grid blocks. The five boundaries are:

- B_S (blue): Boundary to the south of the model
- B_W (bright blue): Boundary that covers the entire west side of the model
- B_N (green): Boundary in the north and north-west. Towards the east this boundary ends where one of the main faults of the reservoir intersects the boundary.
- B_NE (yellow): Boundary in the north-east. Towards the west this boundary ends where one of the main faults of the reservoir intersects the boundary. Towards the south this boundary ends at the pressure region boundary between the pressure regions SE_NE and NE.
- B_SE (red): Boundary in the south-east. Towards the north this boundary ends at the pressure region boundary between the pressure regions SE_NE and NE.

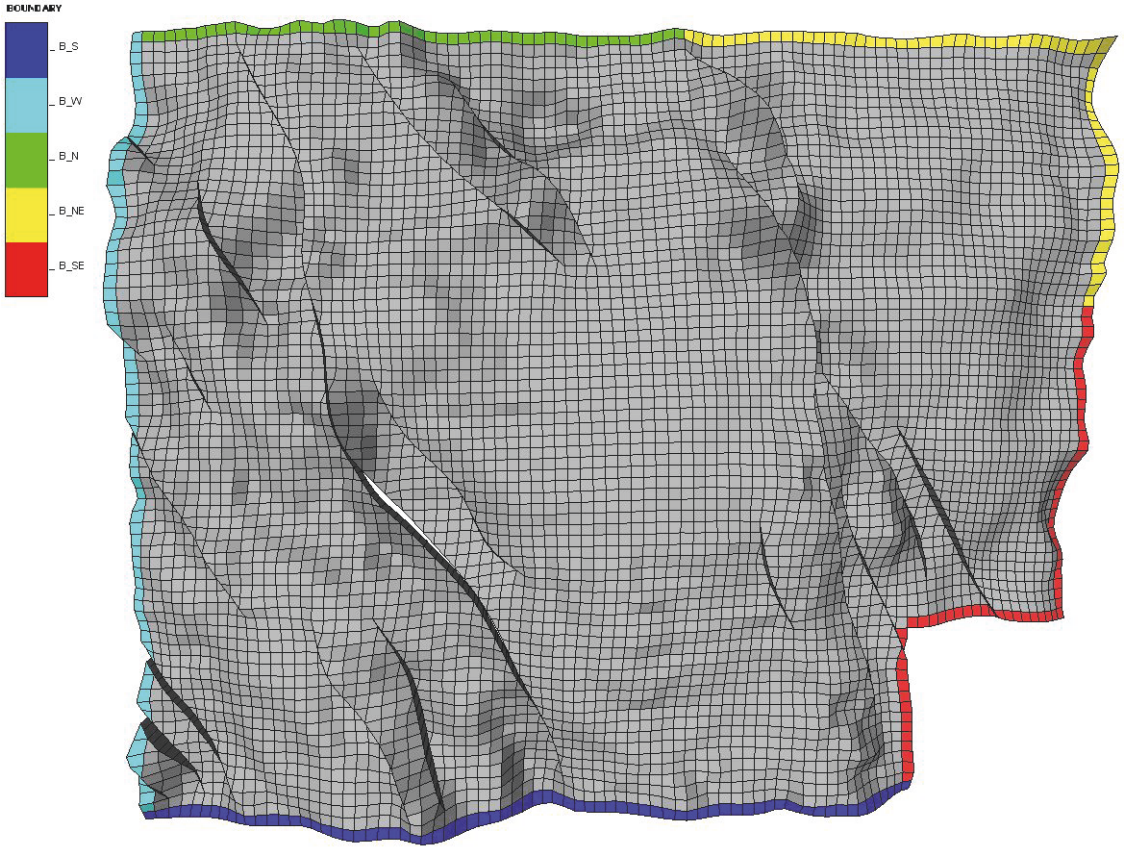

Figure 6.2: Defined boundaries for analytical aquifer attachment in the bottom layer

6.2 Target Pressure Method

The TPM is an option for assisted history matching, which makes it possible to determine water influx requirements (Pichelbauer 2003, Mittermeir 2003). This method makes it possible to simulate without prior knowledge of the correct aquifer setup by determining the water influx requirements of the model according to the specified target pressure. The target pressure is the average region pressure of the target area.

Pichelbauer (2003) lists the following boundary block properties, which are all true for the generated boundaries as described in Section 6.1.1:

- Boundary grid blocks are fully saturated with water with constant salinity.
- Intersection of boundaries are not possible.
- Boundaries are allowed to be discontinuous.
- An unlimited number of volume regions can be connected to a single boundary.
- There can be only one target area per boundary and one boundary per target area.
- No active grid blocks are present on the outside of an outer boundary.

- Boundary grid blocks do not belong to volume regions.

The process of the TPM can be described in four steps, which are performed at the beginning of each time step:

1. Determination of the pressure decline rate correction: In this step the corrections to the simulated pressure decline are calculated based on a comparison of the simulated and the actual pressure decline.
2. Pressure decline rate conversion: In this step the deviation of the actual and simulated pressure decline rate is corrected by adjusting the water influx.
3. Injection/ production rate distribution: The in the second step calculated total injection or production rate is distributed along the boundary blocks in a way that a uniform boundary pressure is formed.
4. Adding the water rate to the boundary grid blocks: This step consists of adding the calculated rates for each boundary block to the flow equation system of the simulation model. Here the additional water rate or production is added to the accumulation term of the mole balance equation.

A more detailed description of the individual steps and the calculations methods used can be found in the dissertation of Pichelbauer (2003).

After completion of the simulation the best fitting analytical aquifer model and its parameters is determined. This is done for the Vogt-Wang, Carter-Tracy and Fetkovich aquifer models.

Figure 6.3 shows the general workflow for the TPM as described above.

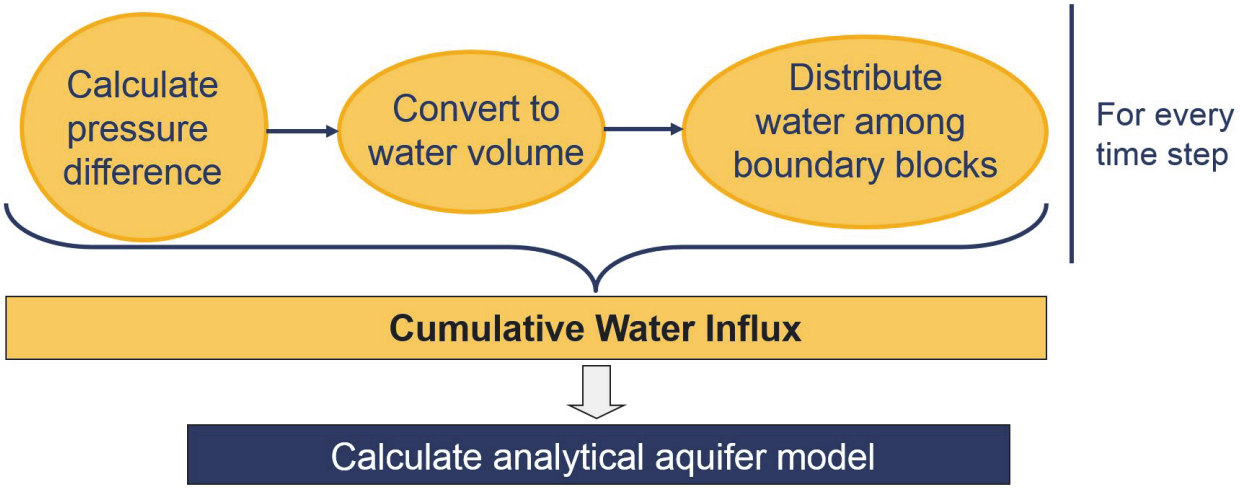

Figure 6.3: Workflow for the Target Pressure Method

6.3 Analytical Water Influx Assessment for the Sabah Field

The analytical water influx assessment using the material balance calculations has been performed with H5. The single porosity material balance option was used. To make material balance calculation for the field it is necessary to create a target volume consisting of all other matrix and fracture regions. The start date for the calculations has been set to 1978/01/01 and the end date to 2014/05/01.

6.3.1 Aquifer Model Determination

The single porosity material balance option was used, which was introduced in the TDD file as follows:

```
MATBAL   TARGET TA_MF-ALL BOUNDARY B_All history
```

where `MATBAL` is the identifier for the material balance option. The keyword `TARGET` specifies the target area `TA_MF-ALL`, which is a volume comprised of all matrix and fracture regions. The boundary `B_ALL` is defined as a boundary to the `TA_MF-ALL` region. The attribute `history` specifies that this is not a prediction, but a history calculation. The boundary is defined as follows:

```
BOUNDARY B_All ptarget AREA TA_MF-ALL HCvol QLIMIT 0 50000 relax 1 &
         TINTER   1985  1996  2000  2002  2005  2008  2011  2014
```

which means that the boundary `B_All` for the area `TA_MF-ALL` is operated under target pressure option. `HCvol` means that the target pressure is defined as average pressure of the hydrocarbon pore volume and `QLIMIT` gives the lower and upper limit for the boundary inflow rate [stb/d]. The keyword `TINTER` gives the possibility to set years at the beginning of which Fetkovich aquifer parameters are calculated. Detailed description about the used identifiers, keywords and attributes can be found in the PRS TDD manual (2015). Figure 6.4 shows the calculated pressures (history) and the measured pressures. Naturally, for the material balance method the calculated values exactly match the measured data.

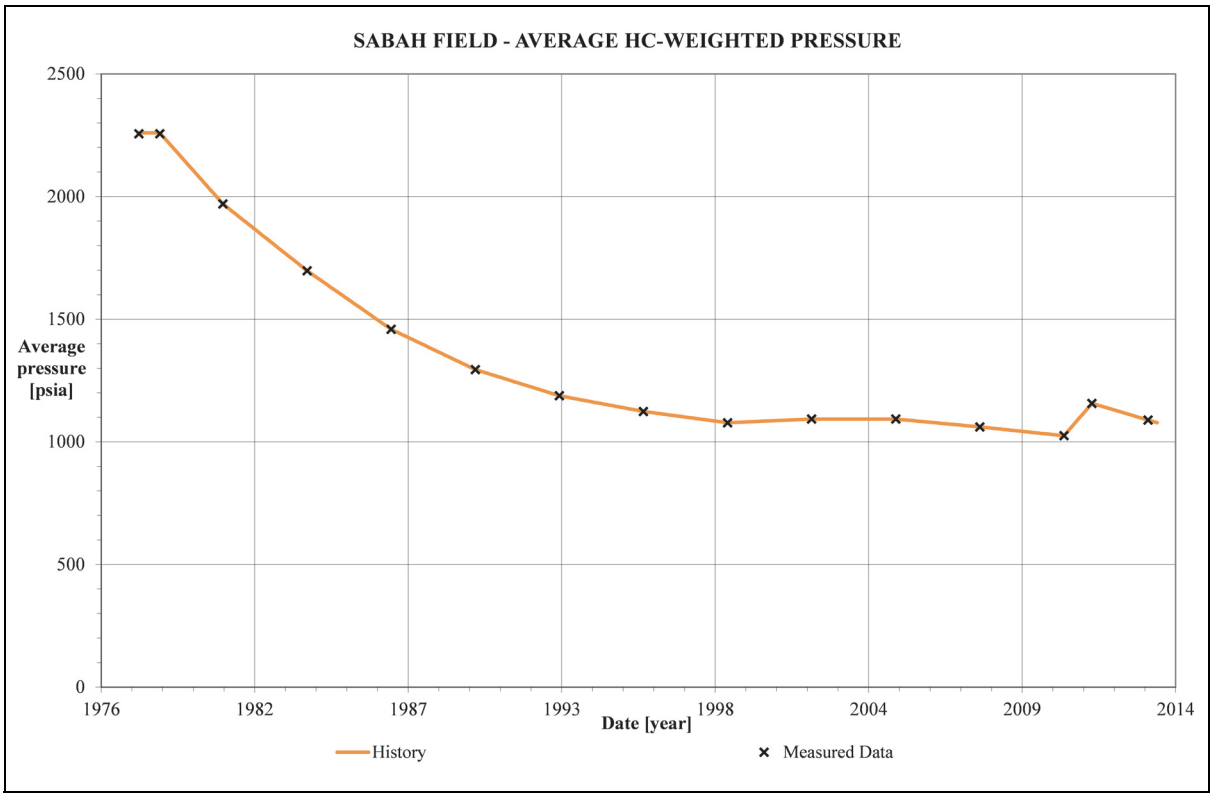

Figure 6.4: Average reservoir pressure from the history compared with the measured data

Exactly the amounts of water and oil according to the field production history is taken out and the necessary water influx is calculated. The best fitting aquifer for was determined to be a Fetkovich aquifer model with a maximum encroachable water amount of water of 4.1378E+09 [bbl] and an aquifer productivity index of 109 [(bbl/d)/psi].

6.3.2 Aquifer Model Applicability Verification

To verify the aquifer it is necessary to use the calculated aquifer parameters and run the simulation again for the same period as in the history run. If the pressure and the water influx from the prediction run shows a good match with the history run data, the calculated aquifer parameters can be viewed as verified. Therefore the following instructions have been included into the TDD file:

```
MATBAL   AREA TA_MF-ALL BOUNDARY B_All prediction

BOUNDARY 1978/01/01 B_All fetkov AQUIWEI 0.41378E+10 AQUIJW 190
```

where the attribute `prediction` indicates that this is a prediction and not a history run. The boundary is defined as a Fetkovich aquifer and `AQUIWEI` is the maximum encroachable amount of water and `AQUIJW` is the aquifer productivity index. The aquifer parameters are held constant

for the entire prediction simulation run. The boundary `B_All` is the same boundary as in the `history` run.

By applying this boundary condition and using the same production history as before the pressure history could be reproduced very well until 2011. After 2011 higher differences between the measured data and the calculated data exist.

It is not clear why these discrepancies at the end of the simulation run occur. However, it should be noted that especially after 2011 the available pressure data is only sparse. Entire pressure regions are without or only a few measurements for the time from 2011 to 2014. Therefore the measured pressure data for this period is afflicted with uncertainty.

The next step is to compare the calculated water influx between history and prediction calculations. As can be seen in Figure 6.6, the two lines for the history and the prediction overlap nearly perfectly. This means that the analytical aquifer is able to reproduce the calculated water influx.

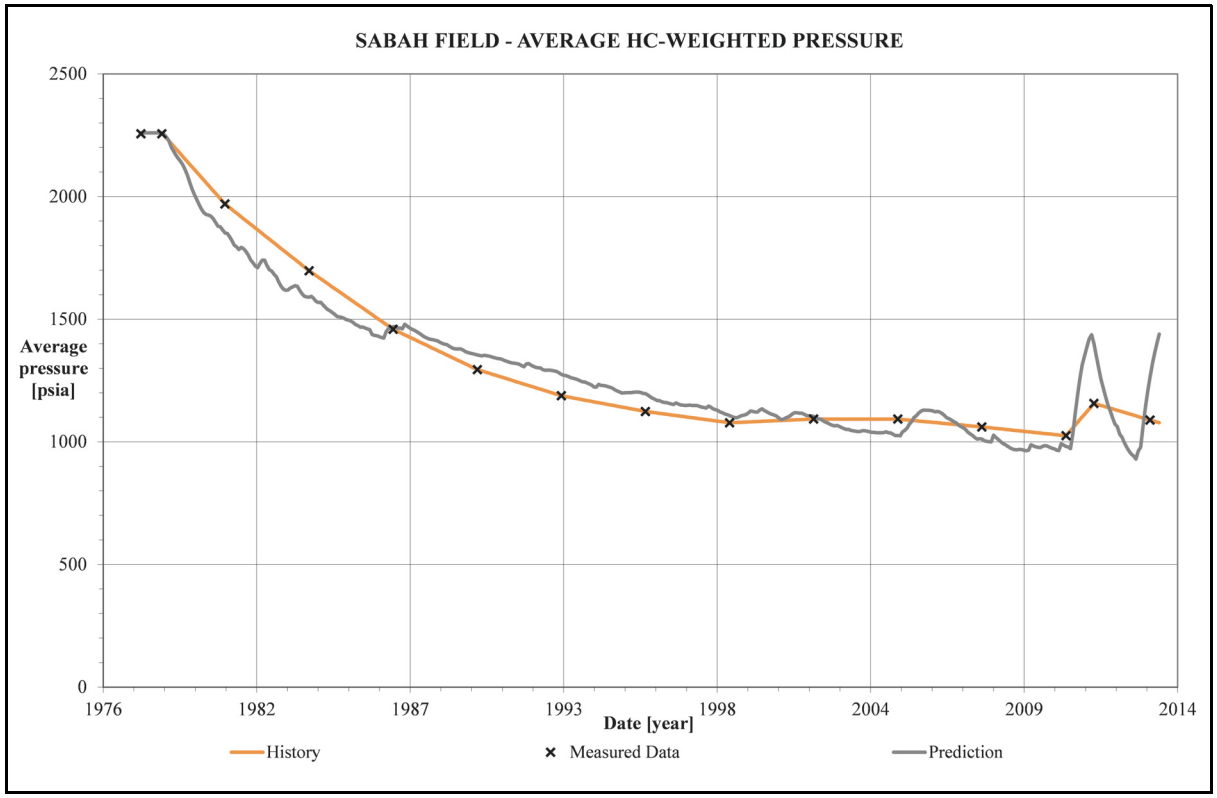

Figure 6.5: Average reservoir pressure using the analytical aquifer (prediction) compared with the history result and the measured data.

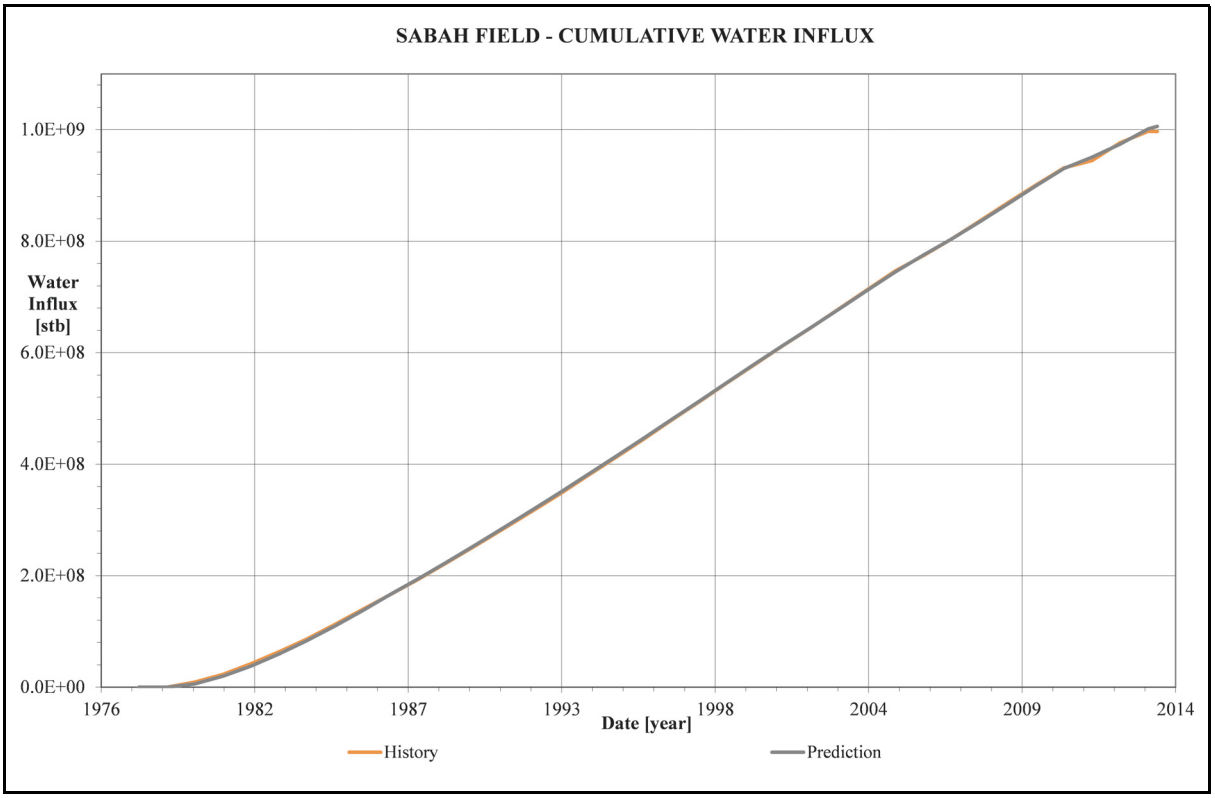

Figure 6.6: Cumulative water influx as a function of time for history and prediction.

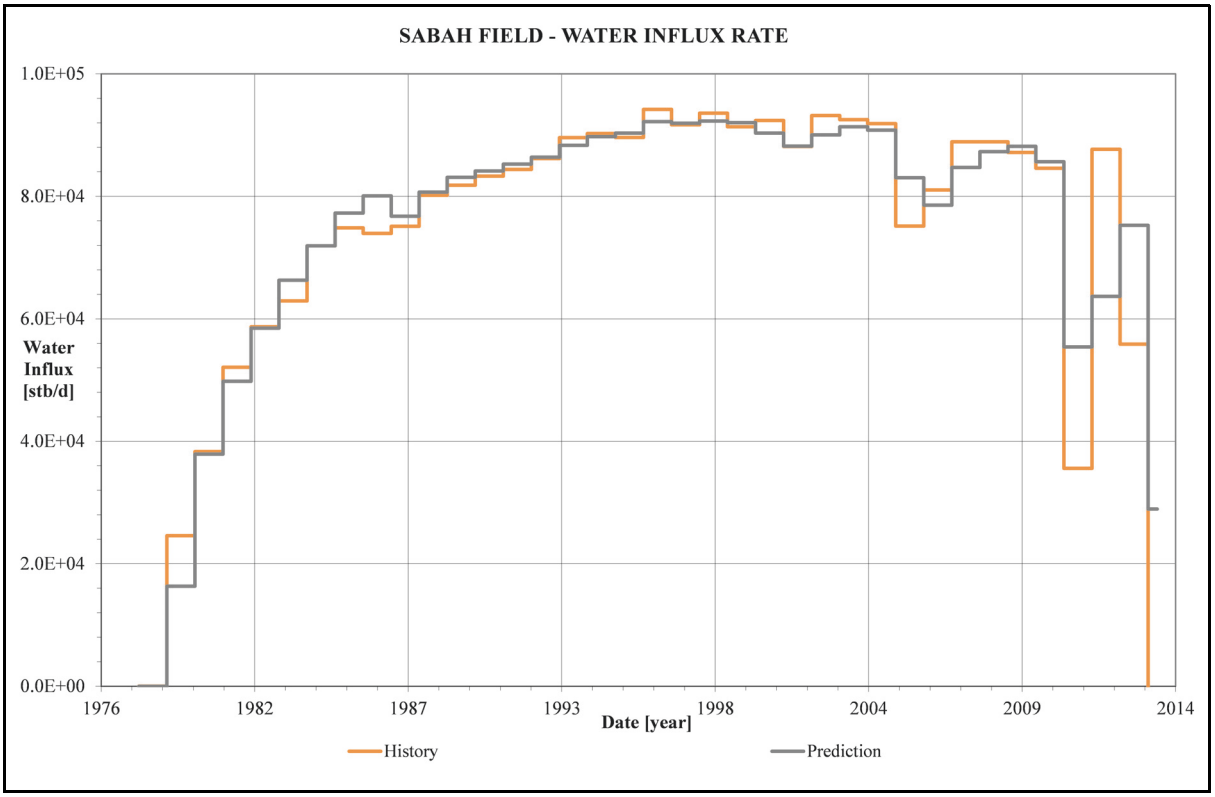

Figure 6.7: Water influx rate as a function of time for history and prediction of the material balance calculation.

6.4 Numerical Water Influx Assessment for the Sabah Field

For the numerical simulation of the Sabah field also H5 was used. Initialization date is 1978/01/01 and the end of the simulation is 2014/05/01. The first part is the determination of analytical aquifer parameters and the second part is the verification of the parameters by re-calculating the historical pressure data with the use of the analytical aquifer models.

6.4.1 Aquifer Model Determination

The application of the TPM requires that target pressures for all five boundaries are assigned. The following region pressures are assigned as target pressures:

Table 6.1: Target regions for the five boundaries of the productive area

Boundary	Target Region
B_S	MS
B_W	SW
B_N	MN_MS
B_NE	NE (ZOC & AGOCO)
B_SE	SE_NE

The wells have been defined to produce the exact amount of reservoir volume as in the production history. This was done using the option `resvol` in the well definition. This means that the reservoir volume will be matched in the simulation, but not necessarily the phase. Therefore it is possible to have a different surface production volume from the simulation than from the measured data because of the different formation volume factors of different phases. However, for the purpose of aquifer matching it is the most important issue to match the production in terms of reservoir volume and less important to match the phase exactly.

For example well G01 is defined as:

```
WELLDEF 1978/01/01 G01      oilprd resvol prdstat
```

which means that G01 is an oil producing well that should produce the reservoir volume given in the production history. The date corresponds to the date of initialization of the simulation. All oil producing wells have been defined this way.

All boundaries have been defined as the following example for the B_W boundary shows:

```
BOUNDARY B_W ptarget AREA TA_SW HCvol QLIMIT 0. 70000. relax 4.0  &
             TINTER  1980     1994     2000     2006     2011
```

The keyword TINTER gives the possibility to set years at the beginning of which Fetkovich aquifer parameters are calculated.

The resulting pressure match for the field level can be seen in Figure 6.8. It can be seen that the measured field pressure data can be reproduced very accurately by the TPM. On a regional level differences between the target pressures and the simulated pressures can be observed. The calculated pressure for the SE_NE region (Figure 6.9), a target pressure region, is perfectly fitting the target pressures. This region is matched with the boundary B_SE. The water influx through this boundary, as can be seen in Figure 6.17, reached a cumulative value of 569.90 million [bbl].

Figure 6.10 shows very good matching calculated pressures for the target pressure region NE, which consists of both the NE_ZOC and the NE_AGOCO region. The calculated average pressure for this region is roughly 20 [psi] too high from 1995 to 2008. However, no water influx over the boundary B_NE is taking place at the times of the too high pressure (Figure 6.18). The cumulative water influx through the boundary B_NE is low with a value of 7.17 million [bbl].

Figure 6.11, which shows the average pressure for the NW region, which is not a target pressure region and consists of the two regions NW_ZOC and NW_AGOCO. The simulated pressure in this region also is lower compared to the measured data for the period between 1988 and 2000. After this period the pressure match is very accurate considering that this is not a target pressure region.

The MN_MS target pressure region (Figure 6.12) shows a very good match between the calculated pressures and the measured pressures. This region is matched by the boundary B_N, which is attached to the NW_AGOCO region to the north of the MN_MS region. It has a cumulative water influx of 38.82 million [bbl]. The water injection rate through the boundary B_N can be seen in Figure 6.19. It can be seen that the water influx is not continuous over the entire production period with most of the water influx happening in the early time between 1980 and 1983.

Figure 6.13 shows the pressure data for the MN_MS_NW region, which is not a target pressure region. In this part of the reservoir that contains 16 wells the calculated pressure is higher than in the measured data with a maximum discrepancy of slightly over 150 [psi]. Surrounding volume regions do not show this overpressure and this hints towards the necessity to revisit the geological model.

Figure 6.14 shows the simulated and measured pressure data for the SW region and a nearly perfect match until the year 1996. After this year the calculated pressure is too high and the TPM therefore stopped water injection over the boundary B_W (Figure 6.20). Water influx from other boundaries increased the pressure in this region too much, which hints towards the necessity to revisited the geological model. The cumulative water influx over the connected boundary B_W is 28.73 million [bbl].

Figure 6.15 shows a nearly perfect pressure match for the target pressure region MS, which is connected to the boundary B_S. The water influx through the boundary B_S can be seen in Figure 6.21. The cumulative water influx for this boundary is 344.68 million [bbl].

The MSS region, which is not a target pressure region but is connected to the boundary B_S shows a good pressure match for the entire production period (Figure 6.16).

The cumulative water influx for all boundaries can be seen in Figure 6.22. It can be seen that nearly all of the water injection takes place through the boundaries B_SE and B_S, both of which lie in the south of the productive area. The water injection rate and the cumulative water influx for the field level can be seen in Figure 6.23.

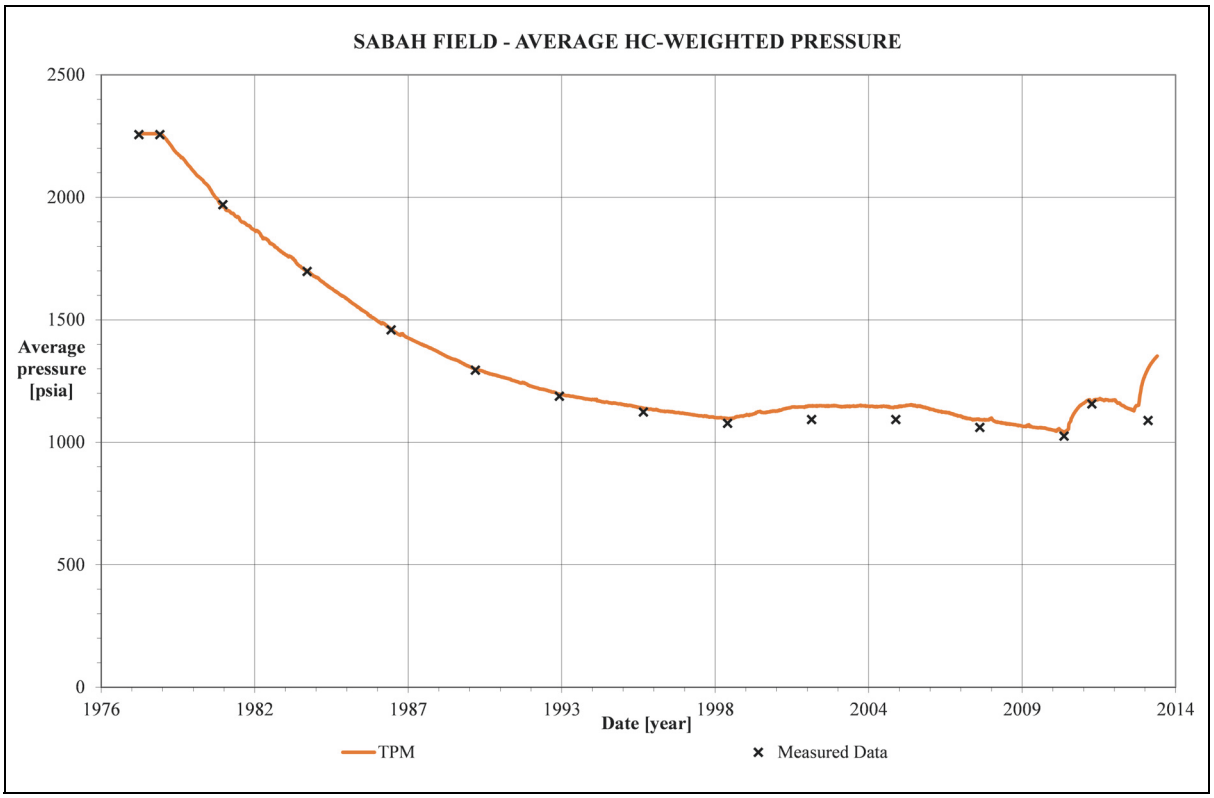

Figure 6.8: TPM simulated and measured field level average pressure.

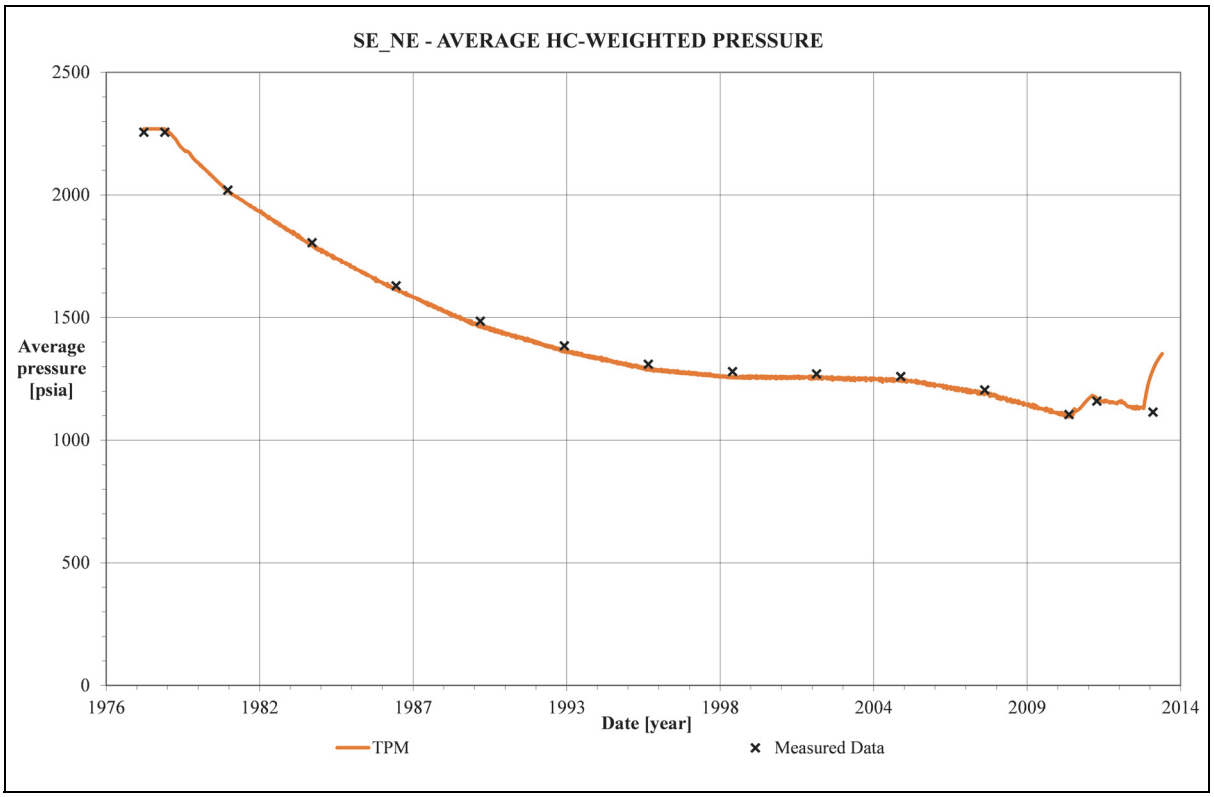

Figure 6.9: TPM simulated and measured average pressure of SE_NE.

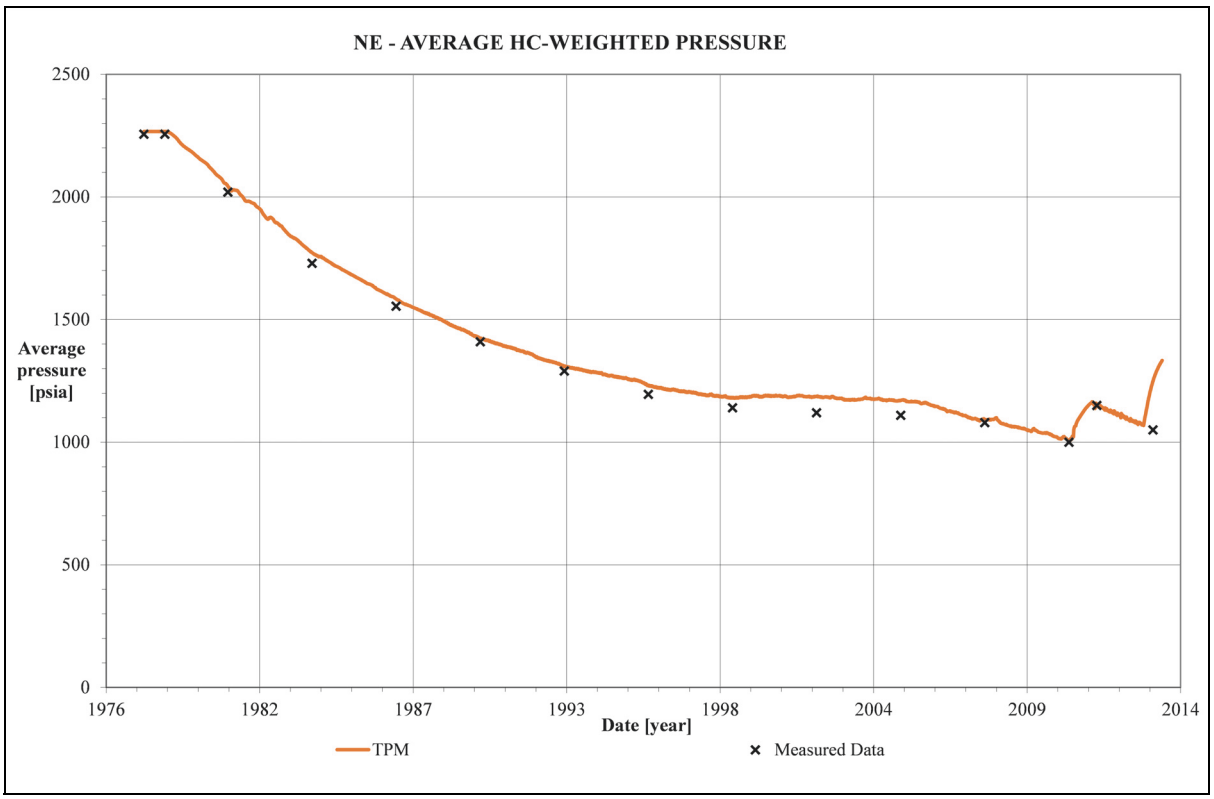

Figure 6.10: TPM simulated and measured average pressure of NE.

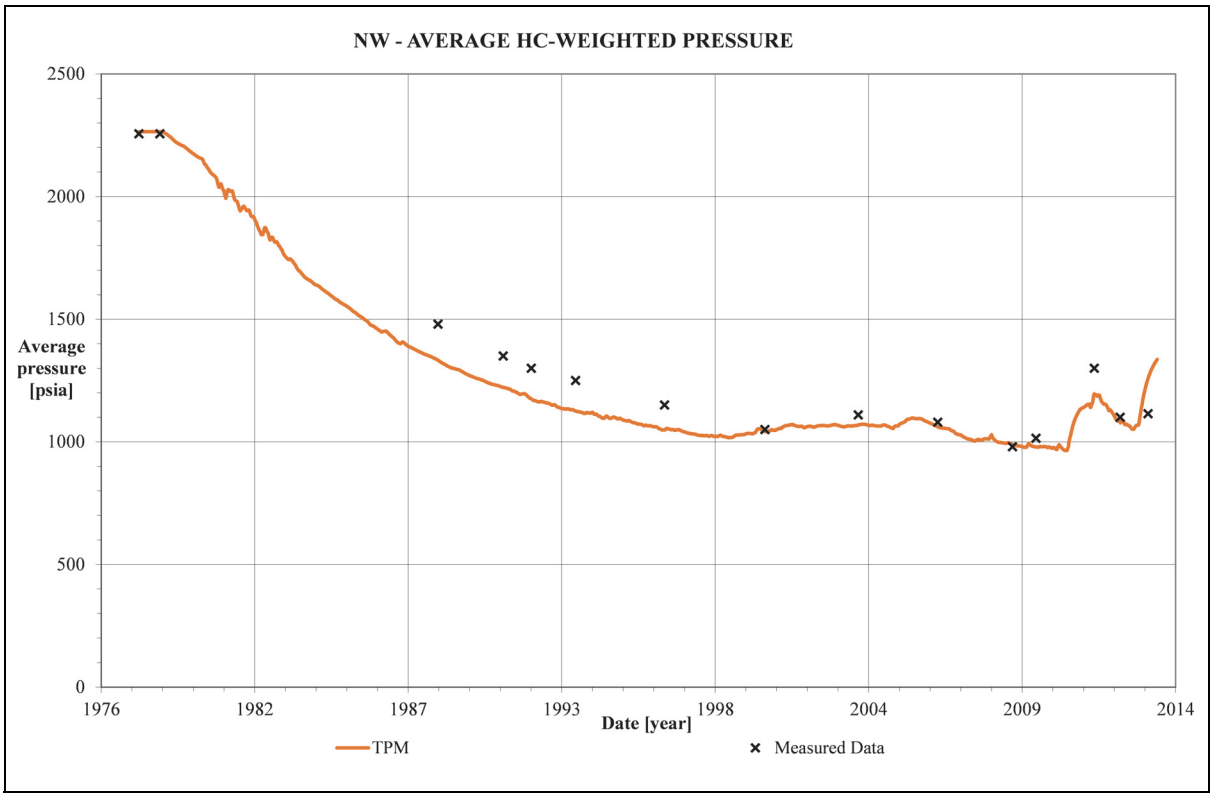

Figure 6.11: TPM simulated and measured average pressure of NW.

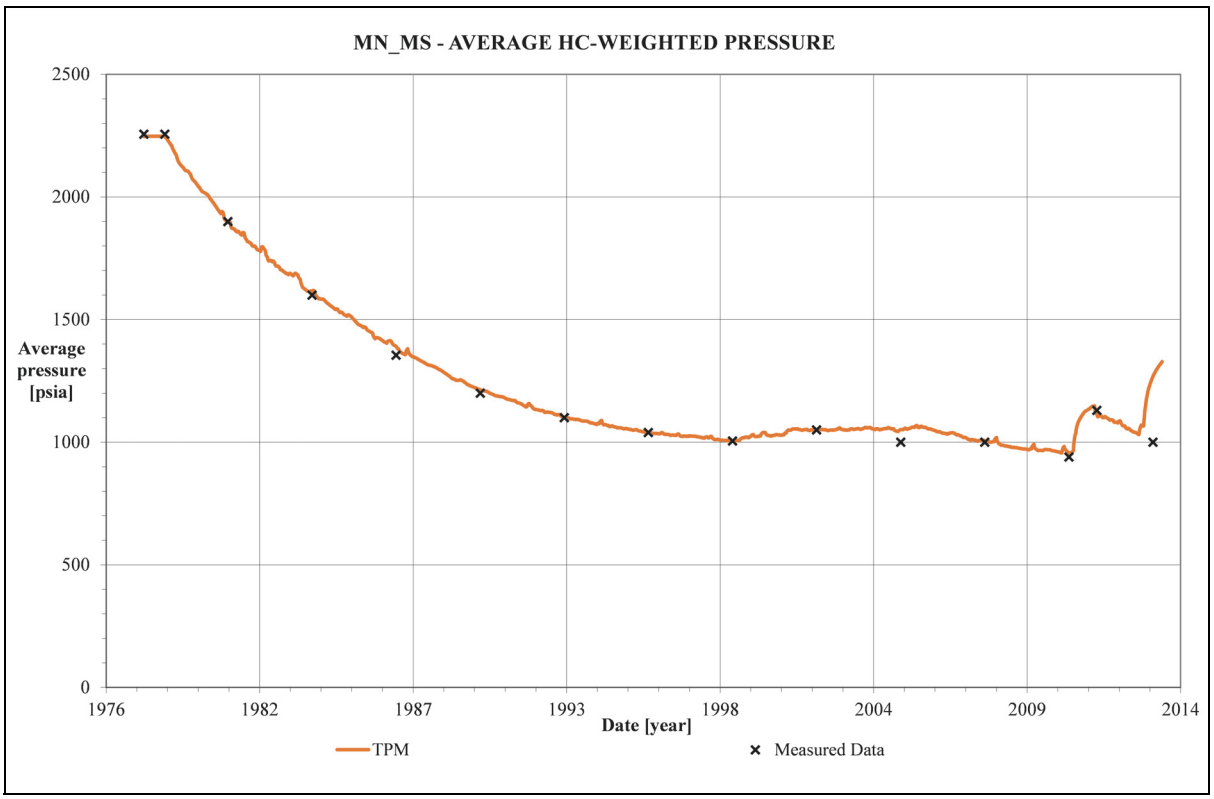

Figure 6.12: TPM simulated and measured average pressure of MN_MS.

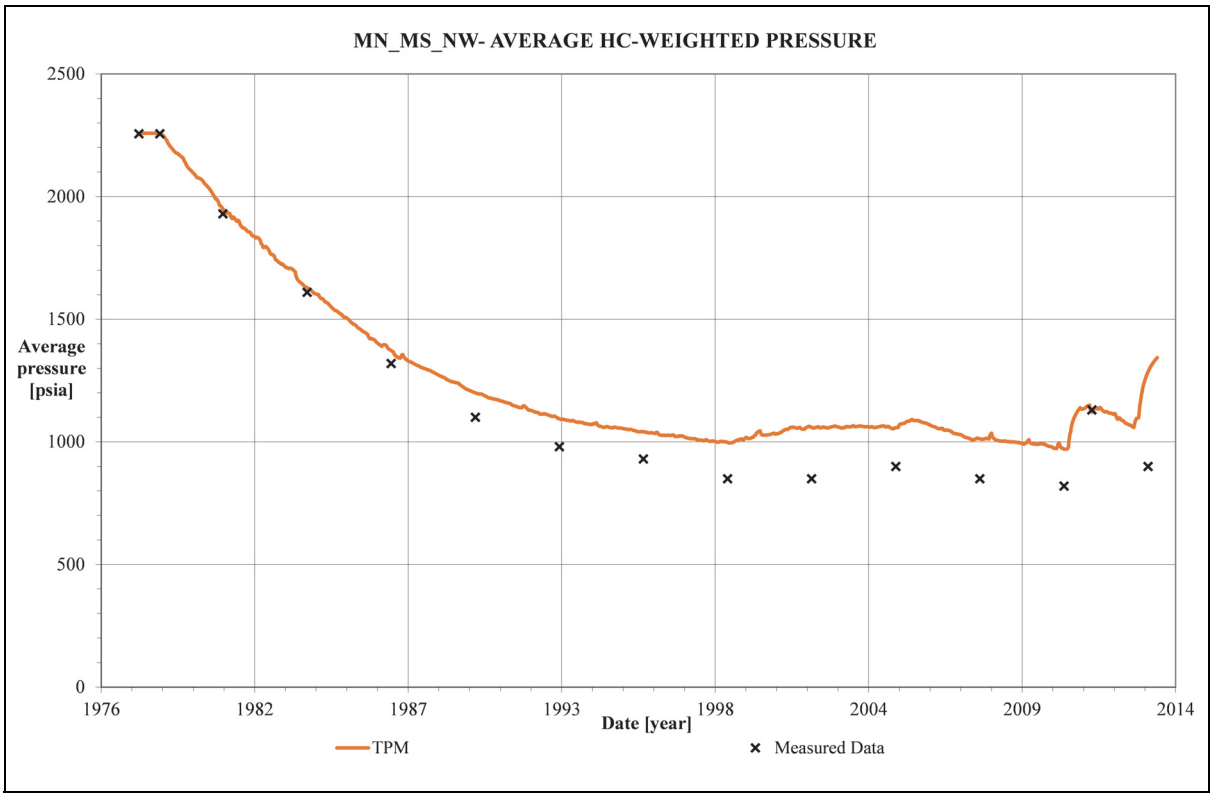

Figure 6.13: TPM simulated and measured average pressure of MN_MS_NW

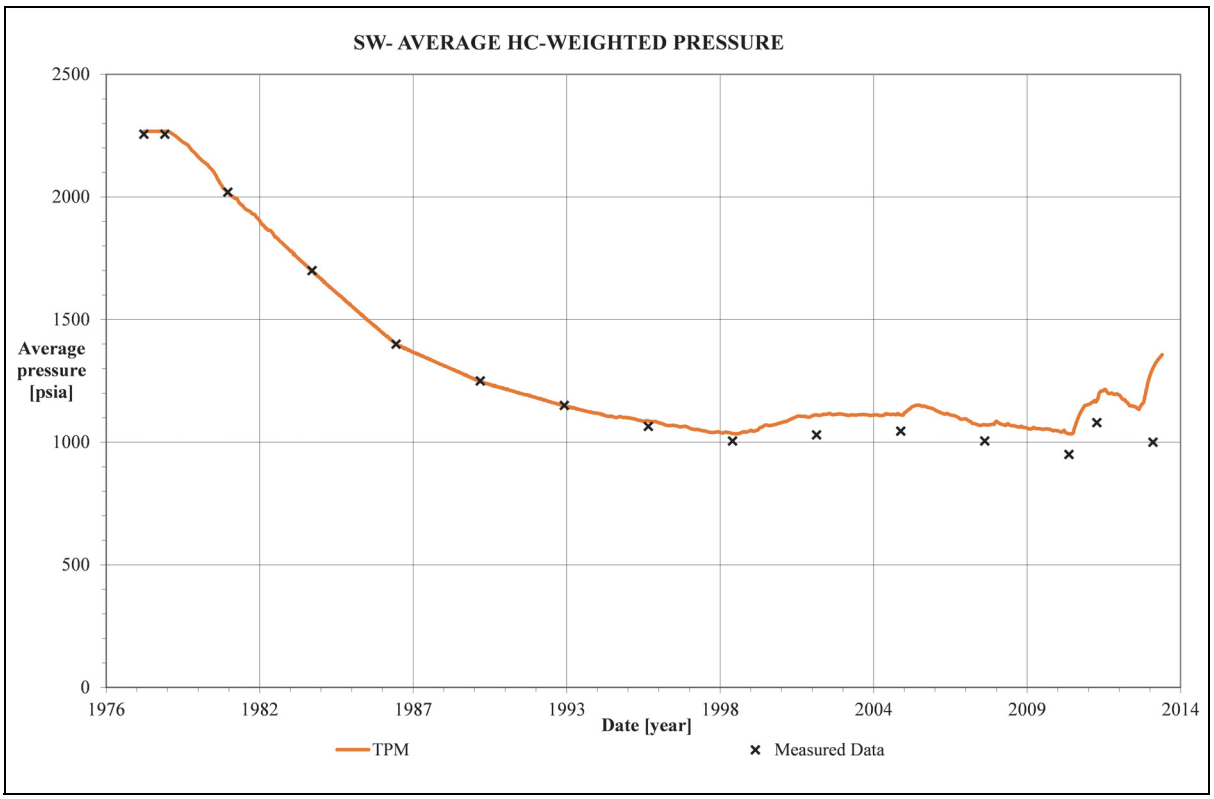

Figure 6.14: TPM simulated and measured average pressure of SW.

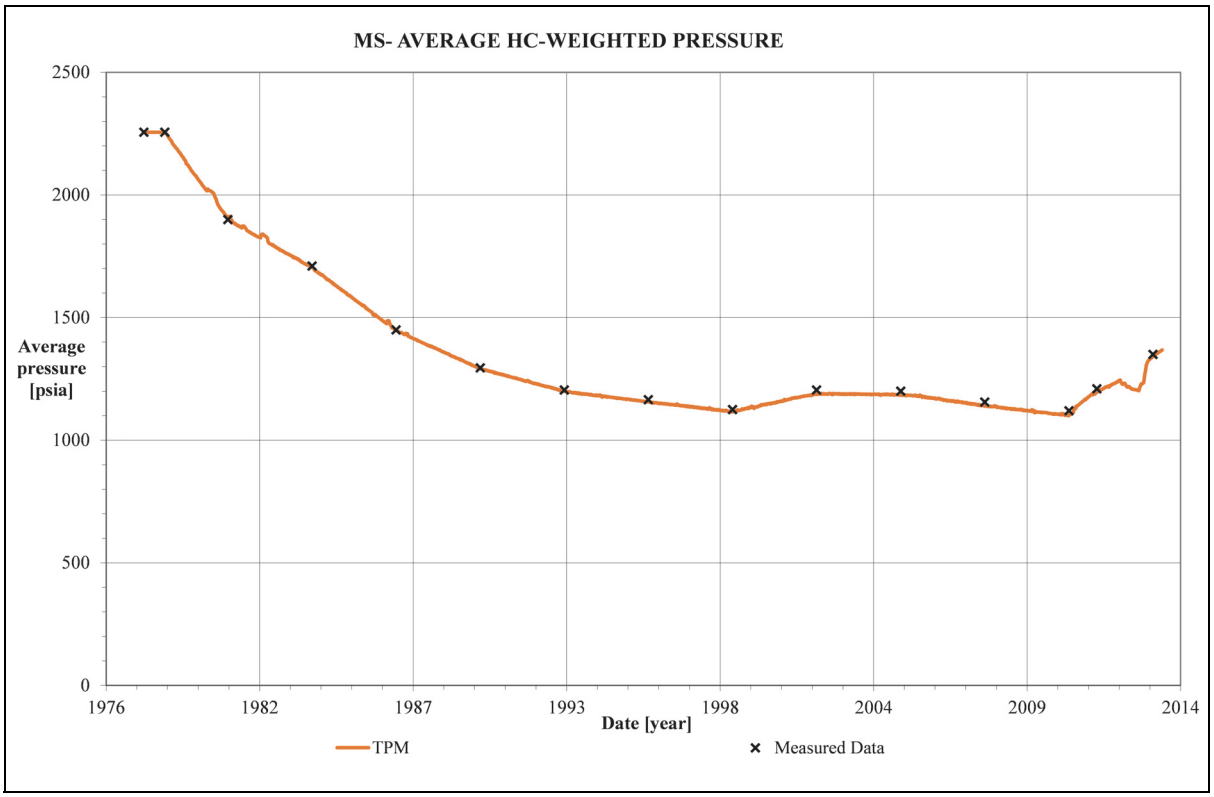

Figure 6.15: TPM simulated and measured average pressure of MS.

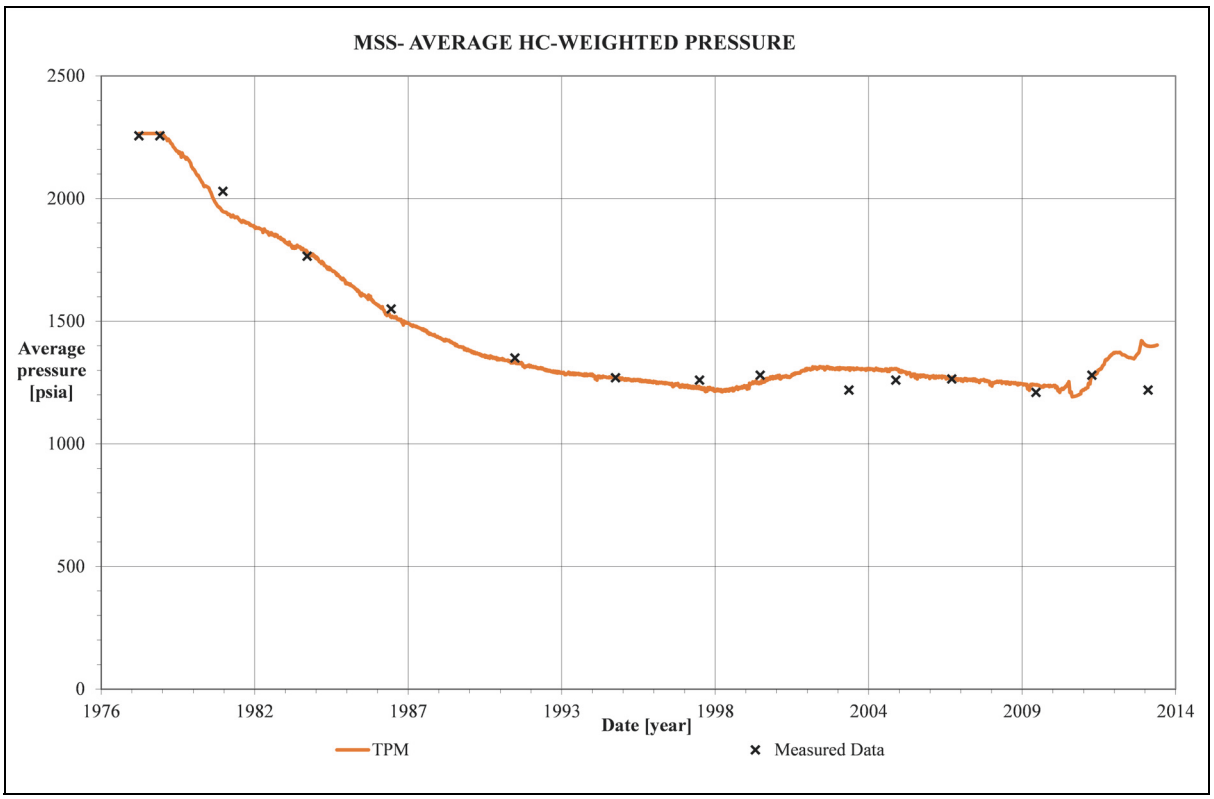

Figure 6.16: TPM simulated and measured average pressure of MSS.

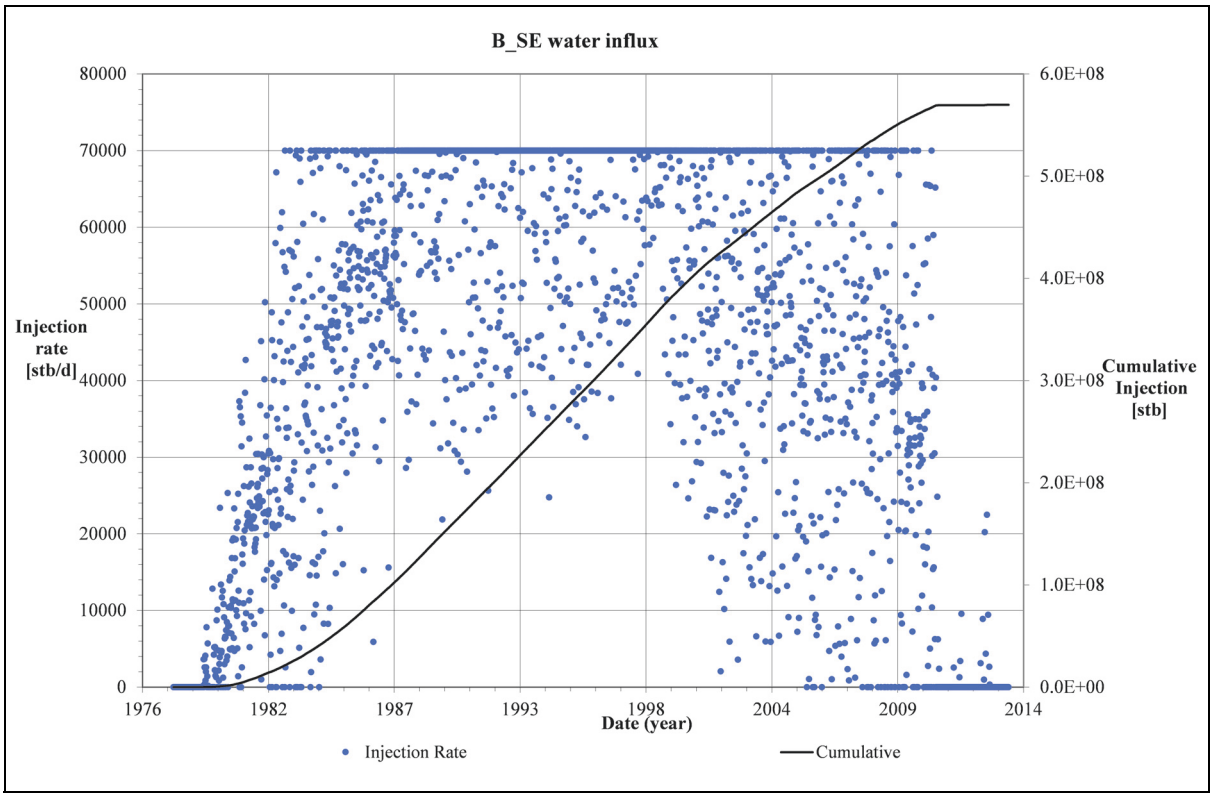

Figure 6.17: Calculated water influx for the B_SE boundary

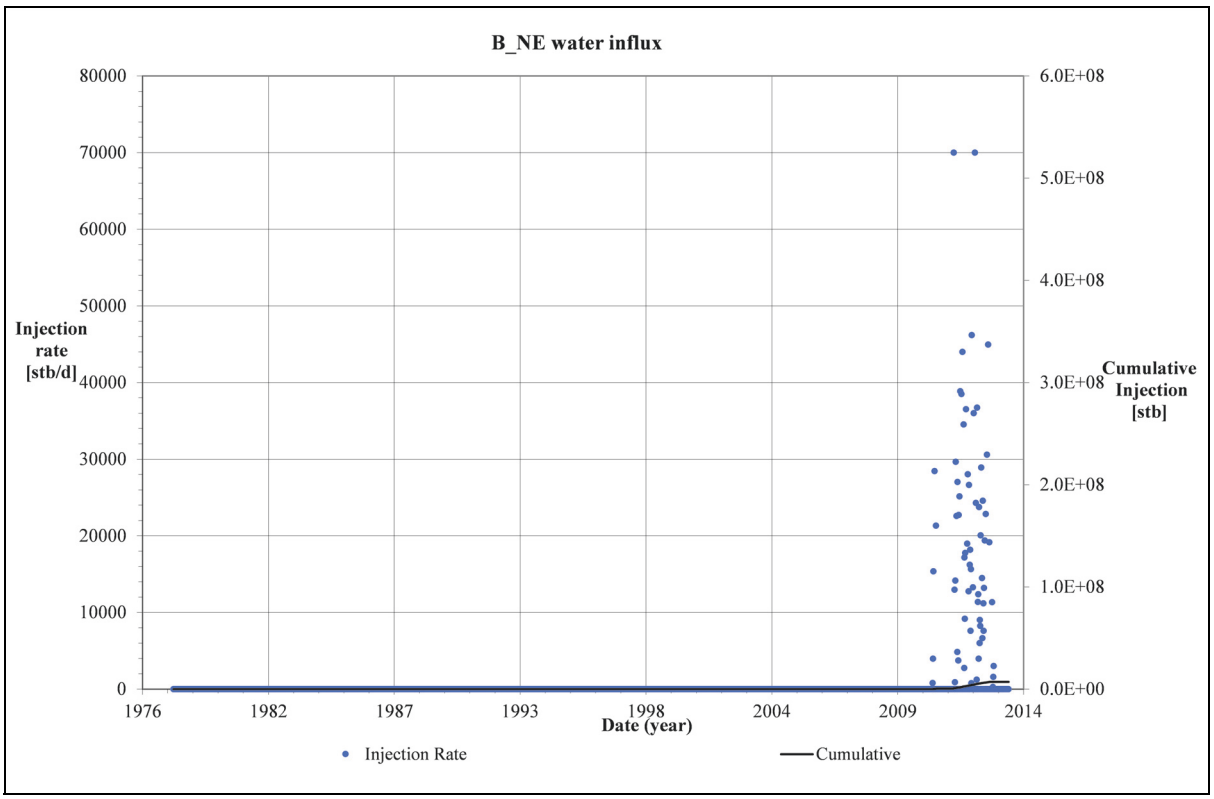

Figure 6.18: Calculated water influx for the B_NE boundary

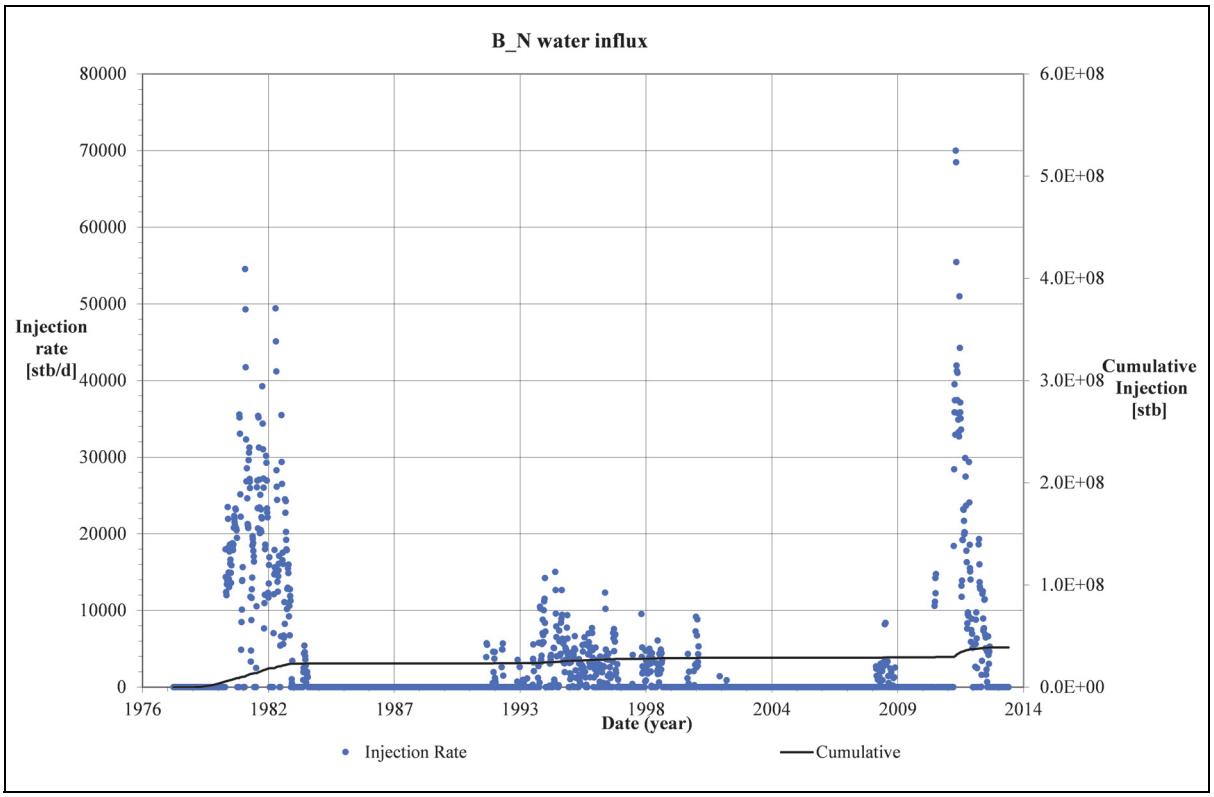

Figure 6.19: Calculated water influx for the B_N boundary

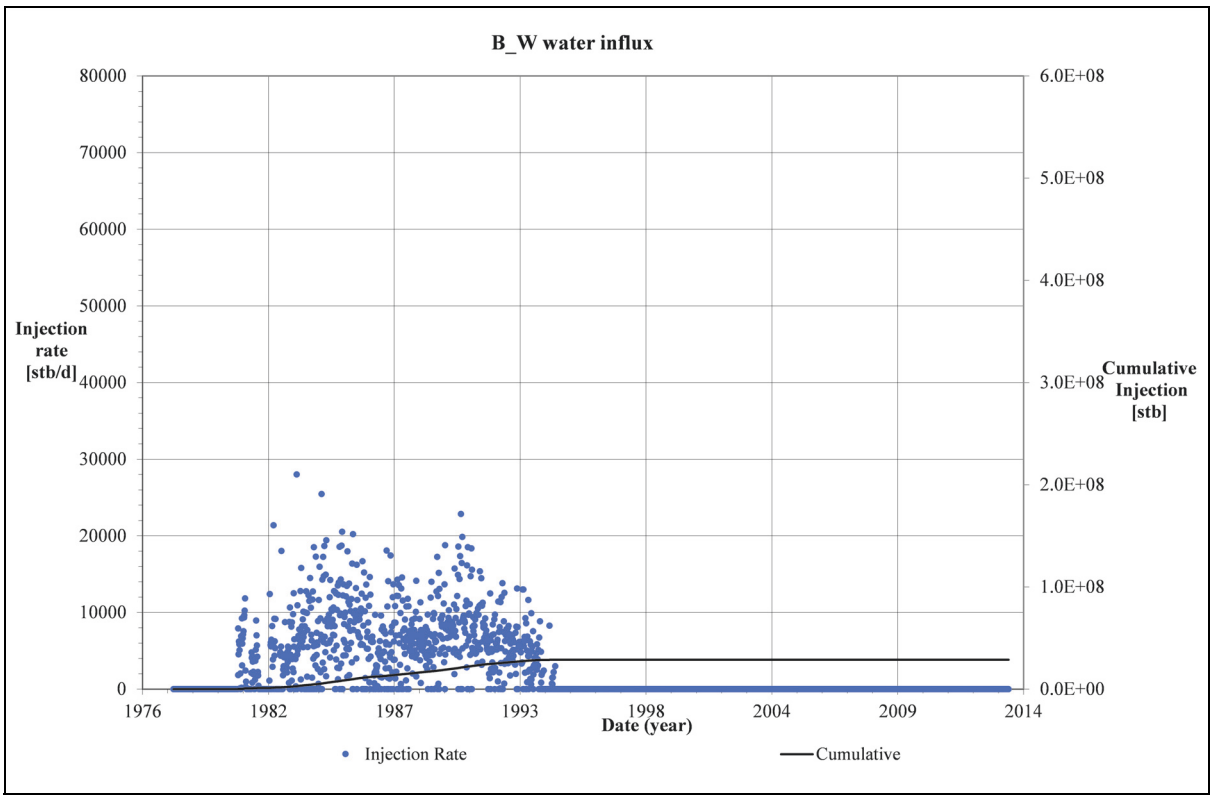

Figure 6.20: Calculated water influx for the B_W boundary

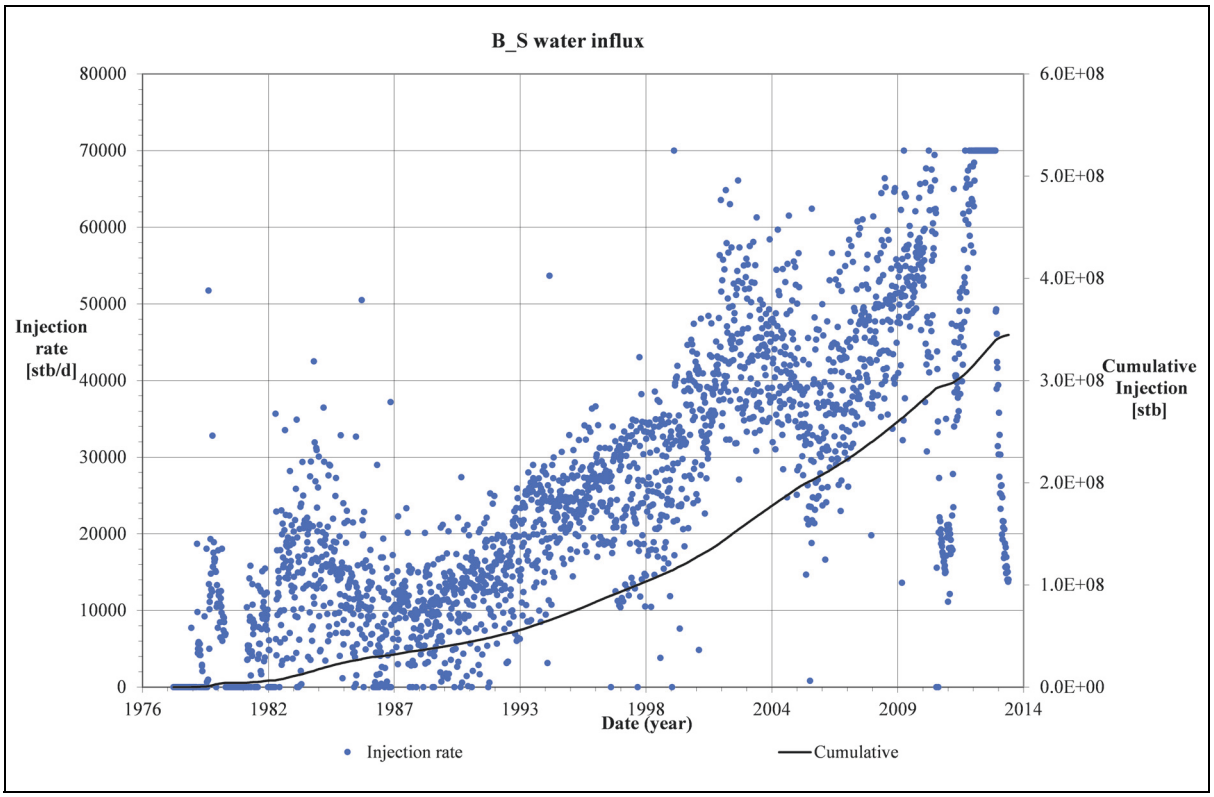

Figure 6.21: Calculated water influx for the B_S boundary

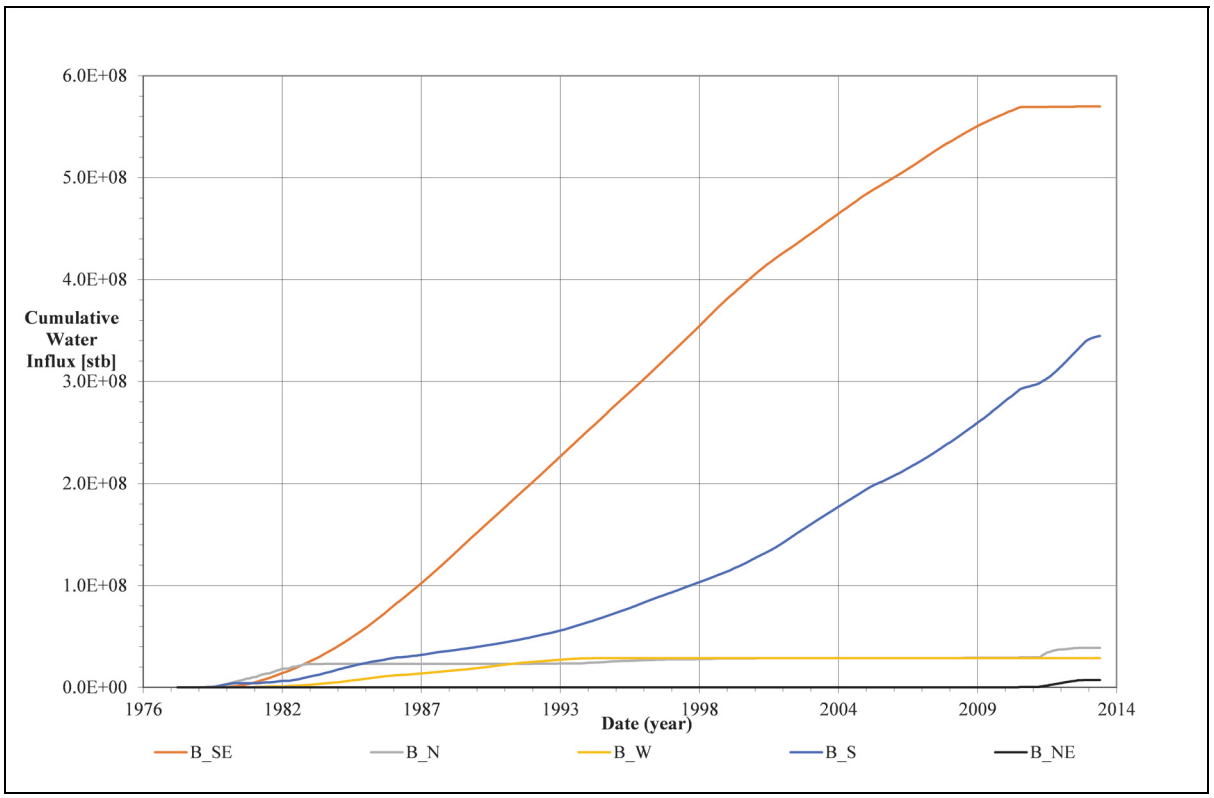

Figure 6.22: Calculated cumulative water influx for all boundaries

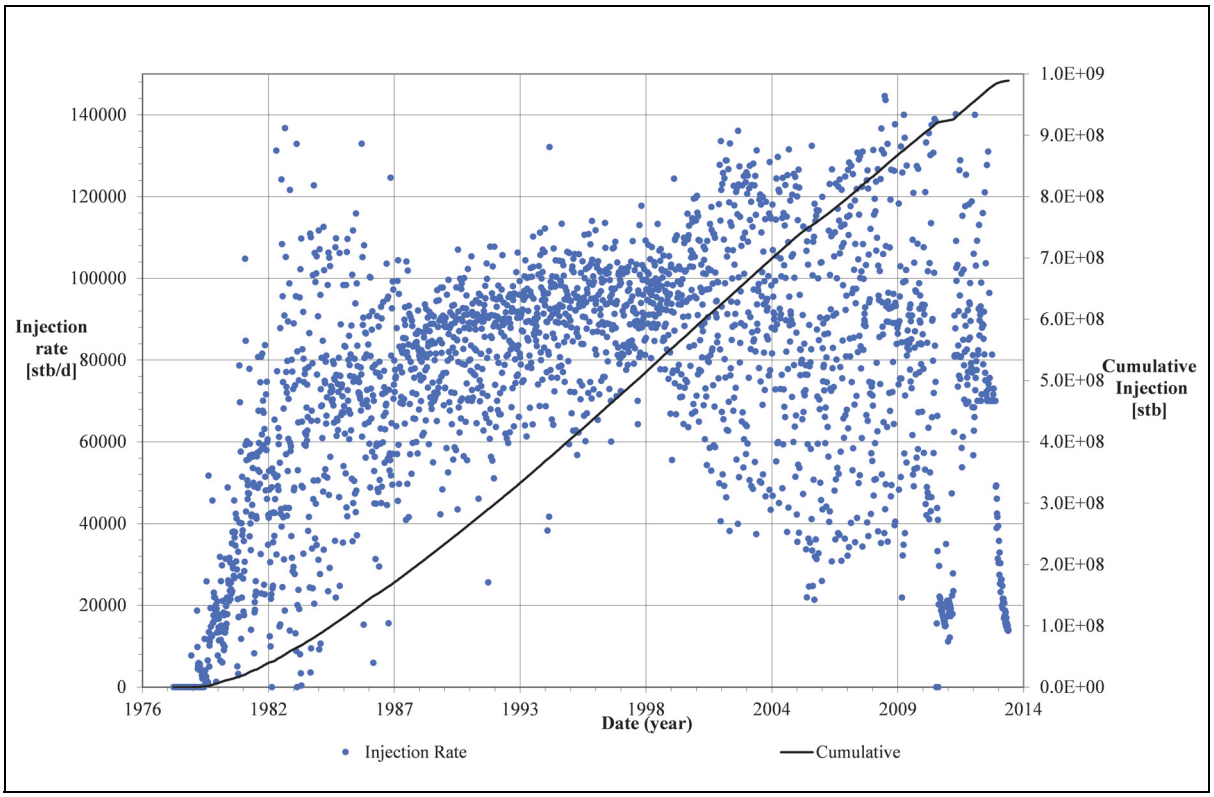

Figure 6.23: Calculated water influx for the Sabah field.

The Target Pressure Method determined analytical aquifer parameters and the time dependent Fetkovich parameters can be seen in Table 6.2. The time intervals for the Fetkovich aquifer models was set in the commands for the boundary definition using the keyword `TINTER`.

Table 6.2: Analytical aquifer parameters as calculated by the TPM

Boundary	**Date (YYYY/MM/DD)**	**Max. encroachable water [bbl]**	**Aquifer productivity index [(bbl/d)/psi]**
B_SE	1978/01/01	1.896E+09	171.5
	1995/12/01	1.896E+09	238.1
	1999/11/29	1.896E+09	249.0
	2005/12/17	1.896E+09	212.3
	2010/12/04	1.896E+09	69.9
B_NE	1978/01/01	2.377E+06	0.3
	1995/12/01	2.377E+06	0.3
	1999/11/29	2.377E+06	0.1
	2005/12/17	2.377E+06	0.3
	2010/12/04	2.377E+06	0.1

Table 6.2: Analytical aquifer parameters as calculated by the TPM

Boundary	Date (YYYY/MM/DD)	Max. encroachable water [bbl]	Aquifer productivity index [(bbl/d)/psi]
B_N	1978/01/01	5.910E+07	728.6
	1982/12/18	5.910E+07	1209.2
	1990/12/14	5.910E+07	3.1
	1995/12/01	5.910E+07	17.8
	1999/11/29	5.910E+07	6.1
	2005/12/17	5.910E+07	5.0
	2010/12/04	5.910E+07	2235.2
B_W	1978/01/01	5.942E+07	2.4
	1979/12/09	5.942E+07	29.1
	1993/12/23	5.942E+07	56.6
	1999/11/29	5.942E+07	143.1
	2005/12/17	5.942E+07	2.4
	2010/12/04	5.942E+07	2.4
B_S	1978/01/01	1.936E+12	19.5
	1995/12/01	1.936E+12	27.9
	1999/11/29	1.936E+12	45.5
	2005/12/17	1.936E+12	47.7
	2010/12/04	1.936E+12	57.7

6.4.2 Aquifer Model Applicability Verification

The same approach as with the via material balance calculated aquifer is taken here. To verify the aquifer it is necessary to use the calculated aquifer parameters and run the simulation again for the same period as in the TPM run. If the pressure the prediction run shows a good match with the history run data, the calculated aquifer parameters can be viewed as verified.

As demonstrated for the example boundary B_SE, the boundaries are defined as follows:

```
BOUNDARY 1978/01/01 B_SE fetkov AQUIWEI 0.189641E+10 AQUIJW 0.171456E+03
BOUNDARY 1995/12/01 B_SE fetkov AQUIWEI 0.189641E+10 AQUIJW 0.238112E+03
BOUNDARY 1999/11/29 B_SE fetkov AQUIWEI 0.189641E+10 AQUIJW 0.248980E+03
BOUNDARY 2005/12/17 B_SE fetkov AQUIWEI 0.189641E+10 AQUIJW 0.212265E+03
```

```
BOUNDARY 2010/12/04 B_SE fetkov AQUIWEI 0.189641E+10 AQUIJW 0.699120E+02
```

where AQUIWEI is the maximum encroachable water [bbl] and AQUIJW is the aquifer productivity index [(bbl/d)/psi]. The values are taken from the TPM results that can be seen in Table 6.2.

Figure 6.24 shows the calculated average reservoir pressure for the history (TPM), the prediction, using the analytical aquifers, and the measured data. The chosen analytical aquifer models are able to reproduce the values from the TPM very accurately with the exception of the pressure behavior in the last years. However, the input data of the years beyond 2009 is only sparse and therefore the measured data is very uncertain in this period.

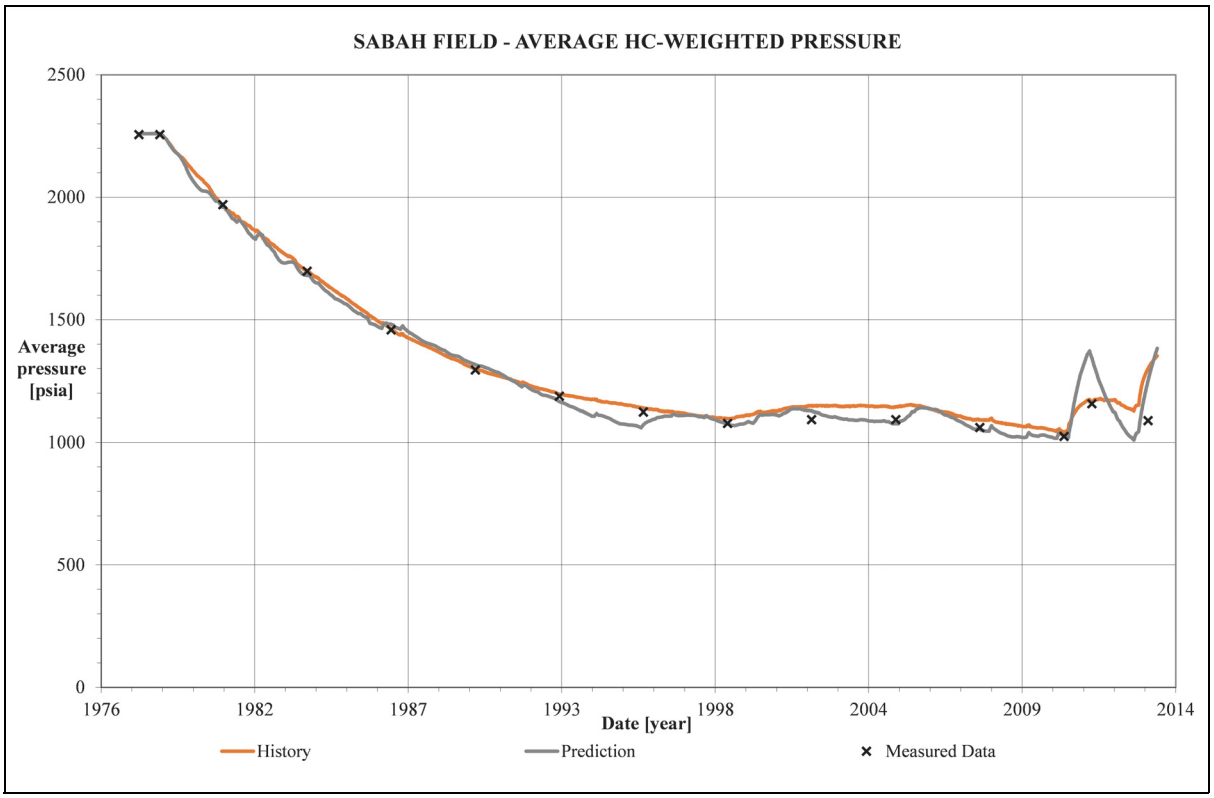

Figure 6.24: Average reservoir pressure using the analytical aquifer models (prediction) compared with the TPM result and the measured data.

A closer look at all the individual pressure regions is presented in the figures Figure 6.25 - Figure 6.32. A general trend is that the pressures using the analytical aquifer models is slightly lower than the pressures calculated with the TPM. The biggest discrepancy between TPM and the prediction simulation can be seen in Figure 6.30, which shows the SW region.

Overall the analytical aquifer models can be considered to be applicable, since the pressure history could be reconstructed with the simulation in prediction mode.

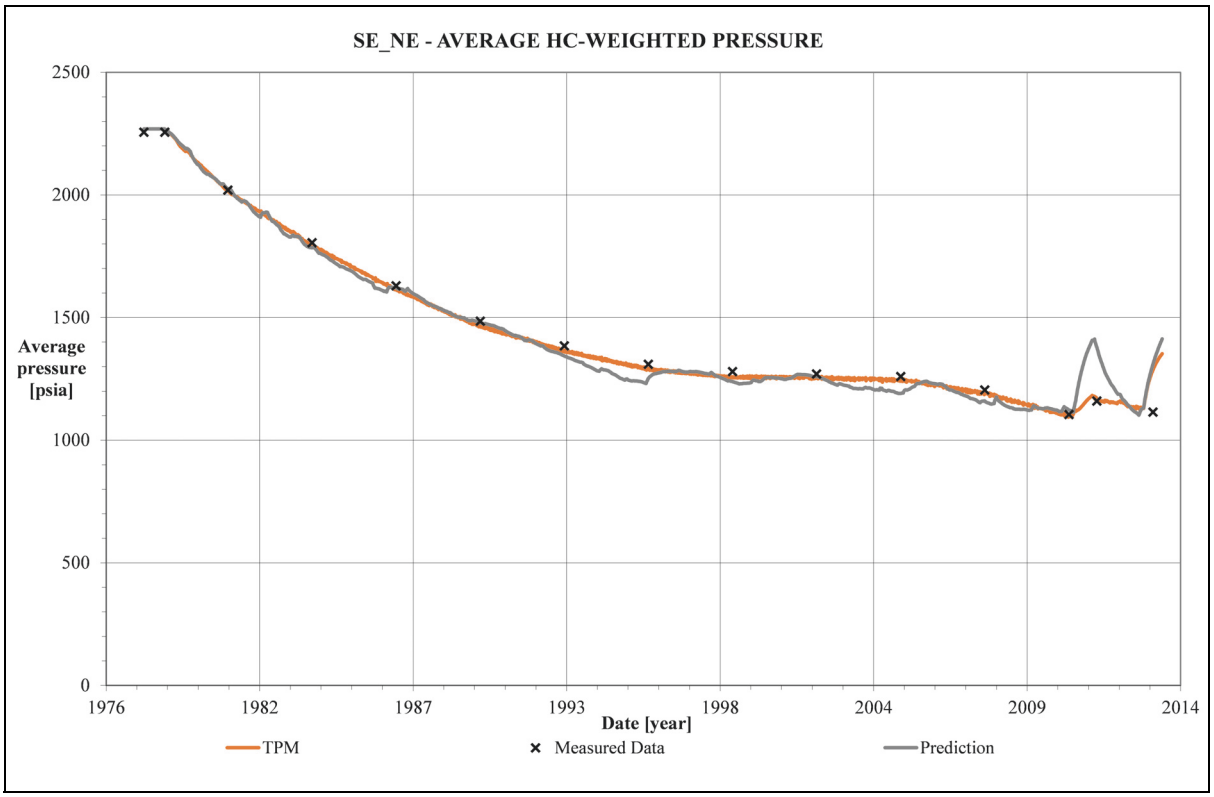

Figure 6.25: Average pressure of the SE_NE region using the analytical aquifer model (prediction) compared with the TPM result and the measured data.

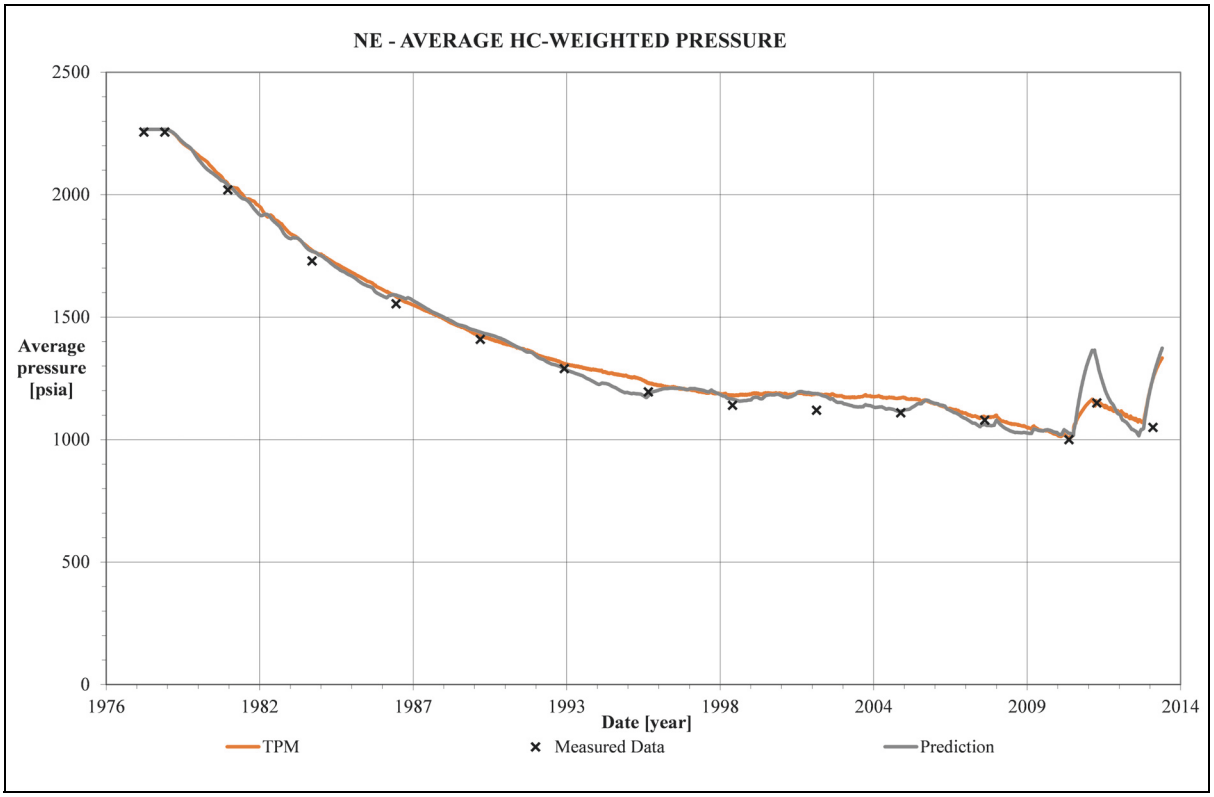

Figure 6.26: Average pressure of the NE region using the analytical aquifer model (prediction) compared with the TPM result and the measured data.

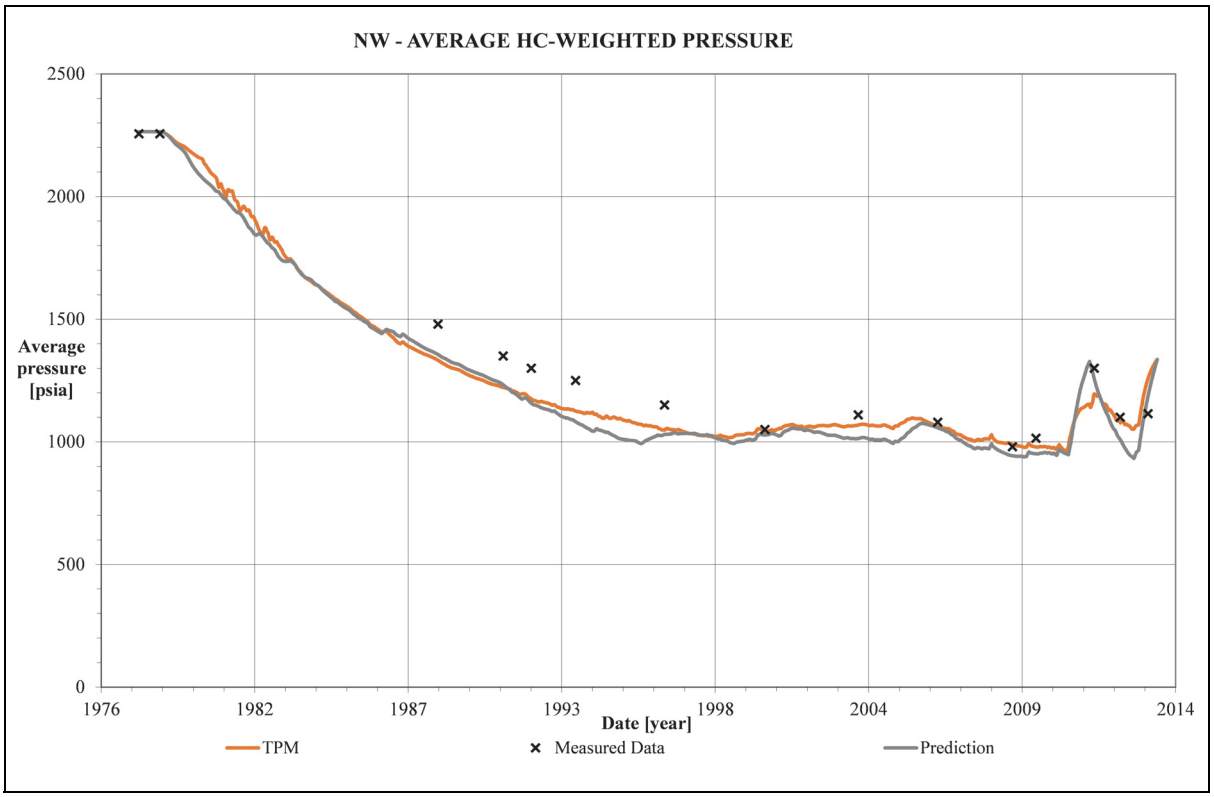

Figure 6.27: Average pressure of the NW region using the analytical aquifer model (prediction) compared with the TPM result and the measured data.

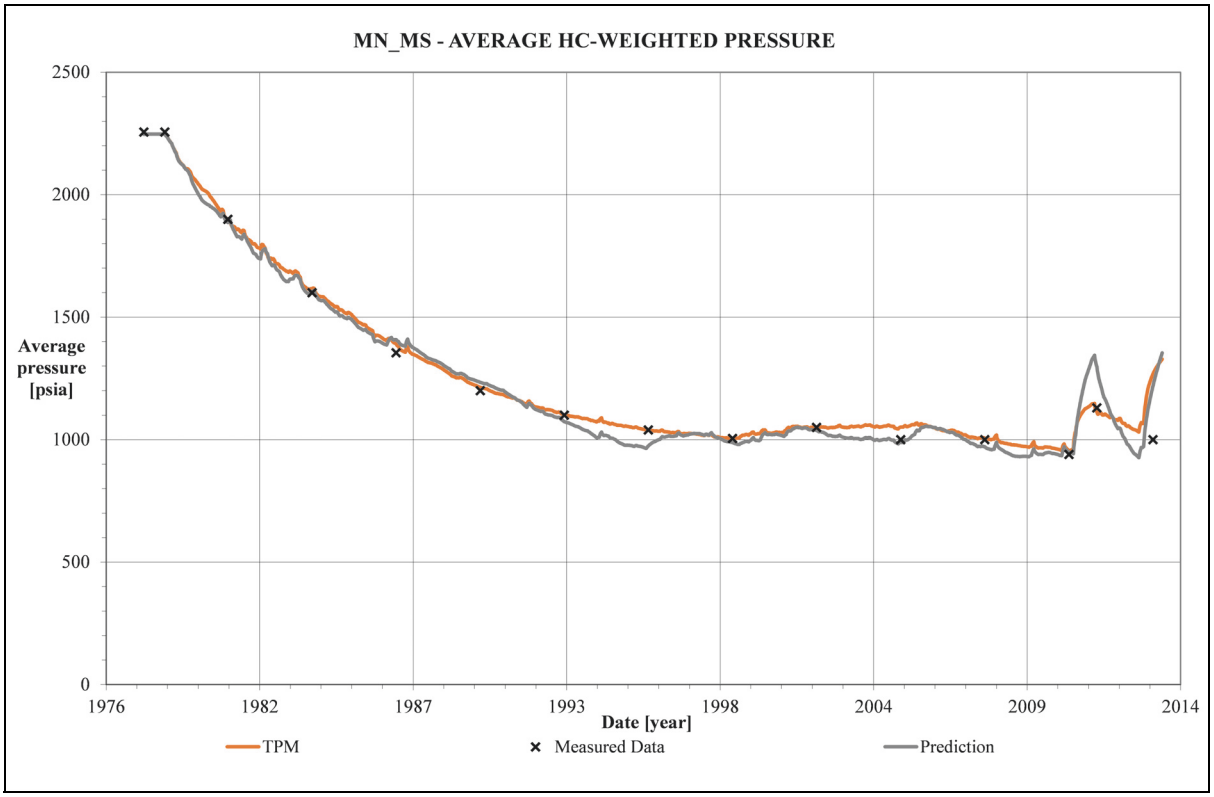

Figure 6.28: Average pressure of the MN_MS region using the analytical aquifer model (prediction) compared with the TPM result and the measured data.

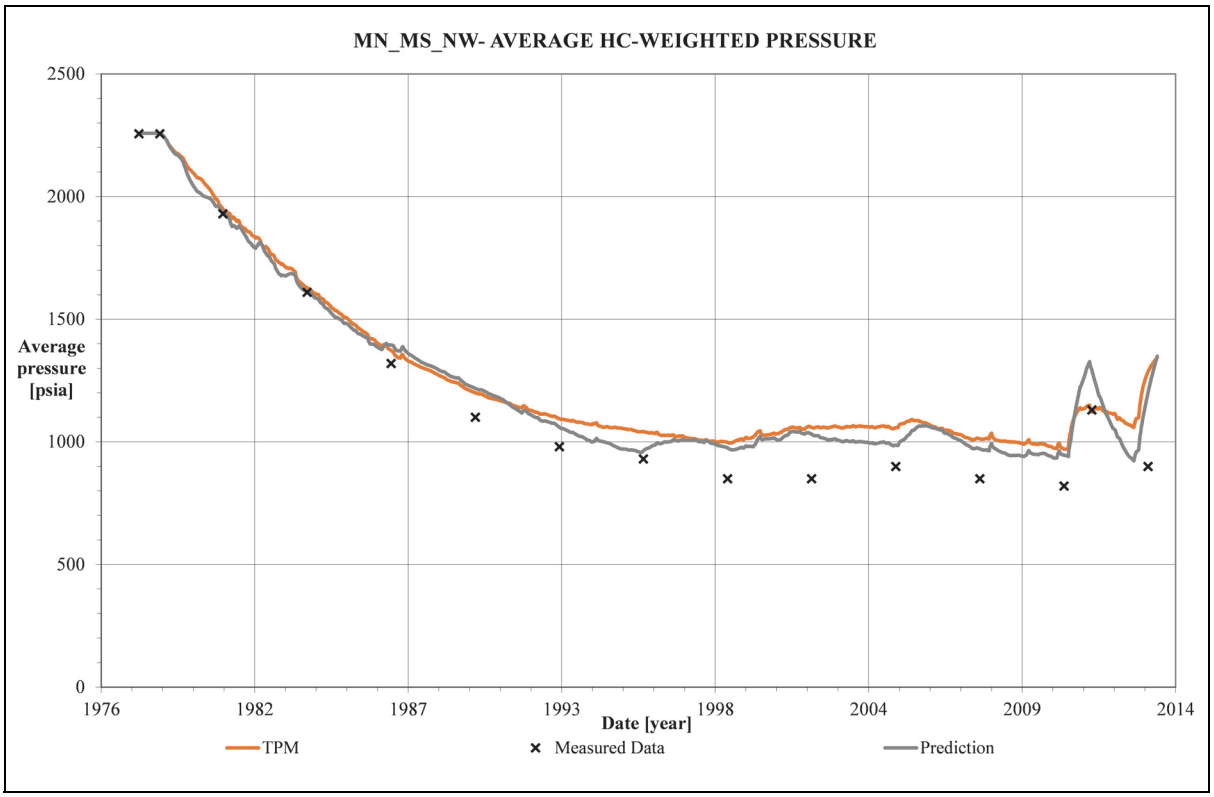

Figure 6.29: Average pressure of the MN_MS_NW region using the analytical aquifer model (prediction) compared with the TPM result and the measured data.

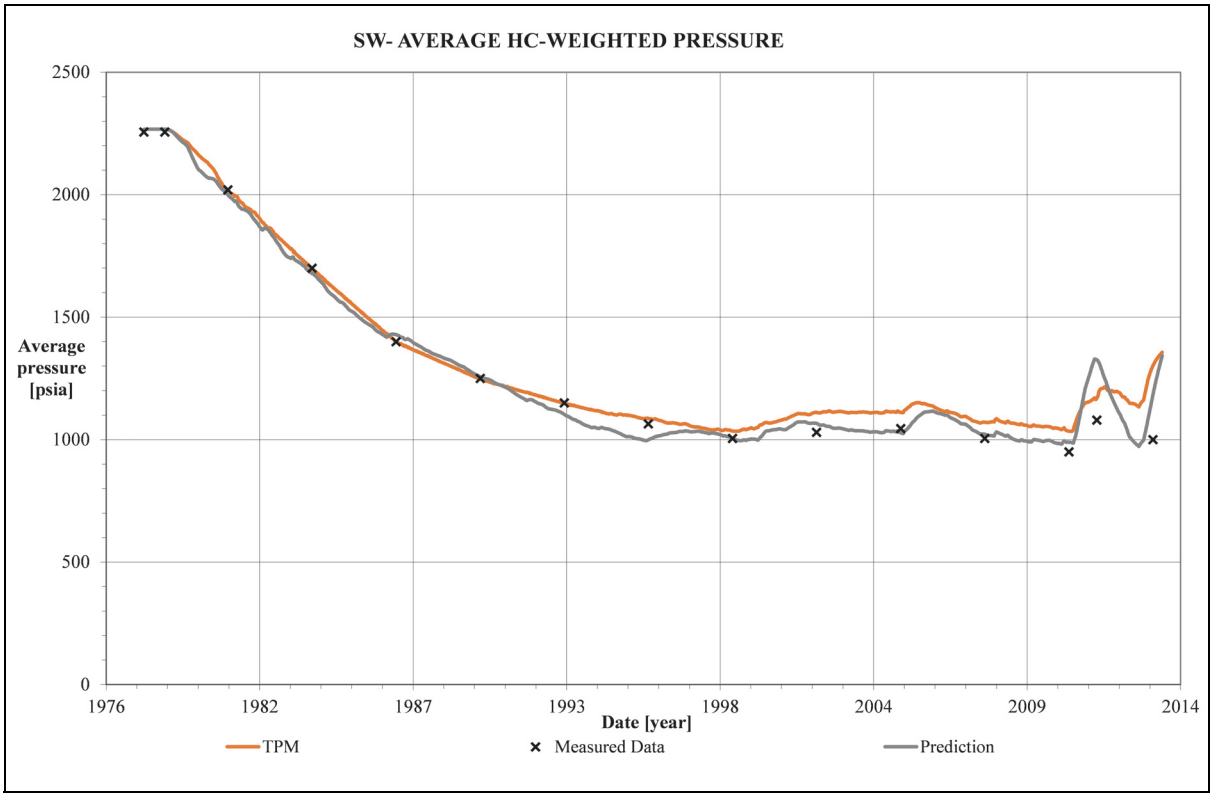

Figure 6.30: Average pressure of the SW region using the analytical aquifer model (prediction) compared with the TPM result and the measured data.

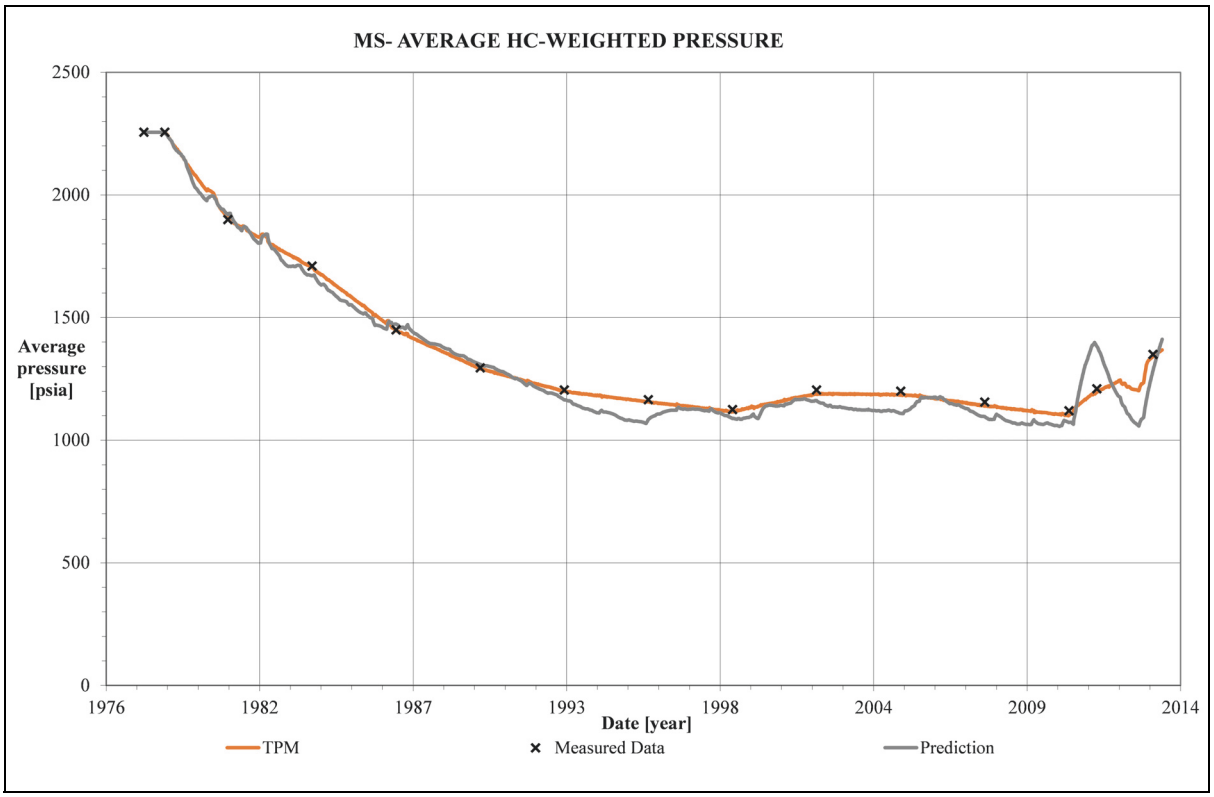

Figure 6.31: Average pressure of the MS region using the analytical aquifer model (prediction) compared with the TPM result and the measured data.

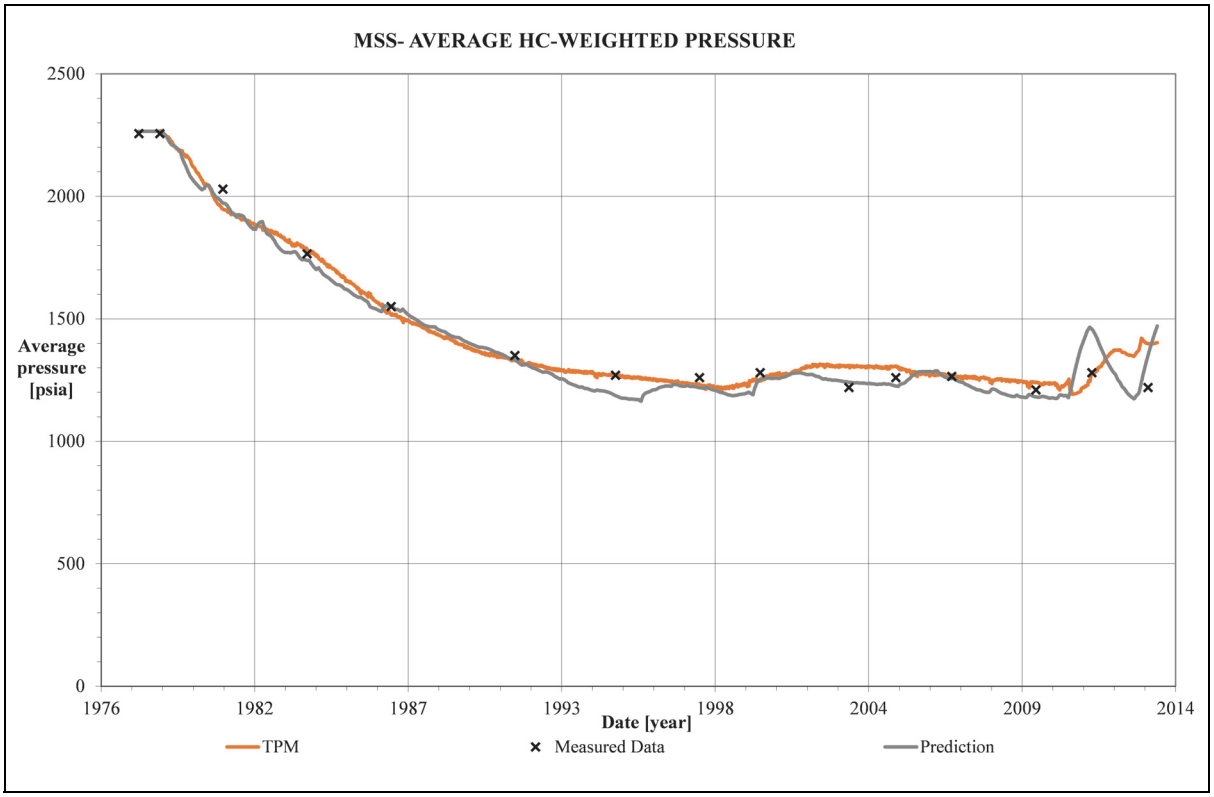

Figure 6.32: Average pressure of the MSS region using the analytical aquifer model (prediction) compared with the TPM result and the measured data.

6.4.3 Aquifer Model Applicability Verification With Schlumberger ECLIPSE

The TPM in H5 also calculates the aquifer model parameters directly into a format that can be interpreted by ECLIPSE. The TPM output can be copied into the SOLUTION section of the ECLIPSE input. In case the TINTER option is used, the aquifer model parameters have to be copied into the SCHEDULE section to the according date.

This step is performed to verify the applicability of the aquifer model, as calculated using the TPM, which is implemented in H5, with a different commercial software package. If the calculations with H5 and ECLIPSE show the same results with the analytical aquifer model, the calculation of ECLIPSE aquifer model parameters using H5 is correct. If the pressure from both prediction runs show a good match with the TPM run data, the calculated aquifer parameters can be viewed as verified.

The aquifer parameters can be seen in Table 6.3. It should be noted that although similar to the used values in H5, the parameters are not identical and use different units.

In ECLIPSE the boundaries are not named but numbered. The aquifer ID numbers correspond to the following named boundaries:

- 1 corresponds to B_SE
- 2 corresponds to B_NE
- 3 corresponds to B_N
- 4 corresponds to B_W
- 5 corresponds to B_S

Therefore an exemplary command ECLIPSE for setting aquifer parameters at a specific date for all boundaries is:

```
DATES
01 'Dec' 1995 /
/
AQUFETP
1 4700.00 2289.20 0.257471E+11 0.313700E-04 2.32153E+02 1 1* /
2 4700.00 2289.20 0.322748E+08 0.313700E-04 2.52180E+00 1 1* /
3 4700.00 2289.20 0.802451E+09 0.313700E-04 1.73662E+01 1 1* /
4 4700.00 2289.20 0.806738E+09 0.313700E-04 5.51835E+01 1 1* /
5 4700.00 2289.20 0.262816E+14 0.313700E-04 2.71905E+01 1 1* /
/
```

where the first column indicates the aquifer ID number, the second column is the aquifer datum depth [ft], the third column is the initial aquifer pressure [psia], the fourth column is the initial volume of water in the aquifer [stb], the fifth column is the total compressibility of the aquifer

[1/psi] and the sixth column is the aquifer productivity index [(stb/d)/psi]. The last two columns are the number of the PVT region, which is always the same, and the initial salt concentration in the aquifer [lb/stb], which is a defaulted value.

Table 6.3: Analytical aquifer parameters as calculated by TPM for ECLIPSE

Boundary	**Date (YYYY/MM/DD)**	**Initial volume of water in aquifer [stb]**	**Aquifer productivity index [(stb/d)/psi]**
1	1978/01/01	2.575E+10	188.9
	1995/12/01	2.575E+10	238.1
	1999/11/29	2.575E+10	249.0
	2005/12/17	2.575E+10	212.3
	2010/12/04	2.575E+10	69.9
2	1978/01/01	3.227E+07	2.5
	1995/12/01	3.227E+07	2.5
	1999/11/29	3.227E+07	1.2
	2005/12/17	3.227E+07	2.5
	2010/12/04	3.227E+07	10583.0
3	1978/01/01	8.025E+08	35.8
	1982/12/18	8.025E+08	1179.0
	1990/12/14	8.025E+08	3.0
	1995/12/01	8.025E+08	17.4
	1999/11/29	8.025E+08	6.0
	2005/12/17	8.025E+08	4.9
	2010/12/04	8.025E+08	2179.3
4	1978/01/01	8.067E+08	30.0
	1979/12/09	8.067E+08	2.8
	1993/12/23	8.067E+08	55.2
	1999/11/29	8.067E+08	139.5
	2005/12/17	8.067E+08	2.3
	2010/12/04	8.067E+08	2.3

Table 6.3: Analytical aquifer parameters as calculated by TPM for ECLIPSE

Boundary	Date (YYYY/MM/DD)	Initial volume of water in aquifer [stb]	Aquifer productivity index [(stb/d)/psi]
5	1978/01/01	2.628E+13	26.3
	1995/12/01	2.628E+13	27.2
	1999/11/29	2.628E+13	44.4
	2005/12/17	2.628E+13	46.5
	2010/12/04	2.628E+13	56.3

The result for the field level can be seen in Figure 6.33. The field level pressure is very similar for all cases.

The results for the target pressure regions can be seen in Figure 6.34 to Figure 6.38. All target pressure regions show a good match between the H5 and ECLIPSE predictions runs using the analytical aquifer parameters. Therefore also the simulation using Schlumberger ECLIPSE confirms the applicability of the calculated aquifer parameters and also the correct determination of the aquifer parameters by H5 is confirmed.

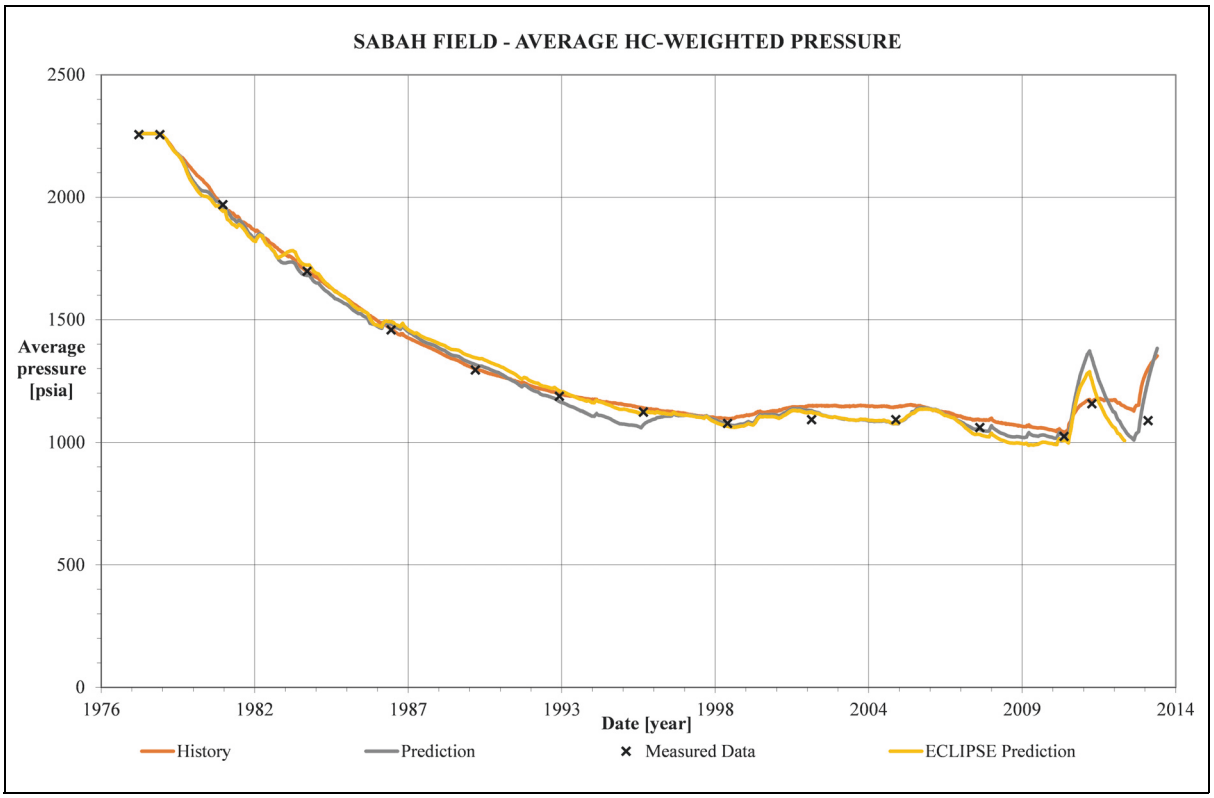

Figure 6.33: Average reservoir pressure comparison between H5 and ELIPSE.

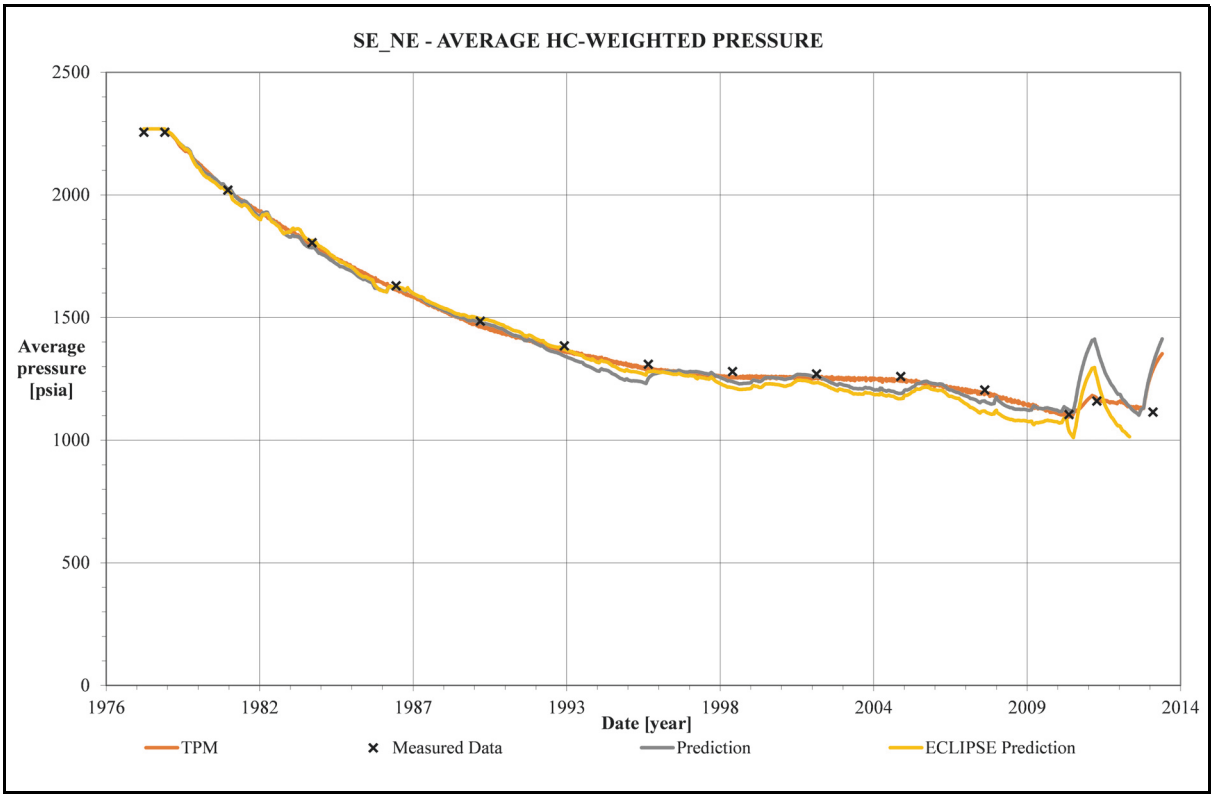

Figure 6.34: SE_NE region pressure comparison between H5 and ELIPSE.

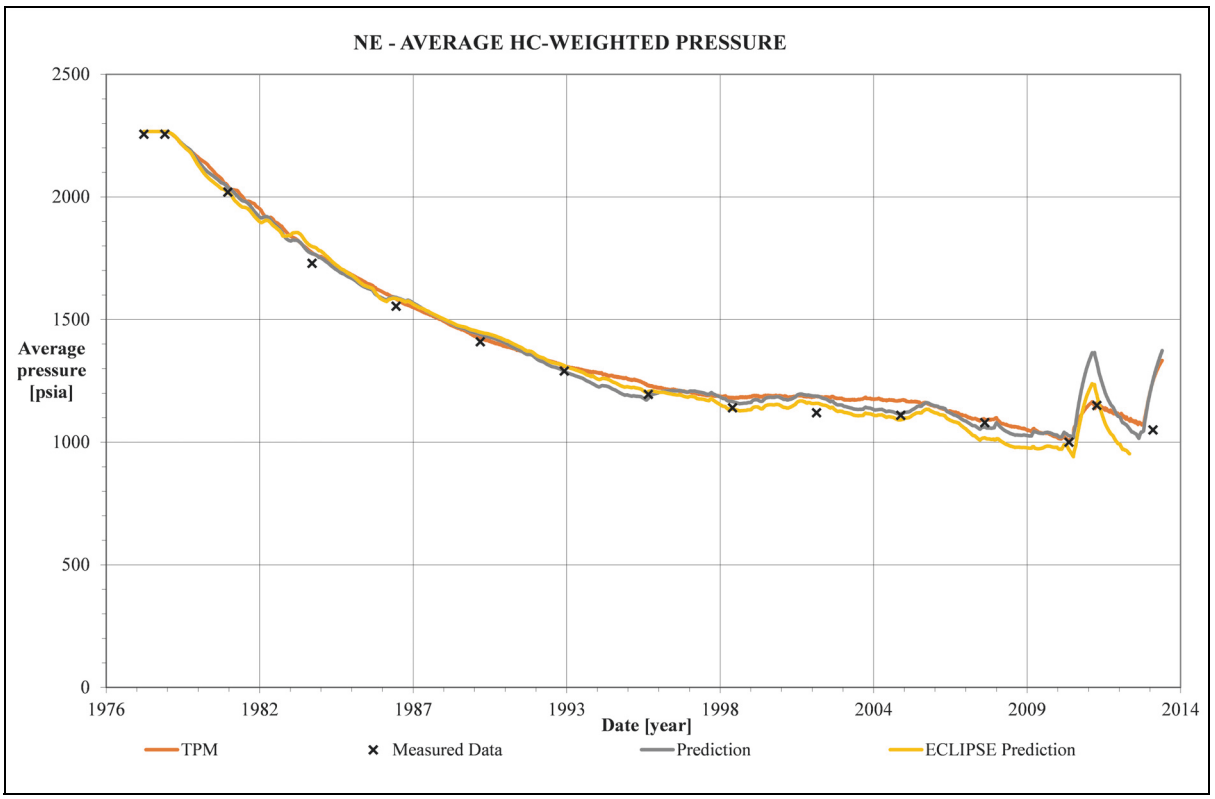

Figure 6.35: NE region pressure comparison between H5 and ELIPSE.

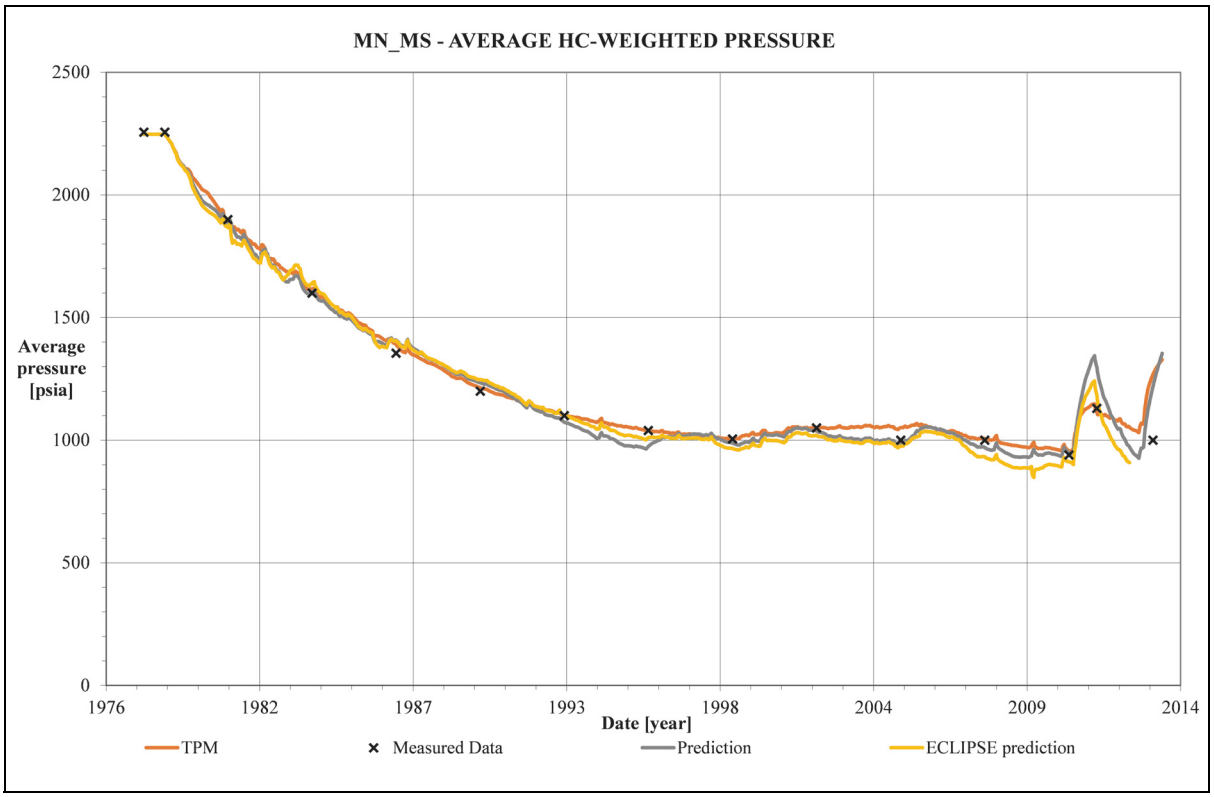

Figure 6.36: MN_MS region pressure comparison between H5 and ELIPSE.

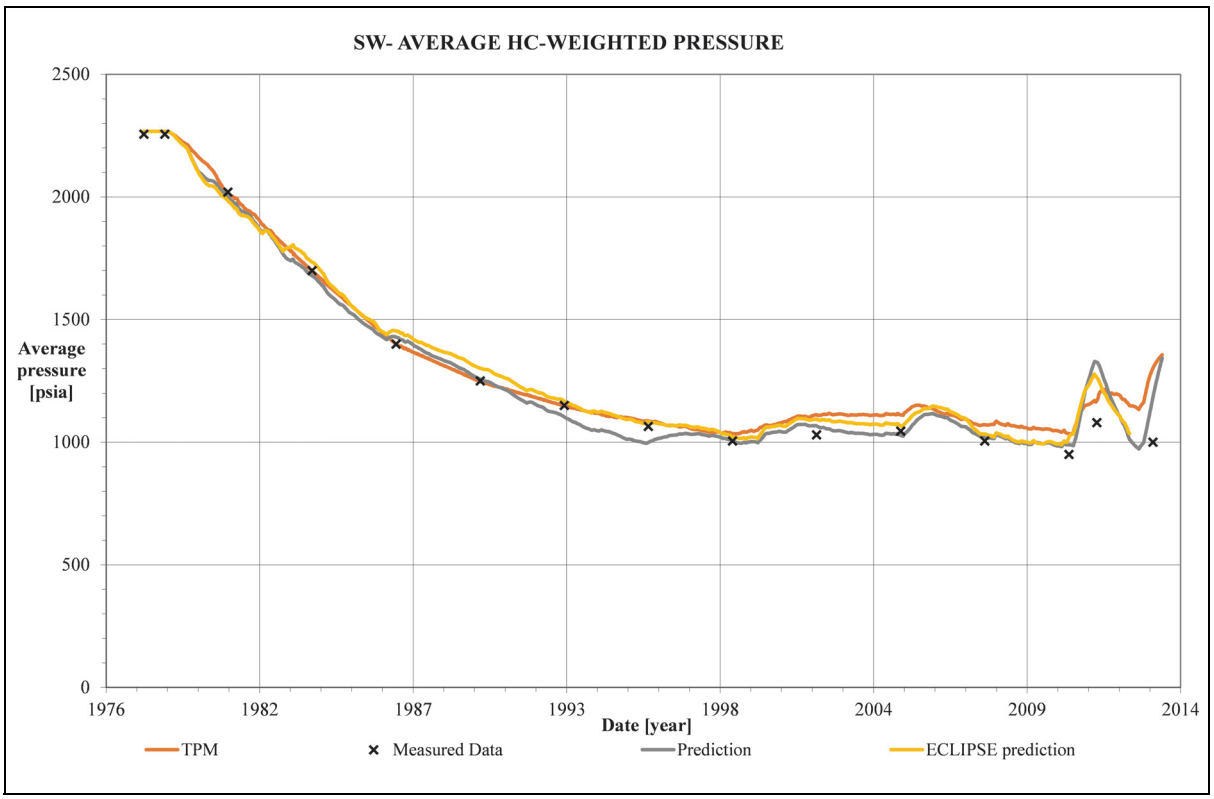

Figure 6.37: SWE region pressure comparison between H5 and ELIPSE.

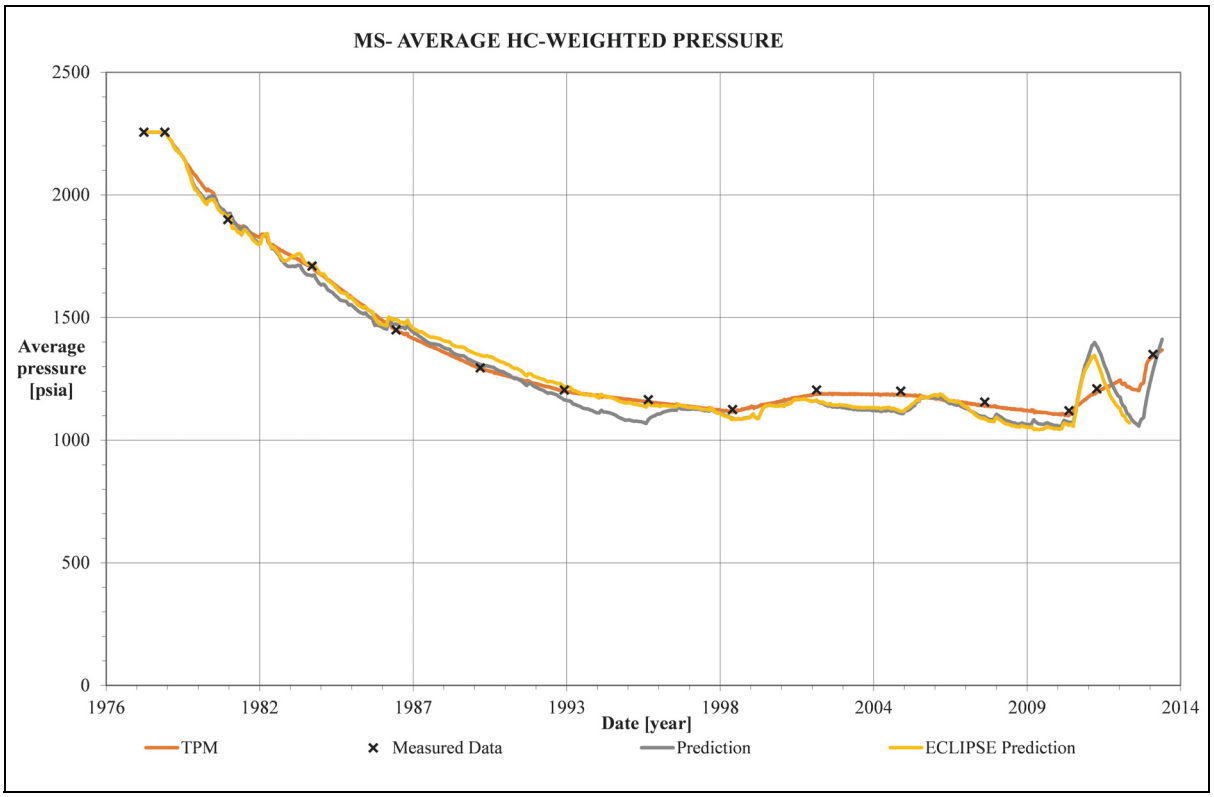

Figure 6.38: MS region pressure comparison between H5 and ELIPSE.

Chapter 7

Conclusions

1. It is possible to determine water influx requirements for a naturally fractured reservoir with the Target Pressure Method by matching the average region pressure of the target region.
2. The average field pressure can be matched with the material balance calculation, but no information about the water influx direction can be obtained.
3. The cumulative water influx calculated with the material balance method is only 0.8% higher than the calculated cumulative water influx using the Target Pressure Method. Therefore it can be concluded that for a quick estimation of only the total cumulative water influx both methods are equally suitable.
4. The Target Pressure Method can be used to give information to the geologist for refining the model at a very early stage of the dynamic modeling process. For the Sabah field it is evident that the calculated average pressure for the regions surrounding the central region MN_MS_NW is either exact or even below the measured data. But average hydrocarbon weighted pressure of the MN_MS_NW region is higher than the measured data. This is a strong indication that improvements to the geological model in the area of the central region MN_MS_NW are possible.
5. Water influx into the Sabah Field mainly happens from the South. This can be seen by the fact that the boundaries B_SE and B_S contribute 92% of all calculated water influx.
6. The results given by the H5 simulator have been confirmed by comparing the results with Schlumbergers ECLIPSE E100 black oil reservoir simulator.

Chapter 8

References

Aanonsen, S.I. et al. 2009. The Ensemble Kalman Filter in Reservoir Engineering - a Review. *SPE Journal* **14** (3): 393-412. SPE-117274-PA

Ahmed, T. 2006. *Reservoir Engineering Handbook*., third edition. Oxford, UK: Gulf Professional Publishing, an imprint of Elsevier

Ahmed, T. and McKinney, P.D. 2008. *Advanced Reservoir Engineering*, first edition. Oxford, UK: Gulf Professional Publishing, an imprint of Elsevier

Anterion, F., Eymard, R. and Karcher B. 1989. Use of Parameter Gradients for Reservoir History Matching. Presented at the SPE Reservoir Simulation Symposium, San Antonio, Texas, February 1989. SPE-18433

Birks, J. 1963. Coning Theory and its Use in Predicting Allowable Producing Rates of Wells in Fissured Limestone Reservoir. *Iranian Petroleum Institute Bulletin* **12**: 470-480

Bissell, R.C., Killough, J. and Sharma Y. 1992. Resevoir Histoy Matching Using the Method of Gradients. Presented at the SPE European Petroleum Computer Conference, Stavanger, May 1992. SPE-24265

Campbell, R.A. and Campbell, J.M., Sr. 1978. *Mineral Property Economics: Vol. 3: Petroleum Property Evaluation*. Norman, Oklahoma: Campbell Petroleum Series

Carlson, F.M. and Mones, C.G. 1994. Resolution of the Inconsistency Between Peaceman's Well-block Pressure And the Average Pressure of the Well Block. Presented at the Annual Technical Meeting, Calgary, Alberta, 12-15 June 1994. PETSOC-94-25

Carter, R.D. and Tracy, G.W. 1960. An Improved Method for Calculating Water Influx. *Trans. AIME* **219**: 415-417

Castellini, A., Gullapalli, I., Hoang, V.T., Condon, P.J. 2008. Quantifying Uncertainty in

Production Forecast for Fields With Significant History: A West African Case Study. Presented at the International Petroleum Technology Conference, Doha, Qatar, 21-23 November 2005, IPTC-10987-MS

Christie, M. et al. 2013. Use of Multi-Objective Algorithms in History Matching of a Real Field. Presented at the SPE Reservoir Simulation Symposium, The Woodlands, Texas, 18-20 February 2013, SPE-163580-MS

Coats, K.H. 1970. Mathematical Methods for Reservoir Simulation. Presented by the College of Engineering, Universitys of Texas at Austin, 8-12 June 1970

Coats, K.H., Rapoport, L.A., McCord, J.R. and Drews, W.P. 1964. Determination of Aquifer Influence Functions From Field Data. Presented at 39th Annual Fall Meeting, Houston, Texas, 11-14 October 1964. SPE-897

CORE LABORATORIES. 1977. Reservoir Fluid Study. Prepared for Occidental Petroleum Corporation (Occidental of Libya, INC), G3-74 Well, Sabah Field

CORE LABORATORIES. 1991. Reservoir Fluid Study for Zueitina Oil Co., Sabah/G18, Sabah Field, Libya

Dake, L.P. 2001. *The Practice of Reservoir Engineering (Revised Edition)*, first edition. Amsterdam, Netherlands: Elsevier Science B.V.

Dietz, D.M. 1965. Determination of Average Reservoir Pressure From Buildup Surveys. *J Pet Technol* **17** (8): 955-959

Ding, S. 1990. *The Use Of Semi-Analytical Method for Matching Aquifer Influence Function*. M.Sc. Thesis, Texas A&M University, College Station, Texas (1990).

Fetkovich, M.J. 1971. A Simplified Approach to Water Influx Calculations - Finite Aquifer Systems. *J Pet Technol* **23** (7): 814-828. SPE-2603-PA

Gokturk, E. and Tarhouni, N. 1999. 3D Seismic Interpretation of Sabah Field. November 1999

Hajizadeh, Y., Christie, M.A. and Demanyanov, V. 2009. Ant Colony Optimization Algorithm for History Matching. Presented at the EUROPEC/EAGE Conference and Exhibition, Amsterdam, The Netherlands, 8-11 June 2009. SPE-121193-MS

Havlena, D. and Odeh, A.S. 1963. The Material Balance as an Equation of a Straight Line. *J Pet Technol* **15** (8): 896-900

Heinemann, Z.E. 2012. *PRS a tool for Reservoir Simulation Modeling & Research: Technical Description (TD) Version 2.1*. Leoben, Austria: Heinemann Oil GmbH

Heinemann, Z.E., Mittermeir, G.M., Abrahem, F.A.S., Gherryo, Y.S. and Shatwan, B.B. 2010a. Computer Assisted History Matching - and its Successful Application (1). *OIL GAS European Magazine* **36** (3): 141-146

Heinemann, Z.E., Mittermeir, G.M., Abrahem, F.A.S., Gherryo, Y.S. and Shatwan, B.B. 2010b. Computer Assisted History Matching - and its Successful Application (2). *OIL GAS European Magazine* **36** (4): 207-213

Horner, D.R. 1951. Pressure Buildup in Wells. Proceedings of the Third World Petroleum Congress, Leiden, Netherlands

HOT Engineering GmbH. 2004. *SABAH FIELD Reservoir Simulation Study: Final Report*. Hot Engineering, Leoben

HOT Engineering GmbH (2008). *SABAH FIELD Reservoir Simulation Study Update: Final Report*. Hot Engineering, Leoben

Hutchinson, T. S. and Sikora, V.J. 1959. A Generalized Water Drive Analysis. *Trans. AIME* **216**: 169-178. SPE-1123-G

Katz, D.L., Tek, M.R. and Jones, S.C. 1962. A Generalized Model for Predicting the Performance of Gas Reservoirs Subject to Water Drive. Presented at 37th Annual Fall Meeting of SPE, Los Angeles, California, 7-10 October 1962. SPE-428

Knytl, J., Brydle, G., Greenwood, D., Earth Sciences Society of Libya. National Oil Corporation Libya. 1996. Tectonic History and Structural Development of the Kaf-Themar Trend of the Western Sift Basin. First Symposium on the Sedimentary Basins of Libya in *The Geology of Sirte Basin*, third edition, Salem, M.J., El-Hawat, A.S., and Sbeta, A.M (eds.)**,** 167-200: Amsterdam, Elsevier

Mansur, M.A. 1987. Sabah Field. Geological Report, September 1987

Mattax, C.C. and Dalton, R.L. 1990. *Reservoir Simulation*. Monograph Series Volume 13, Richardson, Texas: Society of Petroleum Engineers of AIME

Matthews, C.S. and Russel, D.G. 1967. *Pressure Buildup and Flow Tests in Wells*. Monograph Series Volume 1, Dallas, Texas: Society of Petroleum Engineers of AIME

Matthews, C.S., Brons; F., and Hazenbrock, P. 1954. A Method for Determination of Average Pressure in a Bounded Reservoir. *Trans. AIME* **201**: 182-189. SPE-296-G

Menissi, M.H., Kenawy, F.A., Mohamed, S.A. and Sallaly, M.E.El. 1998. Development Of Aquifer Influence Function for Undersaturated Oil Reservoir Using Semi-Analytical Model. Presented at the 1998 SPE Asia Pacific Conference on Integrated Modelling for Asset Management, Kula Lumpur, Malaysia, 23-24 March 1998. SPE-39747

Miller, C.C., Dyes, A.B. and Hutchinson, C.A. (1950): "The Estimation of Permeability and Reservoir Pressure from Bottomhole Pressure Builup Characteristics," Trans., AIME (1950) 189, 91-104

Mittermeir, G.M. 2003. *Enhanced strategies for matching aquifer behavior*. Diploma Thesis, Montanuniversität Leoben, Leoben, Austria (August 2003)

Mittermeir, G.M., Pichelbauer, J. and Heinemann, Z.E. 2004. Automated Determination of Aquifer Properties From Field Production Data. Presented at the European Conference on the Mathematics of Oil Recovery (ECMOR IX), Cannes, France, 30 August - 2 September 2004

Muskat, M. 1937. Use of Data on the Buildup of Bottom-hole Pressures. *Trans. AIME* **123** (1): 44-48

Myrseth, I. and Omre, H. 2010. Hierarchical Ensemble Kalman Filter. SPE Journal **15** (2): 569-580. SPE-125851-PA

Numbere, D.T. 1989. Natural Water Influx in Nonsymmetric Reservoir/Aquifer Systems. Presented at the 64th Annual Technical Conference and Exhibition, San Antonio, Texas, 8 - 11 October 1989. SPE-19850

Peaceman, D.W. 1978. Interpretation of Well-Block Pressures in Numerical Reservoir Simulation. SPE Journal **18** (03): 183-194. SPE-6893-PA

Pelissier-Combescure, J. et al. 1979. Applications of the Repeat Formation Tester in the Middle East. Presented at the Middle East Oil Technical Conference, Manama, Bahrein, 25-29 March 1979. SPE-7775-MS

Phelphs, G.D. et al. 1984. The Effect of Filtrate Invasion and Formation Wettability on Repeat Formation Tester Measurements. Presented at the European Petroleum Conference, London, United Kingdom, 22-25 October 1984. SPE-12962-MS

Pichelbauer, J. 2003. A new method of aquifer matching in reservoir simulation. Dissertation, Montanuniversität Leoben, Leoben, Austria (March 2003)

Pirker, B. 2008. A New Approach for Modeling Dual Porosity Reservoir Using Recovery Curves. Dissertation, Montanuniversität Leoben, Leoben, Austria (November 2008)

Satter, A., Iqbal, G. and Buchwalter, J.L. 2008. *Practical Enhanced Reservoir Engineering: Assisted with Simulation Software*, first edition. Tulsa, Oklahoma: Pennwell Corporation

Schilthuis, R.J. 1936. Active Oil and Reservoir Energy. *Trans. AIME* **118** (1): 33-51

Schlumberger. 2011. *ECLIPSE Reference Manual 2012.1*

Schulze-Riegert, R.W., Axmann, J.K., Haase, O., Rian, D.T. and Lou, Y.-L. 2002. Evolutionary Algorithms Applied to History Matching of Complex Reservoirs. *SPE Reservoir Evaluation & Engineering* **5** (2): 163-173. SPE-77301-PA

Shiralkar, G.S. and Stephenson, R.R. 1994. Predictable Control of Reservoir Pressure Through Voidage Replacement. *Journal of Canadian Petroleum Technology* **33** (09): 55-61

Sills, S.R. 1996. Improved Material-Balance Regression Analysis for Waterdrive Oil and Gas Reservoirs. *SPE Reservoir Engineering* **11** (2): 127-133. SPE-28630-PA

Smith, C.R., Tracy, G.W. and Lance Farrar, R. 1992. *Applied Reservoir Engineering. Vol. 2*. Tulsa, Oklahoma: OGCI Publications

Stewart, G. and Wittmann, M. 1979. Interpretation Of The Pressure Response Of The Repeat Formation Tester. Presented at the SPE Annual Technical Conference and Exhibition, Las Vegas, Nevada, 23-26 September 1979. SPE-8362-MS

Tehrani, D.H. 1985. An Analysis of a Volumetric Balance Equation for Calculation of Oil in Place and Water Influx. *J Pet Technol* **37** (09): 1664-1670. SPE-12894-PA

van der Meer, F.D. and Cloetingh, S.A.P.L. 1993. Intraplate stresses and the subsidence history of the Sirte basin, Libya. *Tectonophysics* **226** (1-4):37-58.

van Everdingen, A.F. and Hurst, W. 1949. The Application of the Laplace Transformation to Flow Problems in Reservoirs. *J Pet Technol* **1** (12): 305-324. SPE-949305-G

Van Poollen, H.K., Breitenbach, E.a. and Thurnau, D.H. 1968. Treatment of Individual Wells and Grids in Reservoir Modeling. *SPE Journal* **8** (04): 341-346. SPE-2022-PA

Vogt, J.P. and Wang, B. 1987. Accurate Formulas for Calculating the Water Influx Superposition Integral. Presented at the 1878 SPE Eastern Regional Meeting, Pittsburgh, PA, 21-23 October 1987. SPE-17066-MS

Williams, M.A., Keating, J.F. and Barghouty, M.F. 1997. The Stratigraphic Method: A Structured Approach to History Matching Complex Simulation Models. Presented at the 1997 SPE Reservoir Simulation Symposium, Dallas, Texas, 8-11 June 1997. SPE-38014

Chapter 9

Nomenclature and Metric Conversion Factors

Symbols

A	dimensionless time conversion factor, [day^{-1}]
C	aquifer related constant, [m^3/bar.day]
c_t	total system compressibility, [1/Pa]
h	layer thickness, [m]
$HCPV$	Hydrocarbon pore volume, [bbl]
i	index of block i or index of time step i, [-]
j	index of block j or index of time step j, [-]
J_w	aquifer productivity index, [m^3/bar.day]
k	absolute permeability, [md]
n	number of time steps, number of block
$\bar{p}$	average reservoir pressure [psi]
p	pressure, [bar]
P	*Van Everdingen-Hurst* dimensionless function, [-]
p^*	false extrapolated pressure, [psi]
P'	Derivative of *Van Everdingen-Hurst* dimensionless function, [-]
p_{Aq}	constant aquifer pressure, [bar]
$\bar{P}_{field}$	Hydrocarbon weighted average pressure for the field level, [psia]
p_i	aquifer boundary pressure of calculation interval i, [bar]
p_i	initial reservoir pressure, [atm]
p_{ws}	well pressure after shut-in, [atm]

$\tilde{Q}_D(t_D)$	dimensionless inflow function according to *Vogt-Wang,* [-]
$Q_D(t_D)$	dimensionless influx function according to *Van Everdingen-Hurst,* [-]
q_w	water influx rate, [m³/day]
r_D	dimensionless radius, [-]
r_e	outer aquifer radius, [m]
r_w	inner radius of aquifer, [m]
s	skin factor, [-]
t_0	time of constant production, [s]
t_D	dimensionless time, [-]
V	volume, [m^3]
W_e	cumulative water efflux from the aquifer, [m³]
W_{ei}	maximum encroachable water, [m³]
WF	Weighting Factor, [-]

Greek Symbols

α,φ,θ	inflow angle, [deg]
ϑ	shut-in time, [s]
μ	viscosity, [Pa.s]
ϕ	porosity, [-]

SI Metric Conversion Factors

atm x 1.013250	E+05 = Pa
bar x 1.0	E+05 = Pa
cp x 1.0	E-03 = Pa.s
ft x 3.048	E-01 = m
md x 9.869	E-04 = μm^2
psi x 6.894757	E+03 = Pa
bbl x 1.589873	E-01 = m^3